ERDC/GSL TR-11-29

Geotechnical and Structures Laboratory

US Army Corps
of Engineers®
Engineer Research and
Development Center

Laboratory Characterization of Talley Brick

Hannah B. Beatty, Steven S. Graham, Erin M. Williams,
and Paul A. Reed

August 2011

ERDC/GSL TR-11-29
August 2011

Laboratory Characterization of Talley Brick

Hannah B. Beatty, Steven S. Graham, Erin M. Williams, and Paul A. Reed

Geotechnical and Structures Laboratory
U.S. Army Engineer Research and Development Center
3909 Halls Ferry Road
Vicksburg, MS 39180-6199

Final report

Prepared for Headquarters, U.S. Army Corps of Engineers
Washington, DC 20314-1000

Under Military Operations in Urban Terrain-Urban Lethal Technologies Army Technology Objective Materials Characterization

Abstract: Personnel of the Geotechnical and Structures Laboratory, U.S. Army Engineer Research and Development Center conducted a laboratory investigation to characterize the strength and constitutive property behavior of Talley brick. A total of 24 mechanical property tests were successfully completed, i.e., three hydrostatic compression tests, three unconfined compression (UC) tests, 12 triaxial compression (TXC) tests, two uniaxial strain (UX) tests, two uniaxial-strain-load/constant-volumetric-strain-load (UX/CV) tests, and two direct-pull (DP) tests. In addition to the mechanical property tests, nondestructive, pulse-velocity measurements were obtained from each specimen. The TXC tests exhibited a continuous increase in maximum principal stress difference with increasing confining stress. A compression failure surface was developed from the TXC test results at six levels of confining pressure and from the results of the UC tests. The results of the DP tests were used to determine the unconfined tensile strength of Talley brick. The Talley brick specimens displayed tensile strengths of less than 10% of the unconfined compressive strength. The UX/CV stress-path data intersect and then follow the failure surface developed from the TXC tests, as expected.

Contents

Figures and Tables iv

Preface vi

1 Introduction 1

Background 1

Purpose and scope 1

2 Laboratory Tests 2

Material description 2

Composition property tests 2

Ultrasonic pulse-velocity determinations 2

Mechanical property tests 4

Specimen preparation 5

Test devices 6

Test instrumentation 8

Test descriptions 9

Definition of stresses and strains 11

Results 12

3 Analysis of Test Results 13

Hydrostatic compression (HC) tests 13

Triaxial compression (TXC) tests 16

Direct-pull (DP) tests 29

Uniaxial strain (UX) tests 29

Strain path tests 32

4 Summary 36

Conclusions 36

References 37

Plates 1-23

Distribution List

Report Documentation Page

Figures and Tables

Figures

Figure 1. Typical test specimen setup. 6
Figure 2. 600-MPa pressure vessel details. 7
Figure 3. Spring arm lateral deformeter mounted on test specimen. 9
Figure 4. Pressure-volume responses from the HC tests. 13
Figure 5. Pressure-time histories from the HC tests. 14
Figure 6. Pressure-volume responses from selected TXC tests. 15
Figure 7. Pressure-volume responses from selected HC and TXC tests. 15
Figure 8. Stress-strain responses from UC tests. 16
Figure 9. Stress difference-volumetric strain during shear from UC tests. 17
Figure 10. Stress-strain responses from TXC tests at a confining pressure of 10 MPa. 17
Figure 11. Stress difference-volumetric strain during shear from TXC tests at a confining pressure of 10 MPa. 18
Figure 12. Stress-strain responses from TXC tests at a confining pressure of 35 MPa. 18
Figure 13. Stress difference-volumetric strain during shear from TXC tests at a confining pressure of 35 MPa. 19
Figure 14. Stress-strain responses from TXC tests at a confining pressure of 50 MPa. 19
Figure 15. Stress difference-volumetric strain during shear from TXC tests at a confining pressure of 50 MPa. 20
Figure 16. Stress-strain responses from TXC tests at a confining pressure of 100 MPa. 20
Figure 17. Stress difference-volumetric strain during shear from TXC tests at a confining pressure of 100 MPa. 21
Figure 18. Stress-strain responses from TXC tests at a confining pressure of 200 MPa. 21
Figure 19. Stress difference-volumetric strain during shear from TXC tests at a confining pressure of 200 MPa. 22
Figure 20. Stress-strain responses from TXC tests at a confining pressure of 300 MPa. 22
Figure 21. Stress difference-volumetric strain during shear from TXC tests at a confining pressure of 300 MPa. 23
Figure 22. Stress-strain responses from TXC tests at confining pressures from 10 to 300 MPa. 26
Figure 23. Stress difference-volumetric strain during shear from TXC tests at confining pressures from 10 to 300 MPa. 26
Figure 24. Radial strain-axial strain data during shear from TXC tests at confining pressures from 10 to 300 MPa. 27
Figure 25. Failure data from UC and TXC tests. 28
Figure 26. Failure data from UC and TXC tests and recommended failure surface. 28
Figure 27. Stress paths and failure data from DP tests. 29
Figure 28. Stress-strain responses from UX tests. 30

Figure 29. Pressure-volume data from UX tests. 30
Figure 30. Stress paths from UX tests and failure surface from TXC tests. 31
Figure 31. Comparison of pressure-volume data from HC and UX tests. 32
Figure 32. Stress-strain responses from UX/CV tests. 33
Figure 33. Pressure-volume data from UX/CV tests. 33
Figure 34. Stress paths from UX/CV tests and failure surface from TXC tests. 34
Figure 35. Strain paths from UX/CV tests. 34

Tables

Table 1. Physical and composition properties of Talley Brick. 3
Table 2. Completed Talley Brick test matrix. 5

Preface

This laboratory mechanical property investigation of Nammo Talley (Talley) brick was conducted by personnel at the U.S. Army Engineer Research and Development Center (ERDC). The study was conducted with funds provided by the Headquarters, U.S. Army Corps of Engineers, under the Military Operations in Urban Terrain-Urban Lethal Technologies Army Technology Objective Materials Characterization Work Package. This study was conducted during May and June 2008 by staff members of the Impact and Explosion Effects Branch (IEEB), Engineering Systems and Materials Division (ESMD), Geotechnical and Structures Laboratory (GSL), ERDC, under the general direction of Henry S. McDevitt, Jr., Chief, IEEB; Dr. Larry N. Lynch, Chief, ESMD; Dr. William P. Grogan, Deputy Director, GSL; and Dr. David W. Pittman, Director, GSL.

The Principal Investigator for this project was Rayment E. Moxley, IEEB. Steven S. Graham, IEEB, and Erin M. Williams, IEEB, served as co-investigators for this project. Graham processed the material property data, and Hannah B. Beatty, IEEB, prepared this report. Laboratory characterization tests were performed by Paul A. Reed, IEEB, under the technical direction of Williams. Instrumentation support was provided by Johnny L. Morrow, Computational Science and Engineering Division, Information Technology Laboratory, ERDC.

COL Kevin J. Wilson was Commander and Executive Director of ERDC. Dr. Jeffery P. Holland was Director.

1 Introduction

Background

Personnel of the Geotechnical and Structures Laboratory (GSL), U.S. Army Engineer Research and Development Center (ERDC), conducted a laboratory investigation to characterize the strength and constitutive property behavior of Talley brick, under the U.S. Army Corps of Engineers Military Operations in Urban Terrain-Urban Lethal Technologies Army Technology Objective Materials Characterization Work Package. A total of 24 mechanical property tests were successfully completed. The tests consisted of three hydrostatic compression (HC) tests, three unconfined compression (UC) tests, 12 triaxial compression (TXC) tests, two uniaxial strain (UX) tests, two uniaxial-strain-load/constant-volumetric-strain-load (UX/CV) tests, and two direct-pull (DP) extension tests. In addition to the mechanical property tests, nondestructive, pulse-velocity measurements were obtained from each specimen.

Purpose and scope

The purpose of this report is to document the results from the mechanical property tests conducted on the Talley brick specimens, along with the results of nondestructive, pulse-velocity measurements from each specimen. The physical and composition properties, test procedures, and test results are documented in Chapter 2. Comparative plots and analyses of the experimental results are presented in Chapter 3. A summary is provided in Chapter 4.

2 Laboratory Tests

Material description

The test specimens used in this investigation were prepared from samples cored from bricks provided by Talley. The brick used for the material property tests was also used to build triple-brick walls at Talley for penetration experiments. The material properties determined from the characterization of the material will be used to develop mathematical models of the brick's responses for use in numerical simulations of penetration tests.

Composition property tests

Prior to performing the mechanical property tests, the height, diameter, and weight of each test specimen were obtained. These measurements were used to compute the specimen's wet, bulk, or "as-tested" density. Results from these determinations are provided in Table 1. Measurements of posttest water content[1] were conducted in accordance with procedures given in American Society for Testing and Materials (ASTM) D 2216 (ASTM 2005d). Based on the appropriate values of posttest water content, wet density, and an assumed grain density of 2.89 Mg/m^3, values of dry density, porosity, degree of saturation, and volumes of air, water, and solids were calculated (Table 1). Also listed in Table 1 are maximum, minimum, and mean values, as well as the standard deviation about the mean for each quantity. The Talley brick specimens had a mean wet density of 1.872Mg/m^3, a mean water content of 0.25%, and a mean dry density of 1.867 Mg/m^3.

Ultrasonic pulse-velocity determinations

Prior to performing the mechanical property tests, ultrasonic pulse-velocity measurements were obtained from each test specimen. This involved measuring the transit distance and time for each P-wave (compressional) or S-wave (shear) pulse to propagate through a given specimen. The velocity was then computed by dividing the transit distance by the transit time. A matching pair of 1-MHz piezoelectric transducers was used to transmit and receive the ultrasonic P-waves, while a pair of 2.25-MHz piezoelectric

[1] Water content is defined as the weight of water removed during drying in a standard oven divided by the weight of dry solids multiplied by 100.

Table 1. Physical and composition properties of Talley Brick.

Test Number	Type of test	Plate No.	Wet Density Mg/m^3	Posttest Water Content, %	Dry Density, Mg/m^3	Porosity, %	Degree of Saturation, %	Volume of Air, %	Volume of Water, %	Volume of Solids, %	Axial P Wave Velocity, km/s	Radial P Wave Velocity, km/s	Axial S Wave Velocity, km/s	Radial S Wave Velocity, km/s
1	UC	5	1.860	0.14	1.857	35.75	0.73	35.49	0.26	64.25	2.57	2.64	1.78	1.64
2	UC	6	1.861	0.21	1.857	35.74	1.09	35.35	0.39	64.26	2.68	2.64	1.85	1.68
3	UC	7	1.890	0.39	1.883	34.84	2.11	34.11	0.73	65.16	2.88	2.87	1.94	1.94
4	HC	1	1.856	0.25	1.851	35.95	1.29	35.48	0.46	64.05	2.48	2.63	1.76	1.64
6	UX	20	1.884	0.70	1.870	35.28	3.71	33.97	1.31	64.72	2.89	2.86	1.97	1.81
7	UX	21	1.861	0.11	1.859	35.69	0.57	35.49	0.20	64.31	2.70	2.79	1.86	1.67
8	TXC/10	8	1.868	0.27	1.863	35.55	1.41	35.05	0.50	64.45	2.72	2.72	1.88	1.82
9	TXC/10	9	1.862	0.19	1.859	35.68	0.99	35.32	0.35	64.32	2.60	2.95	1.82	1.68
10	TXC/35	10	1.864	0.23	1.860	35.65	1.20	35.22	0.43	64.35	2.66	2.50	1.86	1.75
11	TXC/35	11	1.863	0.15	1.860	35.63	0.78	35.35	0.28	64.37	2.57	2.61	1.80	1.66
12	TXC/50	12	1.868	0.26	1.864	35.52	1.36	35.03	0.48	64.48	2.61	2.63	1.81	1.63
13	TXC/50	13	1.854	0.31	1.848	36.06	1.59	35.49	0.57	63.94	2.48	2.47	1.69	1.47
14	TXC/100	14	1.871	0.28	1.865	35.45	1.47	34.93	0.52	64.55	2.78	2.81	1.91	1.94
15	TXC/100	15	1.871	0.22	1.867	35.41	1.16	35.00	0.41	64.59	2.75	2.75	1.89	1.70
16	TXC/200	16	1.883	0.32	1.877	35.06	1.71	34.46	0.60	64.94	2.96	2.96	1.97	1.87
17	TXC/200	17	1.884	0.25	1.879	34.98	1.34	34.51	0.47	65.02	2.76	2.82	1.93	1.82
20	UX/CV/50	22	1.863	0.22	1.859	35.68	1.15	35.27	0.41	64.32	2.72	2.71	1.83	1.69
21	UX/CV/100	23	1.871	0.24	1.867	35.41	1.27	34.96	0.45	64.59	2.605	2.580	1.819	1.668
22	TXC/300	18	1.914	0.10	1.912	33.84	0.57	33.65	0.19	66.16	2.697	2.589	1.863	1.686
23	TXC/300	19	1.885	0.19	1.882	34.89	1.02	34.53	0.36	65.11	2.767	2.712	1.909	1.912
24	DP		1.865	0.24	1.860	35.63	1.25	35.18	0.45	64.37	2.663	2.612	1.853	1.645
26	DP		1.896	0.28	1.891	34.58	1.53	34.05	0.53	65.42	2.863	2.991	1.948	1.837
27	HC	2	1.874	0.32	1.868	35.37	1.69	34.77	0.60	64.63	2.723	2.823	1.842	1.708
28	HC	3	1.874	0.18	1.870	35.28	0.95	34.95	0.34	64.72	2.673	2.747	1.856	1.695
29	HC	4	1.858	0.29	1.852	35.90	1.50	35.36	0.54	64.10	2.521	2.570	1.801	1.676
N			25	25	25	25	25	25	25	25	25	25	25	25
Mean			1.872	0.25	1.867	35.39	1.34	34.92	0.47	64.61	2.69	2.72	1.86	1.73
Stdv			0.014	0.115	0.014	0.486	0.613	0.533	0.216	0.486	0.125	0.142	0.068	0.112
Max			1.914	0.70	1.912	36.06	3.71	35.49	1.31	66.16	2.96	2.99	1.97	1.94
Min			1.854	0.10	1.848	33.84	0.57	33.65	0.19	63.94	2.48	2.47	1.69	1.47

transducers was used to transmit and receive the ultrasonic S-waves. The transit time was measured with a 100-MHz digital oscilloscope, and the transit distance with a digital micrometer. All of the velocity determinations were made under atmospheric conditions, i.e., no prestress of any type was applied to the specimen. The tests were conducted in accordance with procedures given in ASTM C 597 (ASTM 2005c).

One compressional-wave and one shear-wave velocity were determined axially through each specimen. Six radial P-wave velocities were determined; two measurements were taken transverse to each other at elevations of 1/4, 1/2, and 3/4 of the specimen height. Two radial S-wave velocities were measured; these determinations were made at approximately 1/4 and 3/4 of the specimen height. The various P- and S-wave velocities determined for the test specimens are provided in Table 1. The radial-wave velocities listed in Table 1 are the average values.

Mechanical property tests

Twenty-four mechanical property tests were successfully performed on the Talley brick specimens to characterize the strength and constitutive properties of the material. All of the mechanical property tests were conducted quasi-statically with axial strain rates on the order of 10^{-4} to 10^{-5} per second and times to peak load on the order of 5 to 30 min. Mechanical property data were obtained under several stress and strain paths. Undrained compressibility data were obtained from three HC tests and the hydrostatic loading phases of the TXC tests. Shear and failure data were obtained from UC tests, unconsolidated, undrained TXC tests, and DP tests. One-dimensional compressibility data were obtained from undrained, UX, or $K_{0,}$ tests with lateral stress measurements. One type of undrained, strain path test was conducted during the test program. The strain path test specimens were initially loaded under uniaxial strain boundary conditions to a prescribed level of stress or strain. At the end of the UX loading, a constant axial-to-radial-strain ratio (ARSR) of -2.0 was applied. The ARSR = -2.0 path is a constant-volumetric-strain loading path, and these tests are referred to as UX/CV. The terms undrained and unconsolidated signify that no pore fluid (liquid or gas) was allowed to escape or drain from the membrane-enclosed specimens. The completed test matrix is presented in Table 2. Table 2 lists the test types, number of tests, test numbers for each test type, and the nominal, peak radial stress applied to specimens prior to shear loading, or during the HC, UX, or strain-path loading.

Table 2. Completed Talley Brick test matrix.

Type of test	No. of tests	Test nos.	Nominal peak radial stress, MPa
HC	4	4,27,28,29	380 (4), 400 (27,29)
TXC	3	1,2,3	0
	2	8,9	10
	2	10,11	35
	2	12,13	50
	2	14, 15	100
	2	16,17	200
	2	22,23	300
UX strain	2	6,7	510
UX/CV	1	20	50
	1	21	100
DP	2	24,26	0
Total no. of tests:	25		

Specimen preparation

The mechanical property test specimens were cut from solid Talley bricks using a diamond-bit core barrel, following the procedures provided in ASTM C 42 (ASTM 2005b). Once the test specimens were cut to the correct length, the ends were ground flat and parallel to each other and perpendicular to the sides of the core, in accordance with procedures in ASTM D 4543 (ASTM 2005e). The prepared test specimens had a mean diameter of 50 mm and a mean height of 113 mm.

Prior to testing, each specimen was placed between hardened steel top and base caps. With the exception of the UC and the DP test specimens, two 0.6-mm-thick membranes were placed around each specimen, and the exterior of the outer membrane was coated with a liquid synthetic rubber to inhibit deterioration caused by the confining fluid (Figure 1). The confining fluid used was a mixture of kerosene and hydraulic oil. Finally, the specimen, along with its top and base cap assembly, was placed on the instrumentation stand of the test apparatus, and the instrumentation setup was initiated.

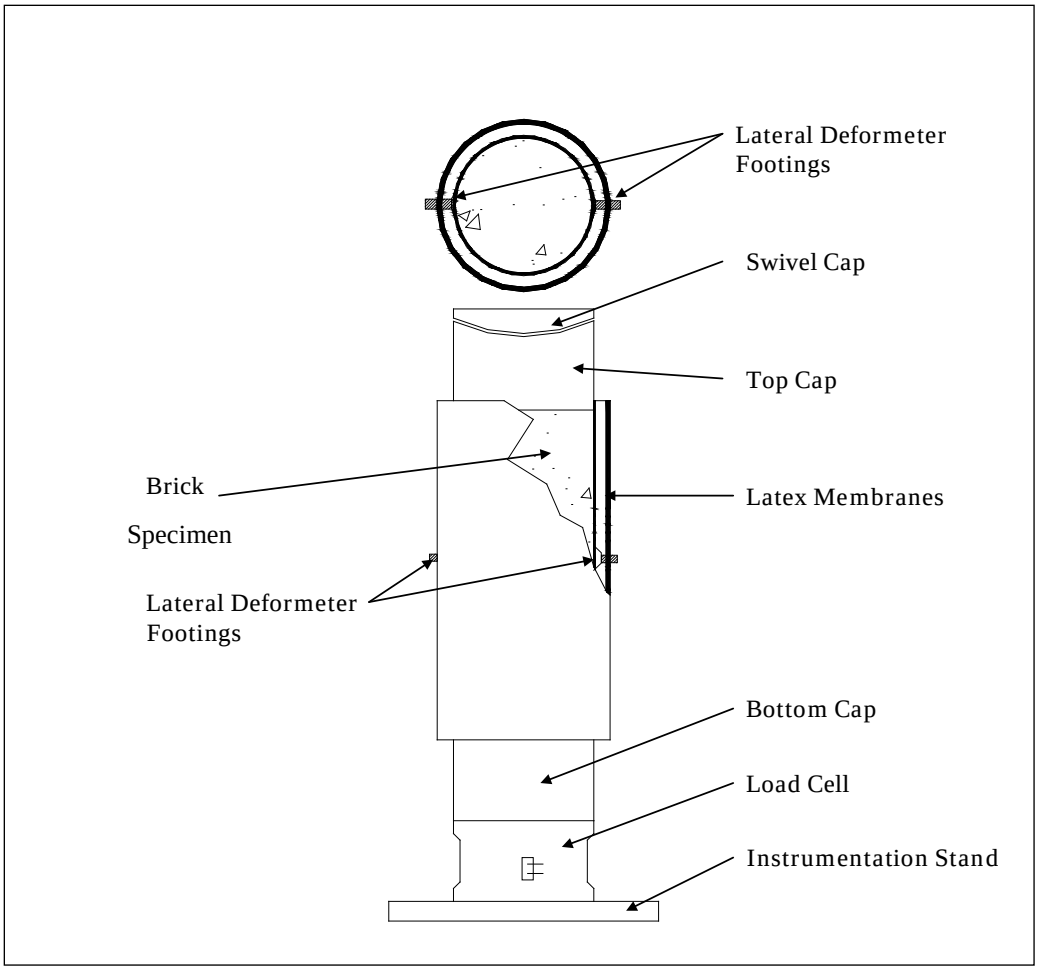

Figure 1. Typical test specimen setup.

Test devices

Three sets of test devices were used during this test program. The axial load for all of the UC tests was provided by a 3.3-MN (750,000-lb) loader. The application of load was manually controlled with this test device. No pressure vessel was required for the UC tests; only top and base caps, a load cell, and vertical and radial deformeters were necessary.

The DP tests were performed by using the DP apparatus in which end caps were attached to unconfined specimens with a high-modulus, high-strength epoxy. A manually-operated hydraulic pump was used to pressurize the DP chamber. When the chamber was pressurized, the piston retracted and produced tensile loading on the test specimens. Measurements of the loading of the specimen were recorded from the output of the load cell.

All of the remaining tests were conducted in a 600-MPa-capacity pressure vessel (Figure 2), and the axial load was provided by an 8.9-MN loader. With this loader, the application of load, pressure, and axial displacement were regulated by a servo-controlled data acquisition system. This servo-controlled system allowed the user to program rates of load, pressure, and axial displacement in order to achieve the desired stress or strain path. Confining pressure was measured externally to the pressure vessel by a pressure transducer mounted in the confining fluid line. A load cell mounted in the base of the specimen pedestal was used to measure the applied axial loads inside the pressure vessel (Figure 1).

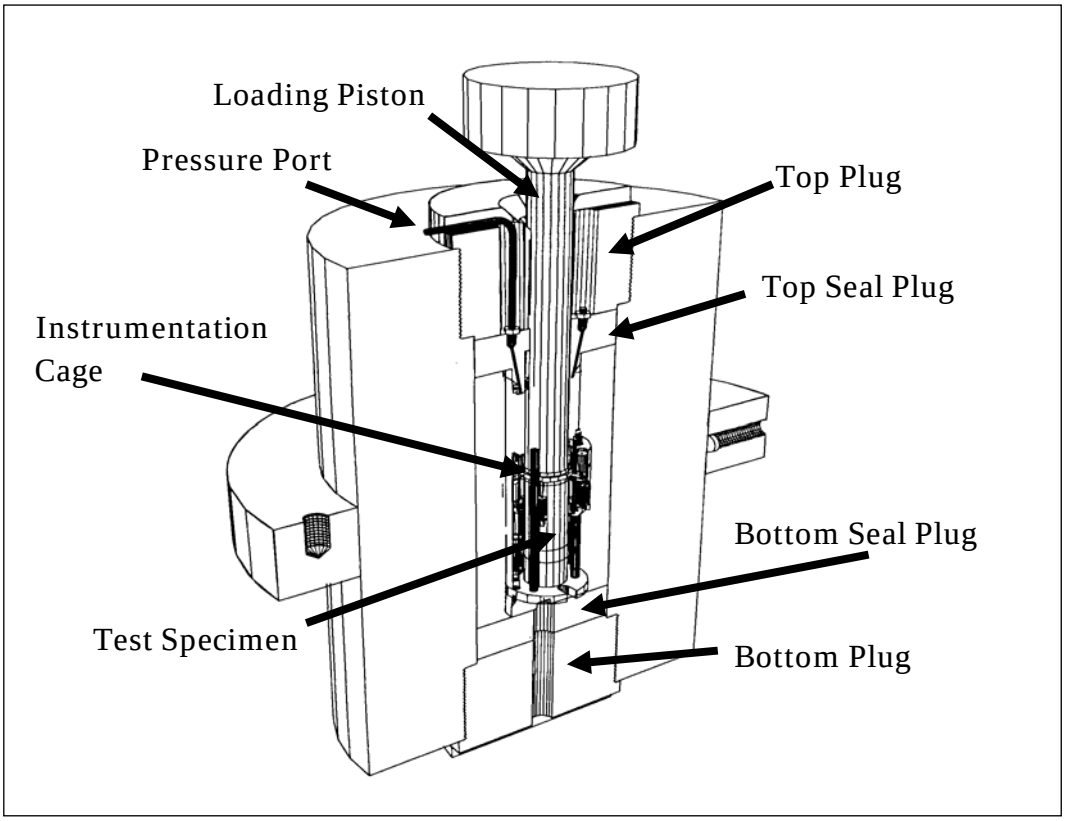

Figure 2. 600-MPa pressure vessel details.

Outputs from the various instrumentation sensors were electronically amplified and filtered, and the conditioned signals were recorded by computer-controlled, 16-bit, analog-to-digital converters. The data acquisition system was programmed to sample the data channels every 1 to 5 sec, convert the measured voltages to engineering units, and store the data for further processing.

Test instrumentation

The vertical deflection measurement system used for all tests, except for the DP tests, consisted of two linear variable differential transformers (LVDTs) mounted vertically on the instrumentation stand and positioned 180-deg apart. They were oriented to measure the displacement between the top and base caps, thus providing a measure of the axial deformation of the specimen. For the confined tests, a linear potentiometer was mounted externally to the pressure vessel to measure the displacement of the piston through which axial loads were applied. This provided a backup to the vertical LVDTs in the event they exceeded their calibrated range or malfunctioned.

Two types of radial deflection measurement systems (lateral deformeters) were used in this test program. The output of each deformeter was calibrated to the radial displacement of the two footings glued to the sides of the test specimen (Figure 1). These two small, steel footings were placed 180-deg apart at the specimen's mid-height and were glued directly to the specimen. The footing faces were machined to match the curvature of the test specimen. A threaded post extended from each footing and protruded through the membranes. Once the membranes were in place, steel caps were screwed onto the threaded posts to seal the membranes to each footing. The lateral deformeter ring was then attached to these steel caps with set screws. The completed specimen lateral deformeter setup is shown in Figure 3.

One of the two types of lateral deformeters used consisted of an LVDT mounted on a hinged ring; the LVDT measured the expansion or contraction of the ring. This lateral deformeter was used over smaller ranges of radial deformation, when the greatest measurement accuracy was required. This lateral deformeter was used for all of the HC, UC, UX, and strain-path tests. This design is similar to the radial deformeter design provided by Bishop and Henkel (1962). When the specimen expanded (or contracted), the hinged-deformeter ring opened (or closed), causing a change in the electrical output of the horizontally mounted LVDT.

The second type of lateral deformeter, used for all of the TXC tests, consisted of two strain-gaged spring-steel arms mounted on a double-hinged ring; the strain-gaged arms deflected as the ring expanded or contracted. When the specimen expanded or contracted laterally, the rigid deformeter ring flexed about its hinge, causing a change in the electrical

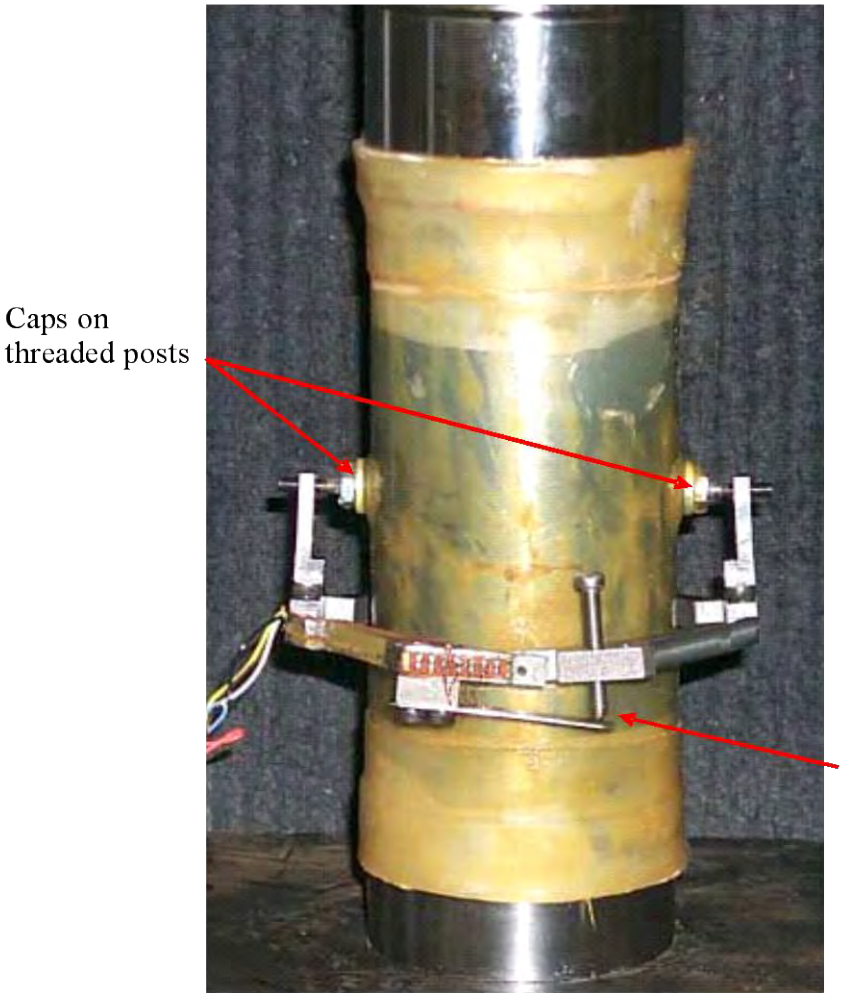

Figure 3. Spring arm lateral deformeter mounted on test specimen.

output of the strain-gaged arm. This deformeter was used when the greatest radial deformation range was required and was slightly less accurate than the LVDT-type deformeter. The output of the strain gages was calibrated to measure the specimen's lateral deformation. Radial strain measurements were not recorded during the DP tests.

Test descriptions

The TXC tests were conducted in two phases. During the initial or hydrostatic-compression phase, the cylindrical test specimen was subjected to an increase in hydrostatic pressure, while measurements of the specimen's height and diameter changes were recorded. The data from this phase are

typically plotted as pressure versus volumetric strain, the slope of which, assuming elastic theory, is the bulk modulus, *K*. The second phase of the TXC test, the shear-loading phase, was conducted after the desired confining pressure was reached during the HC phase. While holding the desired confining pressure constant, axial load was increased, and measurements of the changes in the specimen's height and diameter were made. The axial (compressive) load was increased until the specimen failed. The shear data are generally plotted as principal stress difference versus axial strain, the slope of which represents Young's modulus, *E*. The maximum principal stress difference that a given specimen can support, or the principal stress difference at 15% axial strain during shear (whichever occurs first) is defined as the peak strength of the material.

The UC tests were performed in accordance with ASTM C 39 (ASTM 2005a). The UC test is a type of TXC test in which no confining pressure is applied. The maximum principal stress difference observed during a UC test is defined as the unconfined, compressive strength of the material.

Extension shear data for the brick were obtained by performing DP tests. Similar to the UC tests, no confining pressure was applied during the DP tests. To conduct the DP tests, end caps were attached to the specimen with epoxy. The end caps were screwed into the DP apparatus, and the specimen was pulled apart vertically when pressure was applied to the piston. Extension shear data for the material is generally plotted as principal stress difference versus mean normal stress.

The UX tests were conducted by applying axial load and confining pressure simultaneously, so that as the cylindrical specimen shortened, its diameter remained unchanged; i.e., zero radial strain boundary conditions were maintained. The data are generally plotted as axial stress versus axial strain, the slope of which is the constrained modulus, *M*. The data are also plotted as principal stress difference versus mean normal stress, the slope of which is twice the shear modulus, G, divided by the bulk modulus, *K*, i.e., *2G/K*, or, in terms of Poisson's ratio ν, $3(1-2\nu)/(1+\nu)$.

The strain-path tests in this program were conducted in two phases. Initially, the specimen was subjected to uniaxial-strain loading up to a desired level of mean normal, radial, or axial stress. At the end of the UX loading, a constant axial-to-radial-strain ratio of -2.0 was applied; these tests were

identified earlier as UX/CV tests. In order to conduct these tests, the software controlling the servo-controls had to correct the measured inputs for system compressibility and for the nonlinear calibrations of specific transducers.

Definition of stresses and strains

During the mechanical property tests, measurements were typically made of the axial and radial deformations of the specimen as confining pressure and/or axial load was applied or removed. These measurements along with the pretest measurements of the height and diameter of the specimen were used to convert the measured test data to true stresses and engineering strains.[1]

Axial strain, ϵ_a, was computed by dividing the measured axial deformation, Δh (change in height), by the original height, h_o, i.e., $\epsilon_a = \Delta h / h_o$. Similarly, radial strain, ϵ_r, was computed by dividing the measured radial deformation, Δd (change in diameter), by the original diameter, d_o, i.e., $\epsilon_r = \Delta d / d_o$. For this report, volumetric strain, ϵ_v, was assumed to be the sum of the axial strain and twice the radial strain, i.e., $\epsilon_v = \epsilon_a + 2\epsilon_r$.

The principal stress difference, q, was calculated by dividing the axial load by the cross-sectional area of the specimen, A, which is equal to the original cross-sectional area, A_o, multiplied by $(1 - \varepsilon_r)^2$. In equation form,

$$q = (\sigma_a - \sigma_r) = \frac{\text{Axial Load}}{A_o (1 - \varepsilon_r)^2} \tag{1}$$

where σ_a is the axial stress, and σ_r is the radial stress. The axial stress is related to the confining pressure and the principal stress difference by

$$\sigma_a = q + \sigma_r \tag{2}$$

The mean normal stress, p, is the average of the applied principal stresses. In cylindrical geometry,

$$p = \frac{(\sigma_a + 2\sigma_r)}{3} \tag{3}$$

[1] Compressive stresses and strains are positive in this report.

Results

Results from all the mechanical property tests, except the DP tests, are presented in Plates 1-23. One data plate is presented for each test with reliable results. Results from the HC tests are presented in the plates in four plots, i.e., (a) mean normal stress versus volumetric strain, (b) mean normal stress versus axial strain, (c) radial versus axial strain, and (d) mean normal stress versus radial strain. Each plate for the UC, TXC, UX, and strain-path tests also displays four plots, i.e., (a) principal stress difference versus mean normal stress, (b) principal stress difference versus axial strain, (c) volumetric strain versus mean normal stress, and (d) volumetric strain versus axial strain.

3 Analysis of Test Results

Hydrostatic compression (HC) tests

Undrained, bulk compressibility data were obtained from four HC tests and from the hydrostatic loading phases of the 12 TXC tests. The pressure-volumetric data from the four HC tests are plotted in Figure 4. The initial dry densities of HC test specimens 4, 27, 28, and 29 were 1.851, 1.868, 1.870, and 1.852 Mg/m^3, respectively. The specimens for tests numbers 27 and 28 have essentially the same initial dry densities (~1.869 mg/m^3) but exhibit very different compressibilities. The specimens for tests numbers 4 and 29 also have essentially the same initial dry density (~1.852 mg/m^3) and also exhibit very different compressibilities. These pairs of test specimens also have very similar P- and S-wave velocities with the denser specimens having slightly higher values than the less dense specimens. However, the effects of these velocities are normally at very low stress levels and should not affect the data as plotted in Figure 4. Variations in compressibility for a given material are not unusual and are normally attributed to variations in initial dry density. These data exhibit variations that cannot be explained at this time. Figure 5 presents the pressure-time histories for

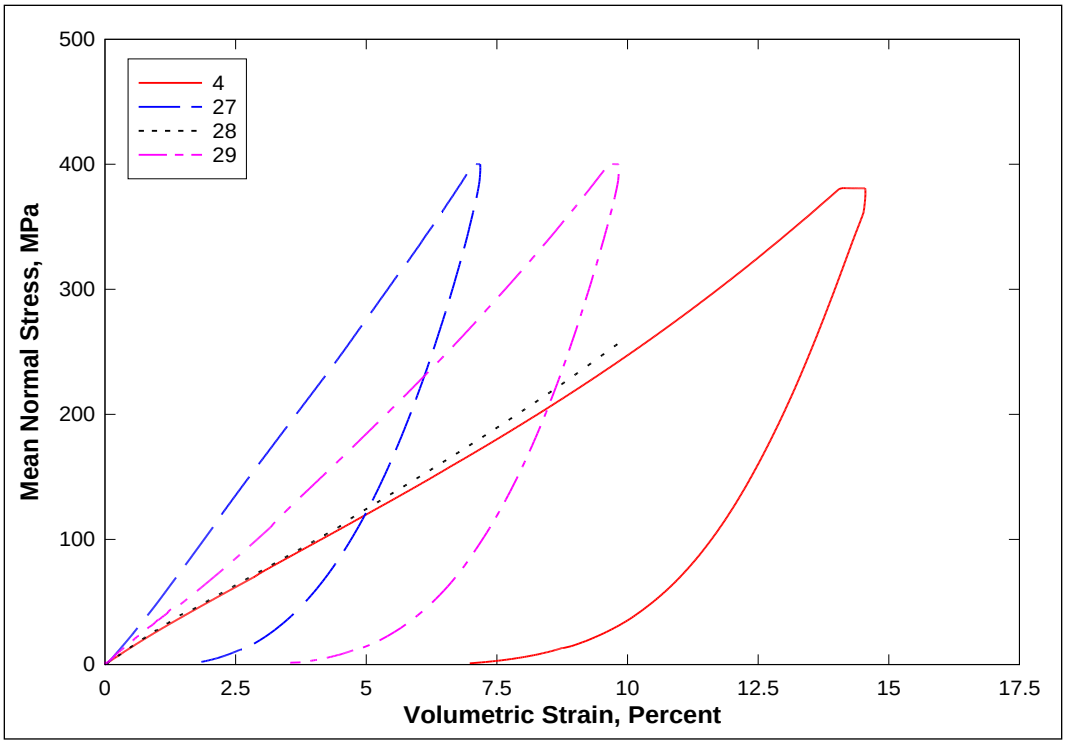

Figure 4. Pressure-volume responses from the HC tests.

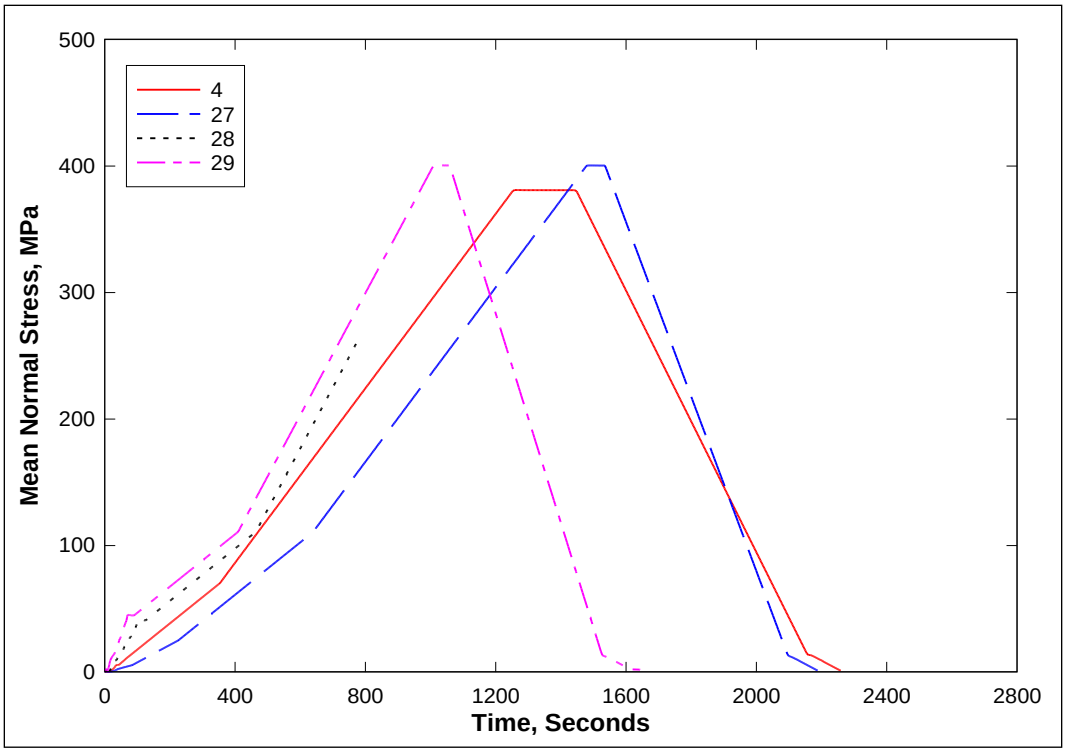

Figure 5. Pressure-time histories from the HC tests.

the HC tests. Once each HC test reached the maximum prescribed pressure, the pressure was intentionally held constant for a period of time. During the pressure hold, the volumetric strains continued to increase, indicating that Talley brick is susceptible to creep (Figures 4 and 5). The pressure for test specimen 4 was held at 380 MPa for 184 sec, during which time a volumetric strain of 0.44% occurred. For test specimen 27, the pressure was held at 400 MPa for 54 sec, during which time a volumetric strain of 0.13% occurred. The pressure for test specimen 29 was also held at 400 MPa for 48 sec, during which time a volumetric strain of 0.17% occurred. Test 28 was stopped after a lateral deformeter malfunction at a mean normal stress of 260 MPa and a volumetric strain of 9.9%.

Pressure-volumetric data were also obtained during the hydrostatic loading phases of the TXC tests (Figure 6). These compressibility variations exhibit the same unexplained differences discussed previously for the HC test data. Pressure-volumetric data from selected TXC tests and the HC data from Figure 4 are plotted in Figure 7. Based on the data from the HC tests, values for the initial bulk modulus (K) of Talley brick ranged from 2.7 to 4.6 GPa. The variations in the initial bulk modulus can be attributed to the differences in the initial dry densities and the ultrasonic pulse-velocities of the HC specimens.

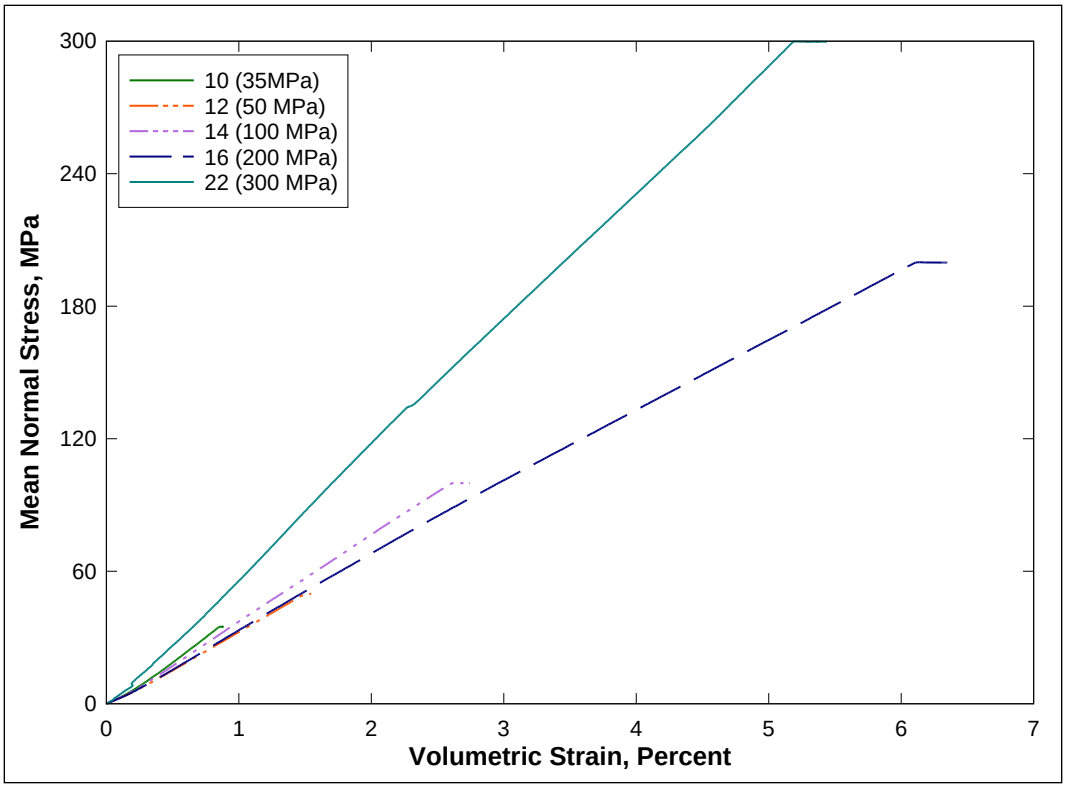

Figure 6. Pressure-volume responses from selected TXC tests.

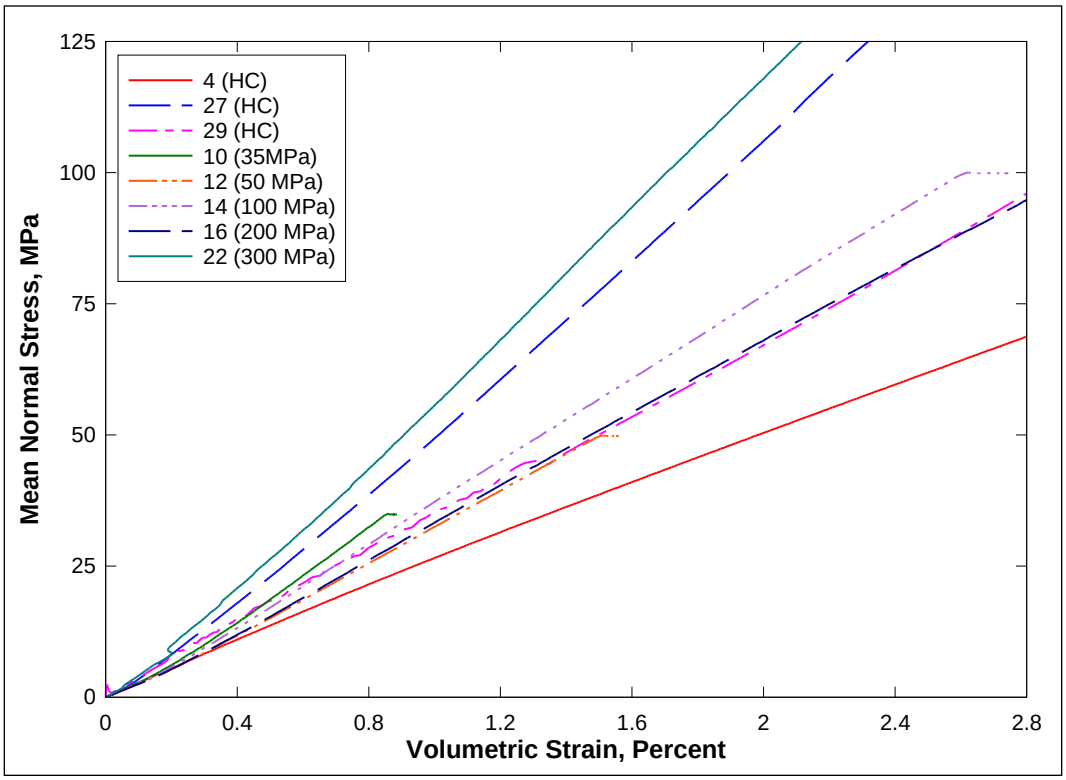

Figure 7. Pressure-volume responses from selected HC and TXC tests.

Triaxial compression (TXC) tests

Shear and failure data were successfully obtained from three unconfined compression tests and 12 unconsolidated, undrained TXC tests. Recall from Chapter 2 that the second phase of the TXC test, the shear-loading phase, was conducted after the desired confining pressure was applied during the HC phase. The UC tests are a special type of TXC test without the application of confining pressure. Results from the UC tests are plotted in Figures 8 and 9, and results from the TXC tests are plotted in Figures 10 through 21. In all figures, the axial and volumetric strains were set to zero at the start of the shear phase; i.e., only the strains during shear are plotted.

Stress-strain data from the three UC tests in Figures 8 and 9 are plotted as principal stress difference versus axial strain during shear and as principal stress difference versus volumetric strain during shear. Deformeters instead of strain gages were used to measure the axial and radial strains of the UC test specimens. During the UC tests, no attempt was made to capture the post-peak (or softening) stress-strain behavior of this material. The mean unconfined compressive strength of Talley brick determined from the three UC tests was 47.5 MPa. The dry densities of the specimens ranged from 1.857 Mg/m^3 to 1.883 Mg/m^3. The results of these three tests indicate increasing strength with increasing initial dry density.

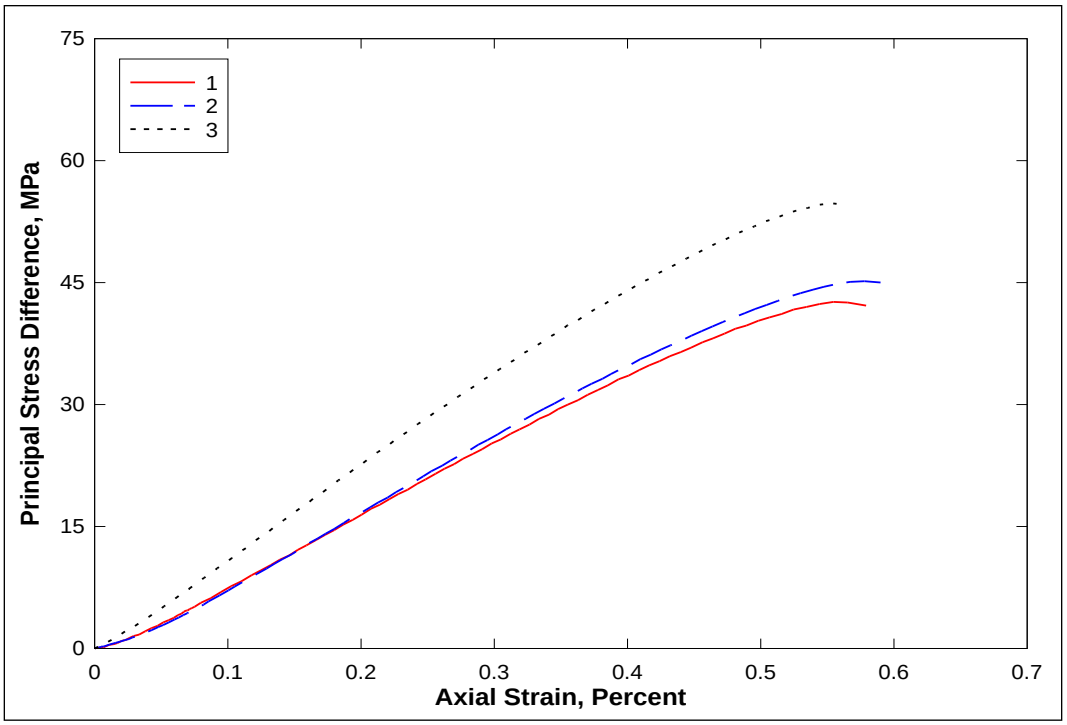

Figure 8. Stress-strain responses from UC tests.

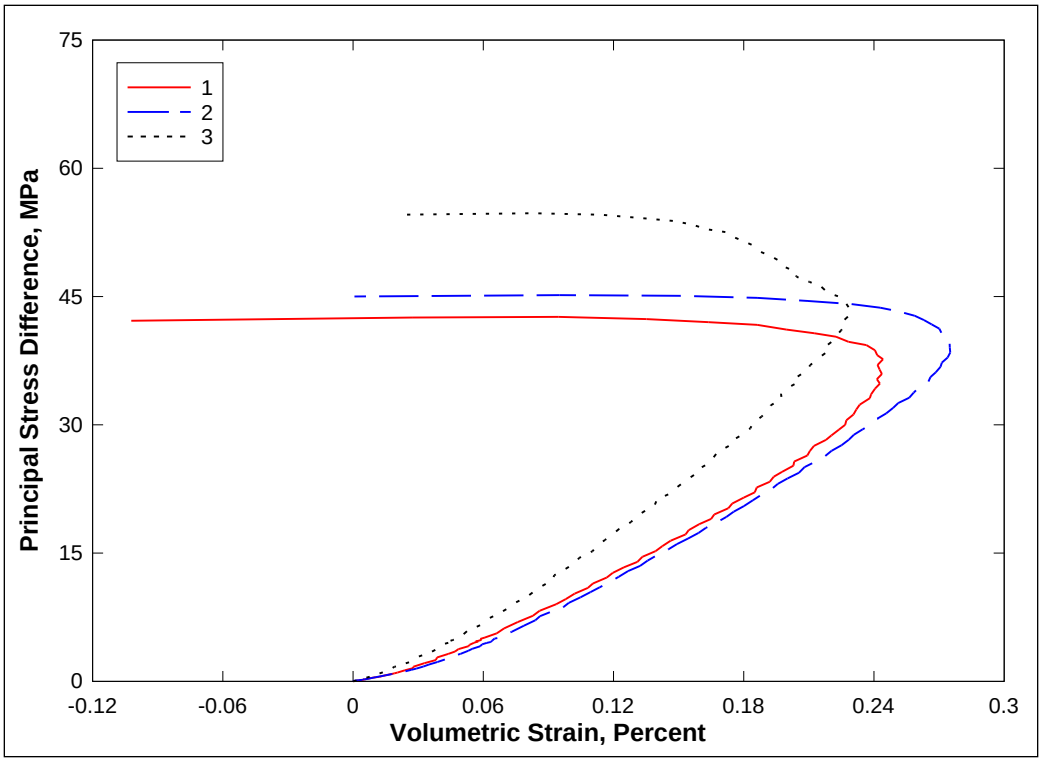

Figure 9. Stress difference-volumetric strain during shear from UC tests.

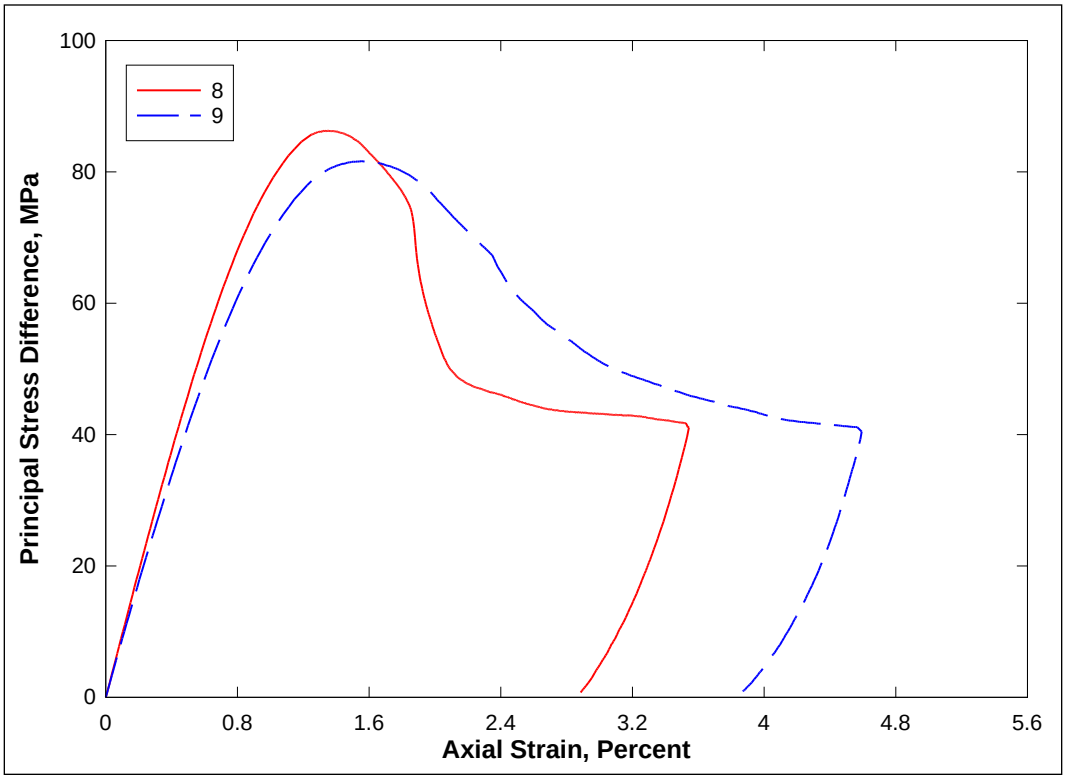

Figure 10. Stress-strain responses from TXC tests at a confining pressure of 10 MPa.

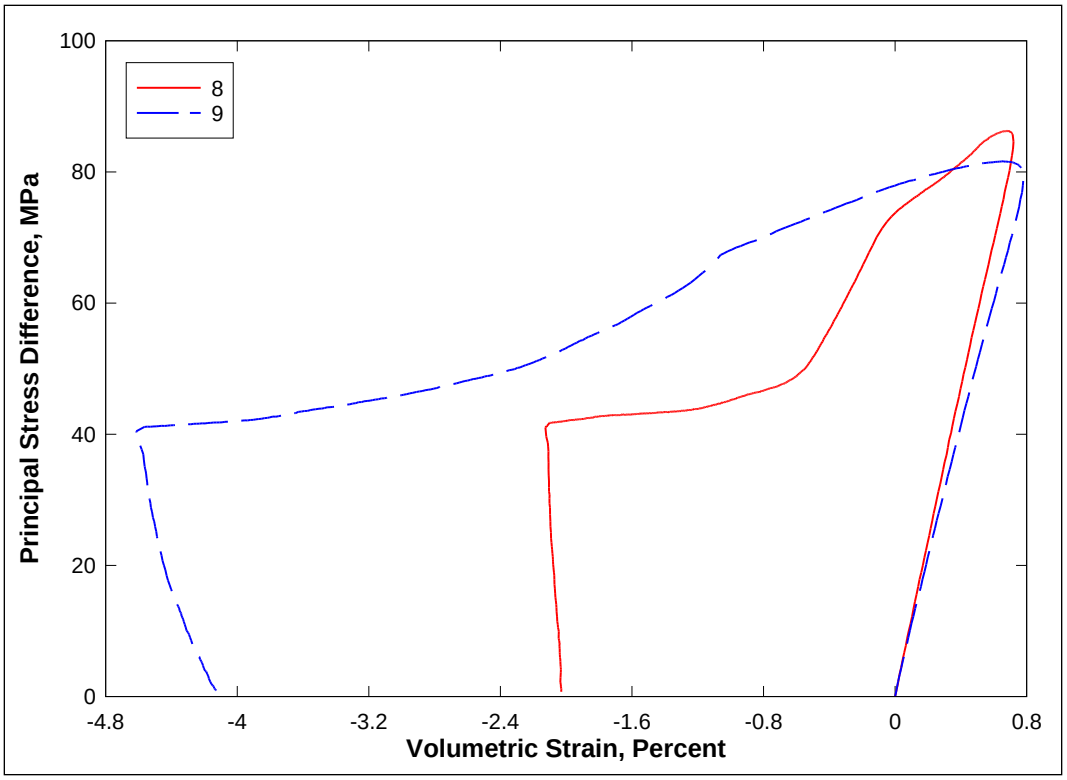

Figure 11. Stress difference-volumetric strain during shear from TXC tests at a confining pressure of 10 MPa.

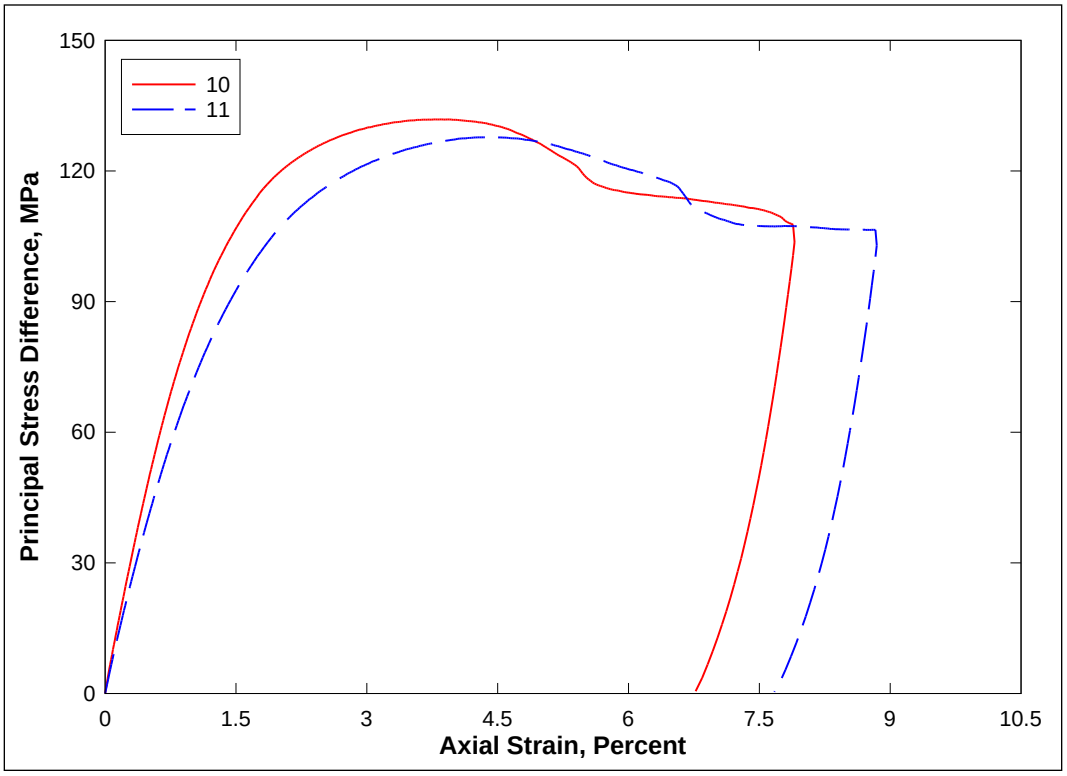

Figure 12. Stress-strain responses from TXC tests at a confining pressure of 35 MPa.

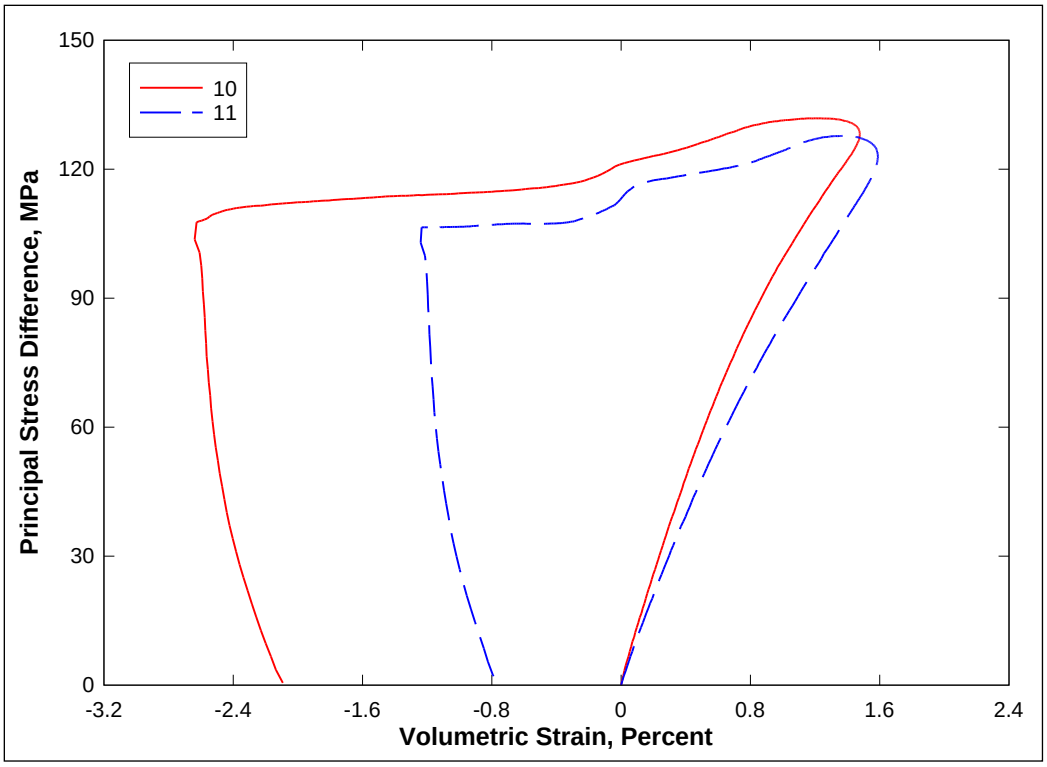

Figure 13. Stress difference-volumetric strain during shear from TXC tests at a confining pressure of 35 MPa.

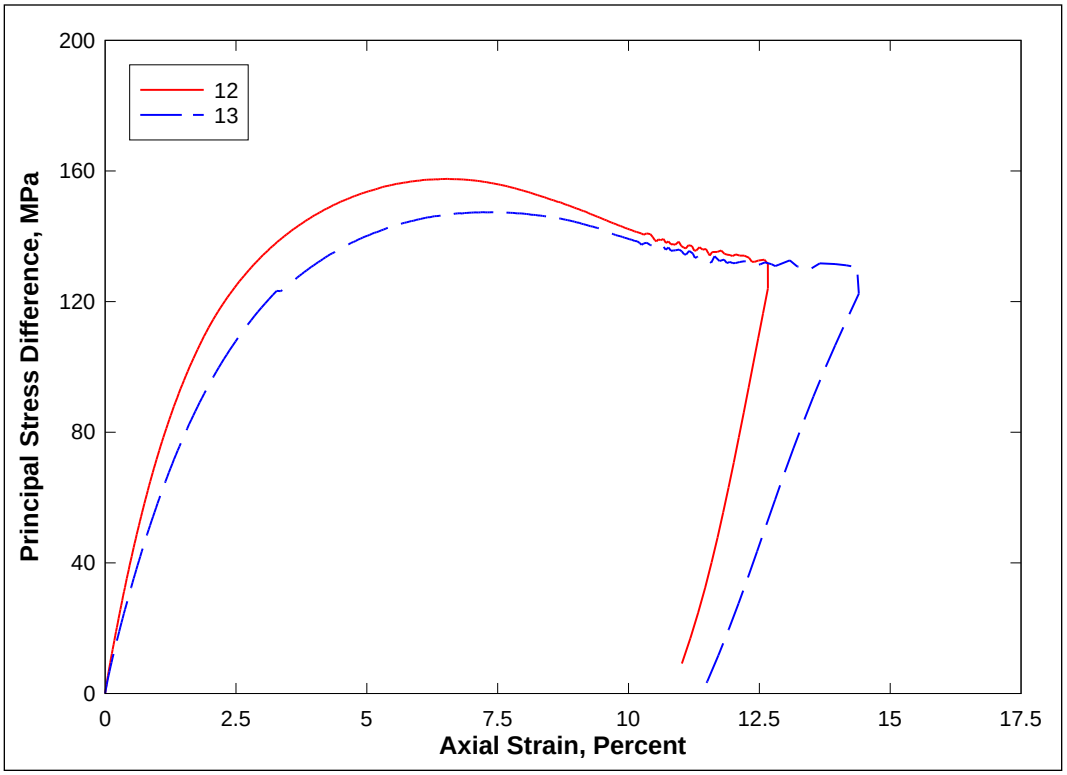

Figure 14. Stress-strain responses from TXC tests at a confining pressure of 50 MPa.

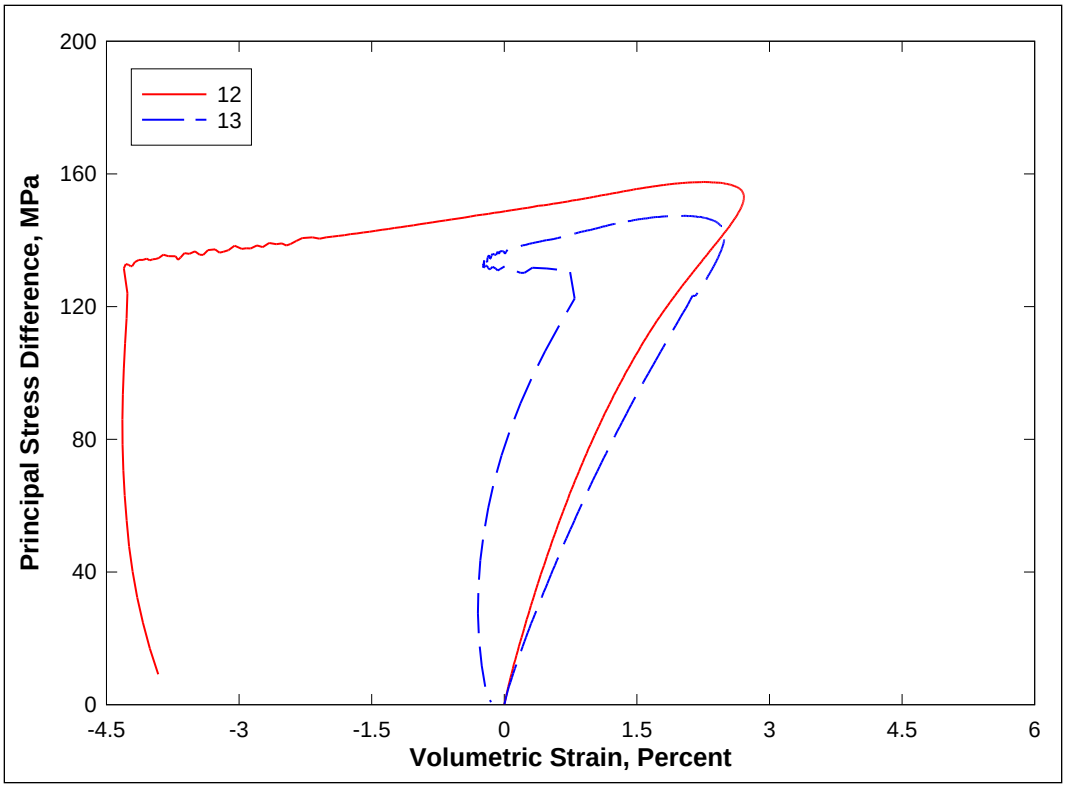

Figure 15. Stress difference-volumetric strain during shear from TXC tests at a confining pressure of 50 MPa.

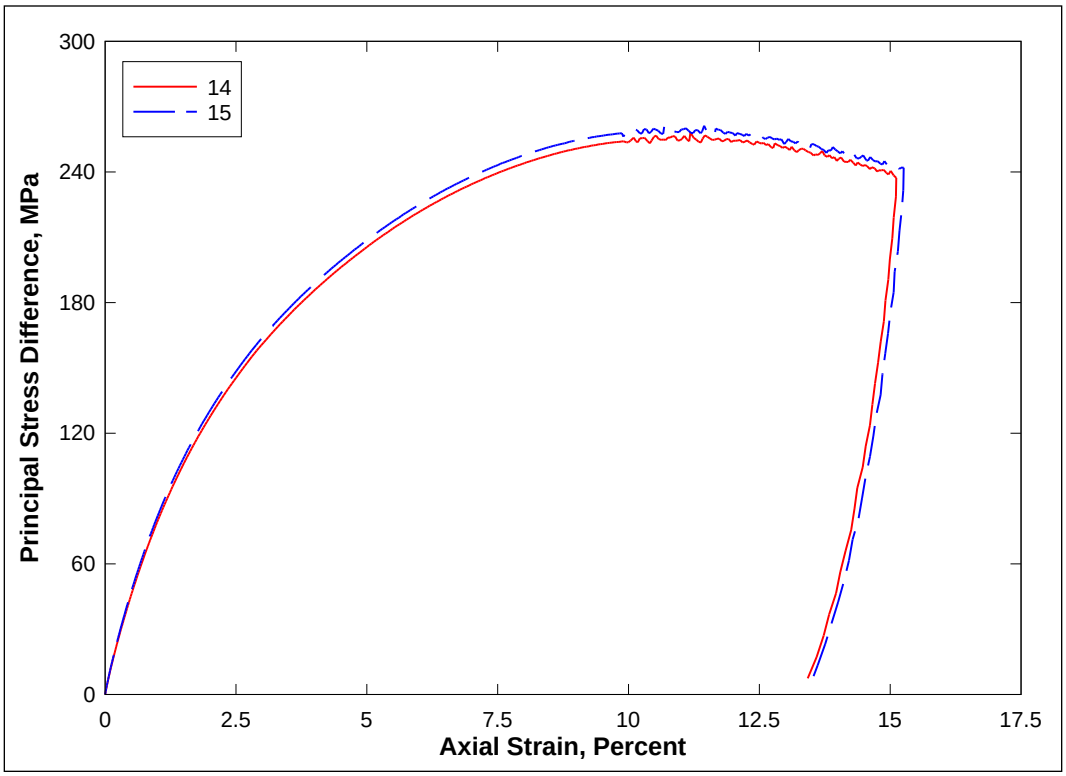

Figure 16. Stress-strain responses from TXC tests at a confining pressure of 100 MPa.

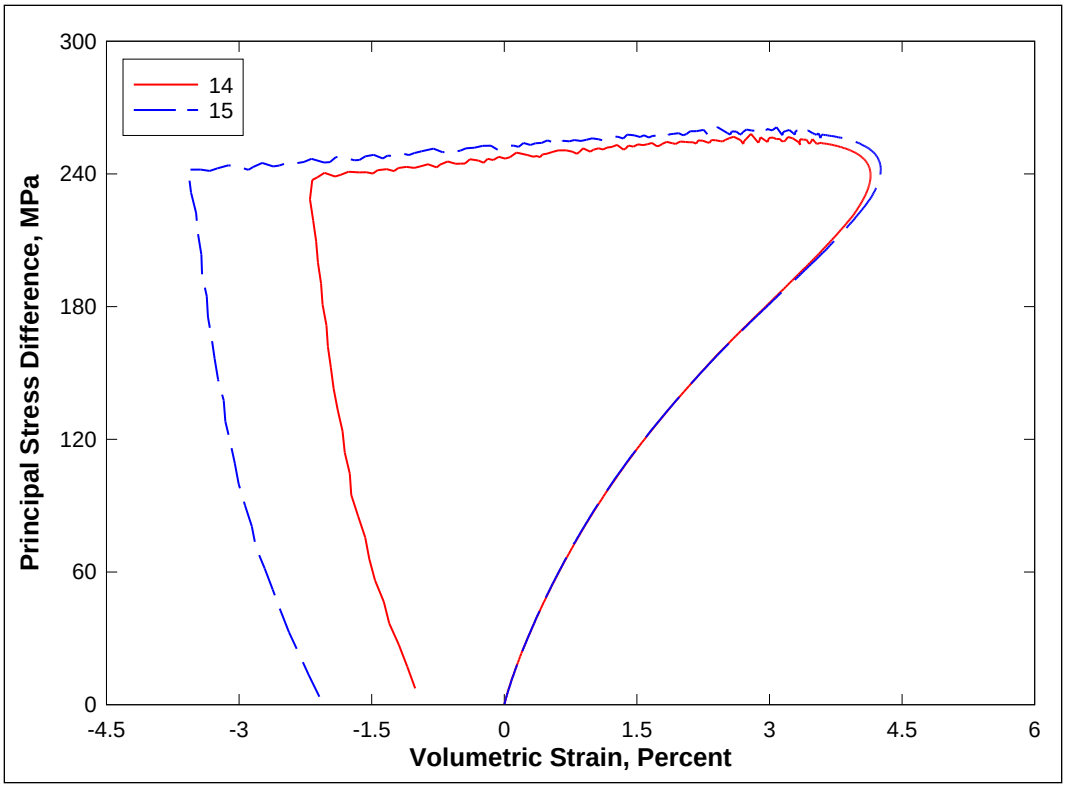

Figure 17. Stress difference-volumetric strain during shear from TXC tests at a confining pressure of 100 MPa.

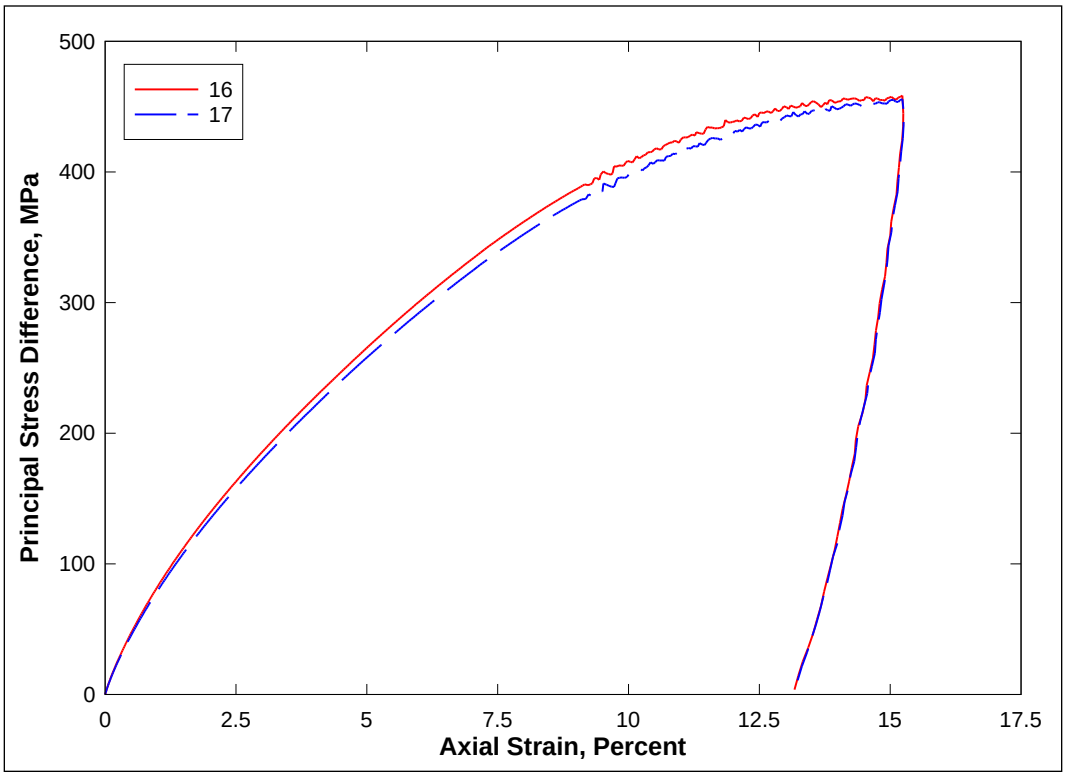

Figure 18. Stress-strain responses from TXC tests at a confining pressure of 200 MPa.

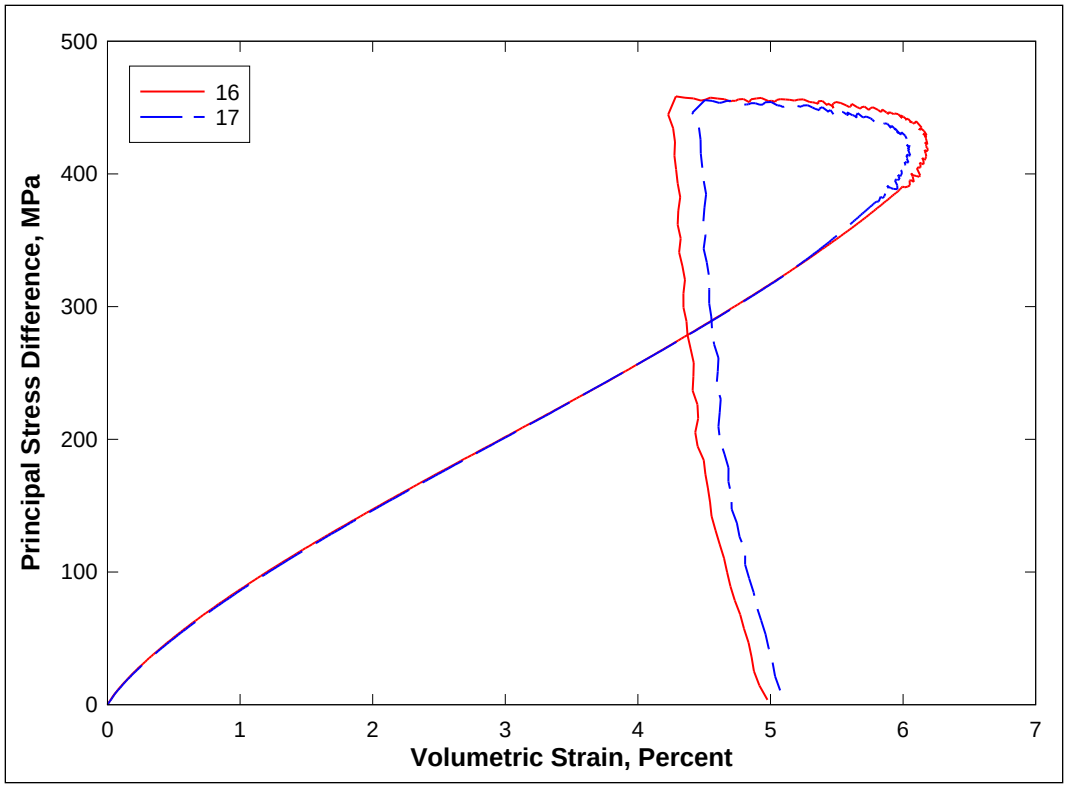

Figure 19. Stress difference-volumetric strain during shear from TXC tests at a confining pressure of 200 MPa.

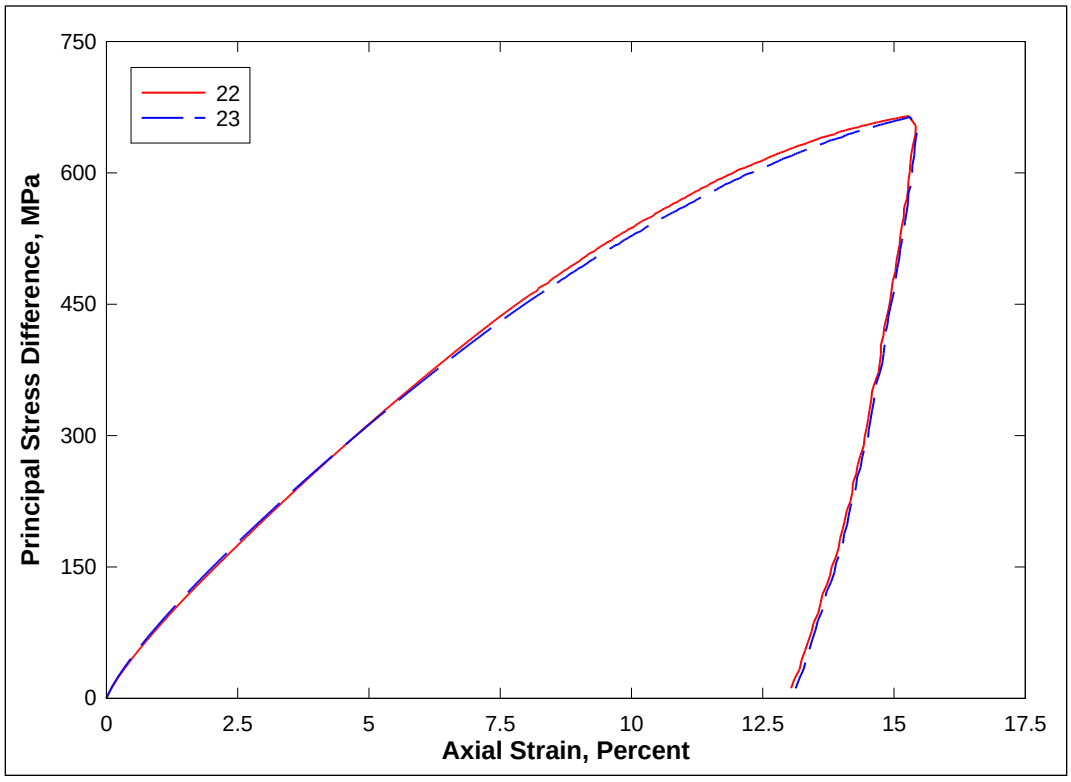

Figure 20. Stress-strain responses from TXC tests at a confining pressure of 300 MPa.

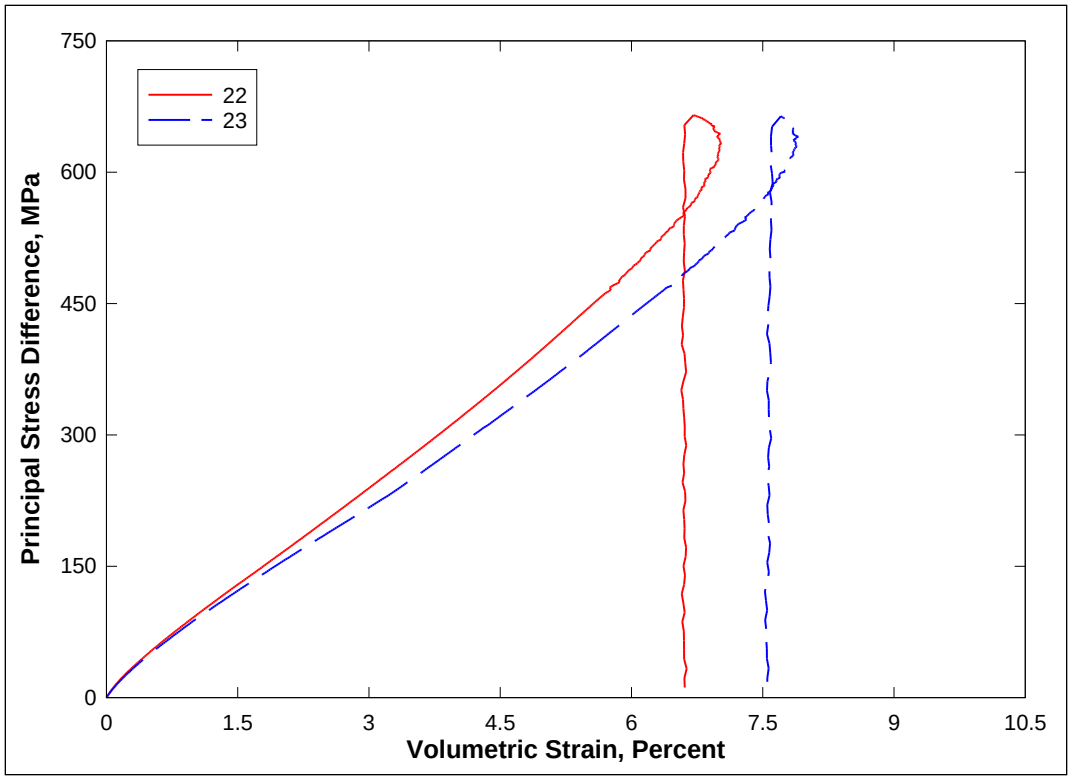

Figure 21. Stress difference-volumetric strain during shear from TXC tests at a confining pressure of 300 MPa.

Figures 10 through 21 present the results from the TXC tests conducted at nominal confining pressures of 10, 35, 50, 100, 200, and 300 MPa. The TXC test results are plotted as principal stress difference versus axial strain during shear and as principal stress difference versus volumetric strain during shear. The results are very good, considering the inherent variations in the initial wet and dry densities and water contents of the specimens. The wet densities of the TXC specimens ranged from 1.854 to 1.914 Mg/m^3, the dry densities ranged from 1.848 to 1.912 Mg/m^3, and the water contents ranged from 0.10% to 0.32%.

Results of TXC tests conducted at a constant confining pressure of 10 MPa are shown in Figures 10 and 11. The initial wet densities of specimens 8 and 9 were 1.868 and 1.862 Mg/m^3, respectively. The initial dry densities of specimens 8 and 9 were 1.863 and 1.859 Mg/m^3, respectively. This difference in initial dry density explains the higher peak principal stress difference reached by specimen 8 (Figure 10). Figure 10 displays post-peak softening in both specimens. The volumetric responses of test specimens 8 and 9 display compressive volumetric strains prior to dilating (Figure 11).

Results of TXC tests conducted at a constant confining pressure of 35 MPa are shown in Figures 12 and 13. The initial dry densities for specimens 10 and 11 were identical with a value of 1.860 Mg/m^3. As with the TXC tests conducted at 10 MPa, the data in Figure 12 display post-peak softening. The volumetric response data in Figure 13 indicate that at 35 MPa confining pressure, both specimens initially experienced compressive volumetric strain before dilating.

Results of TXC tests conducted at a constant confining pressure of 50 MPa are shown in Figures 14 and 15. The initial dry densities for specimens 12 and 13 were 1.864 and 1.848 Mg/m^3, respectively. Figure 14 displays post-peak softening in both specimens. The volumetric responses in Figure 15 indicate that the specimens compacted until just prior to the peak principal stress difference, and then the specimens dilated. The denser test specimen (specimen 12) exhibited a higher strength and a smaller strain at failure.

Results of TXC tests conducted at a constant confining pressure of 100 MPa are shown in Figures 16 and 17. The initial dry densities for specimens 14 and 15 were 1.865 and 1.867 Mg/m^3, respectively. Both specimens exhibited post-peak softening and only a minor difference in peak principal stress difference (Figure 16). The reader should note the decrease in variations in the stress-strain data with increasing pressure even with the slightly-varying dry densities of the test specimens. The UC tests are very sensitive to small differences in dry density and specimen structure (Figures 8 and 9), which result in variations in the initial loading data and peak strength values. The variations are less pronounced as the confining pressure increases. This is a result of the confining pressure reducing the differences in the initial properties of the test specimens. The volumetric response data in Figure 17 indicate that at 100-MPa confining pressure, the test specimens experienced initial compressive volumetric strain followed by dilation.

Test results for TXC tests conducted at a constant confining pressure of 200 MPa are shown in Figures 18 and 19. The initial dry densities for specimens 16 and 17 were 1.877 and 1.879 Mg/m^3, respectively, and exhibited very little difference in peak strength (Figure 18). The volumetric response data in Figure 19 depict initial compaction at the start of shear. The specimens begin dilating prior to reaching the peak principal stress difference and average 1.7% dilation after reaching the peak compressive volumetric strain of approximately 6%.

Test results for TXC tests conducted at a constant confining pressure of 300 MPa are shown in Figures 20 and 21. The initial dry densities for specimens 22 and 23 were 1.912 and 1.882 Mg/m^3, respectively. In spite of the difference in initial specimen density, the data exhibited very little difference in peak strength (Figure 20). The volumetric response data in Figure 21 exhibit initial compaction at the start of shear. The specimens display an average of 7.5% compressive volumetric strain, and then begin dilating just prior to reaching the peak principal stress difference.

Upon completion of the TXC tests, it was determined that none of the specimens reached full saturation during the shear loading, since the stress-strain data continued to exhibit increases in principal stress difference over the entire range of applied confining stresses.

For comparison purposes, stress-strain data from selected TXC tests are plotted in Figure 22 as principal stress difference versus axial strain during shear. In this figure, the results of all tests conducted at and below 100 MPa confining pressure display post-peak softening, while the tests at 200 MPa confining pressure and above exhibit a monatomic increase in stress difference up to the peak strength of the specimen at 15% axial strain. The post-peak softening is a result of the frictional strength along the failure plane, developed after brittle failure of the test specimen.

Stress-strain data from the selected TXC tests in Figure 22 are plotted in Figure 23 as principal stress difference versus volumetric strain during shear. The initial stress-strain loadings of the TXC tests are a function of the material's volume changes during shear, and thus are dependent on the magnitude of the applied confining pressure and the position on the material's pressure-volume response curve. In Figure 23, the compressive volumetric strain during shear loading increased with each increase in confining pressure. The increases in volumetric strain with increasing confining pressure are due to the material's nearly linear pressure-volume relation at high confining stresses (Figure 4). Figure 23 also shows that all the test specimens initially compacted during the shear loading then began to dilate just prior to achieving peak strength.

Results from TXC tests conducted at confining pressures from 10 to 300 MPa are plotted in Figure 24 as radial strain versus axial strain during shear. A contour of zero volumetric strain during shear is also shown in this figure. When the instantaneous slope of a curve is shallower than the

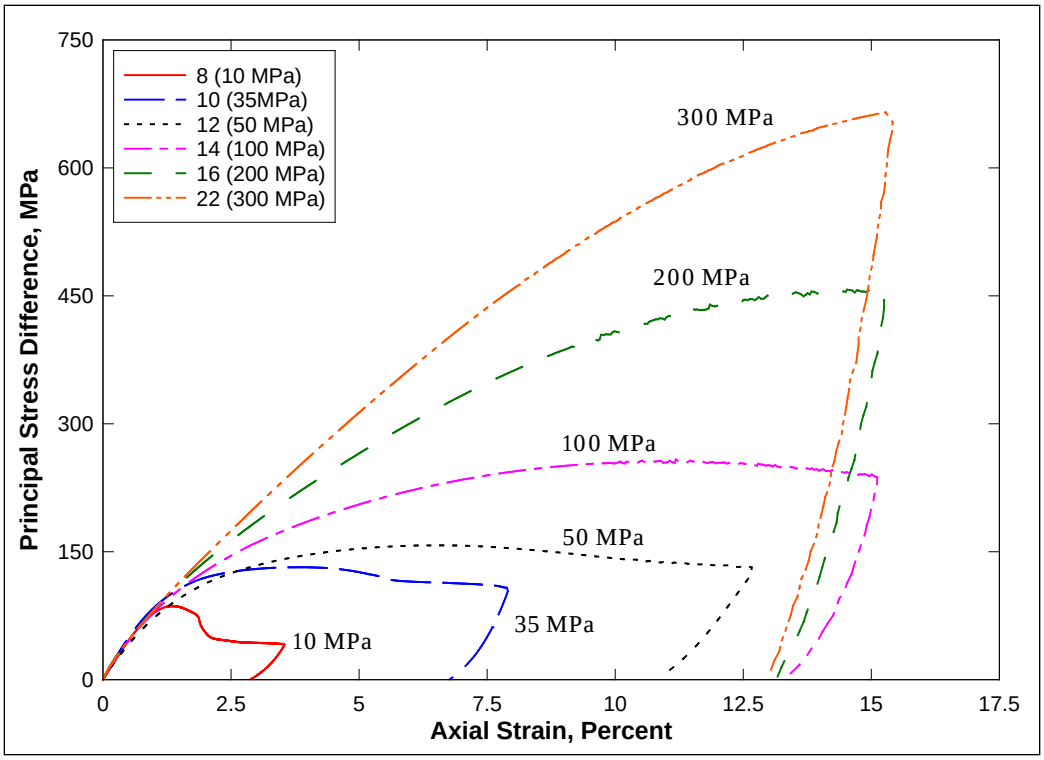

Figure 22. Stress-strain responses from TXC tests at confining pressures from 10 to 300 MPa.

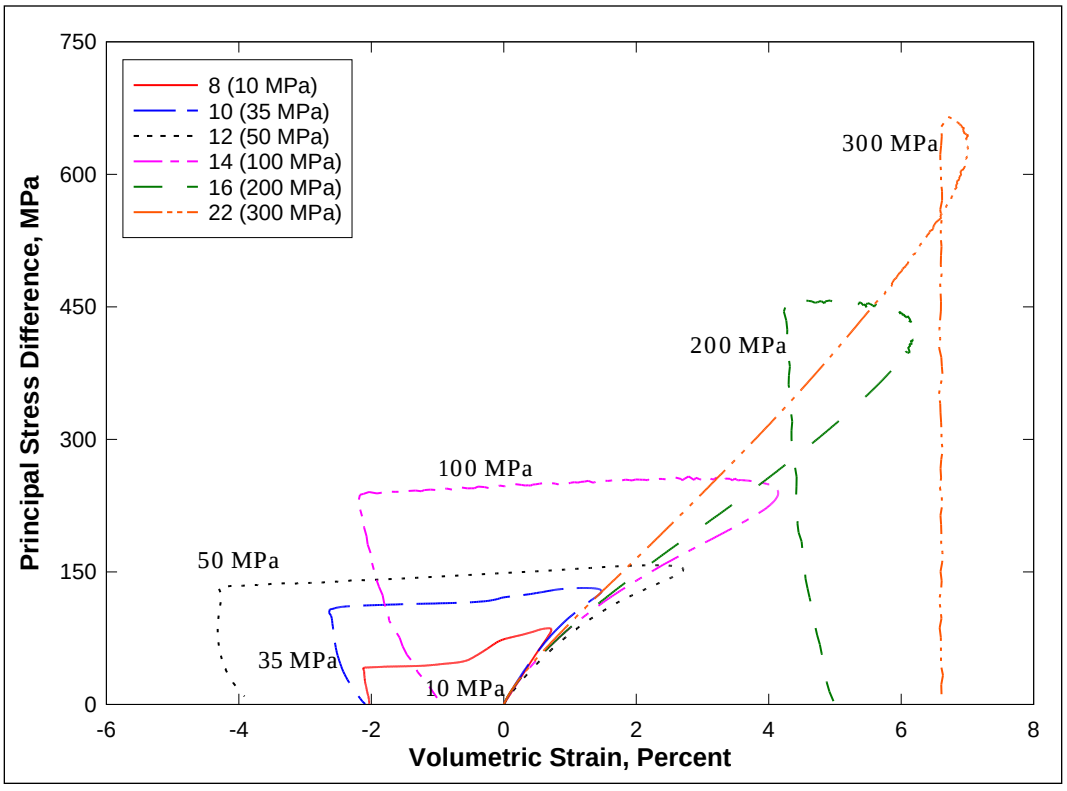

Figure 23. Stress difference-volumetric strain during shear from TXC tests at confining pressures from 10 to 300 MPa.

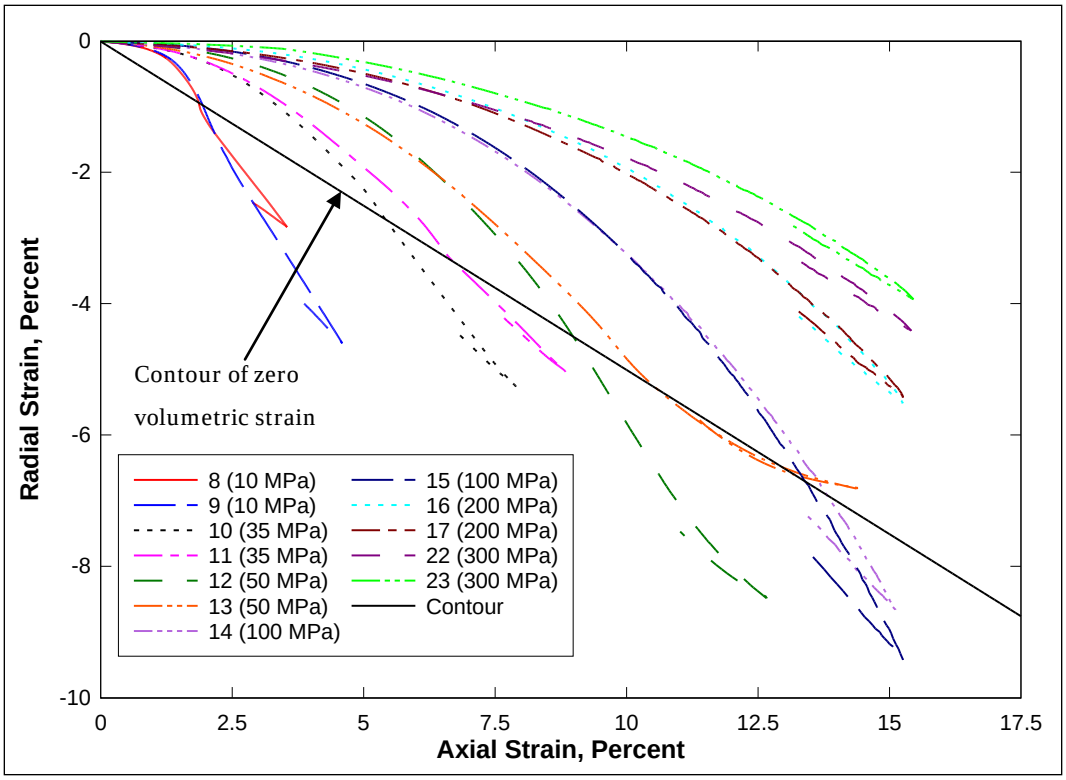

Figure 24. Radial strain-axial strain data during shear from TXC tests at confining pressures from 10 to 300 MPa.

contour of zero volumetric strain, the specimen is in a state of volumetric compression; when steeper, the specimen is in a state of dilation or volumetric expansion. Data points plotting below the contour signify that a test specimen has dilated, and the current volume of the specimen is greater than the volume at the start of shear.

The stress paths and failure data from all the UC and TXC tests are plotted in Figure 25 as principal stress difference versus mean normal stress. In Figure 26, a recommended failure surface is plotted with the failure data from Figure 25. The quality of the failure data is good and exhibits very little scatter. It is important to note that the failure points exhibited a continuous increase in principal stress difference with increasing values of mean normal stress. The response data from the TXC tests indicate that at a mean normal stress of approximately 520 MPa, the brick has not yet reached void closure. Materials such as concrete and brick can continue to gain strength with increasing pressure until all of the specimen's air porosity is forced out.

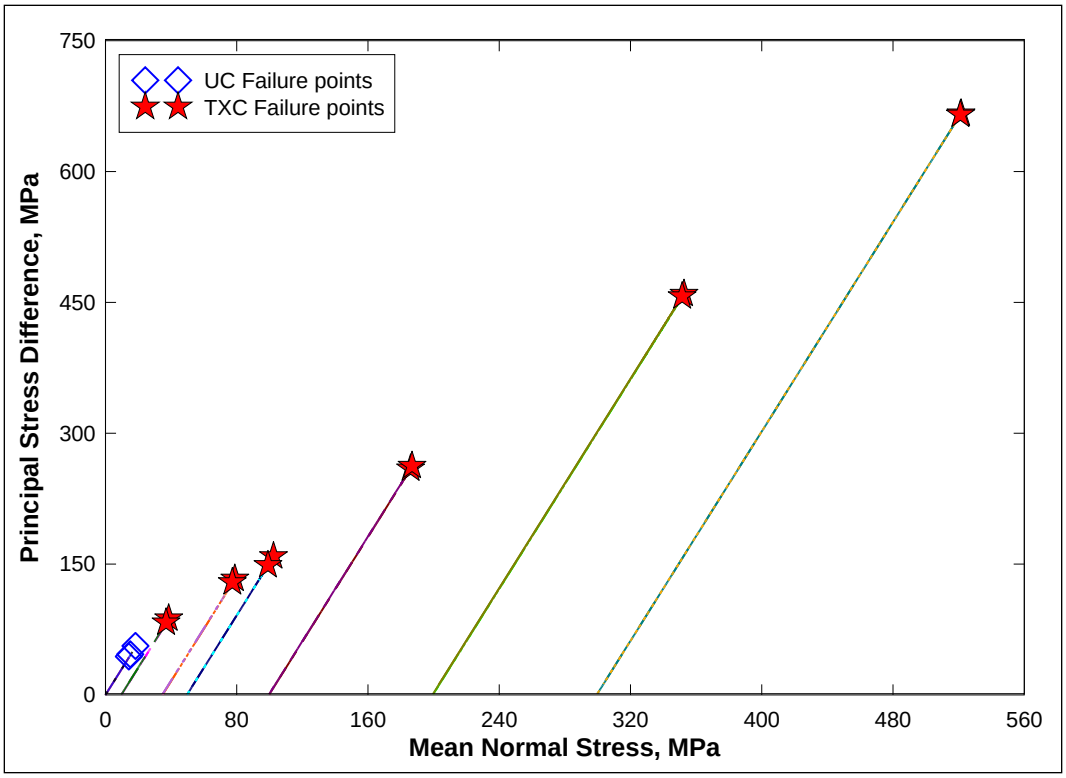

Figure 25. Failure data from UC and TXC tests.

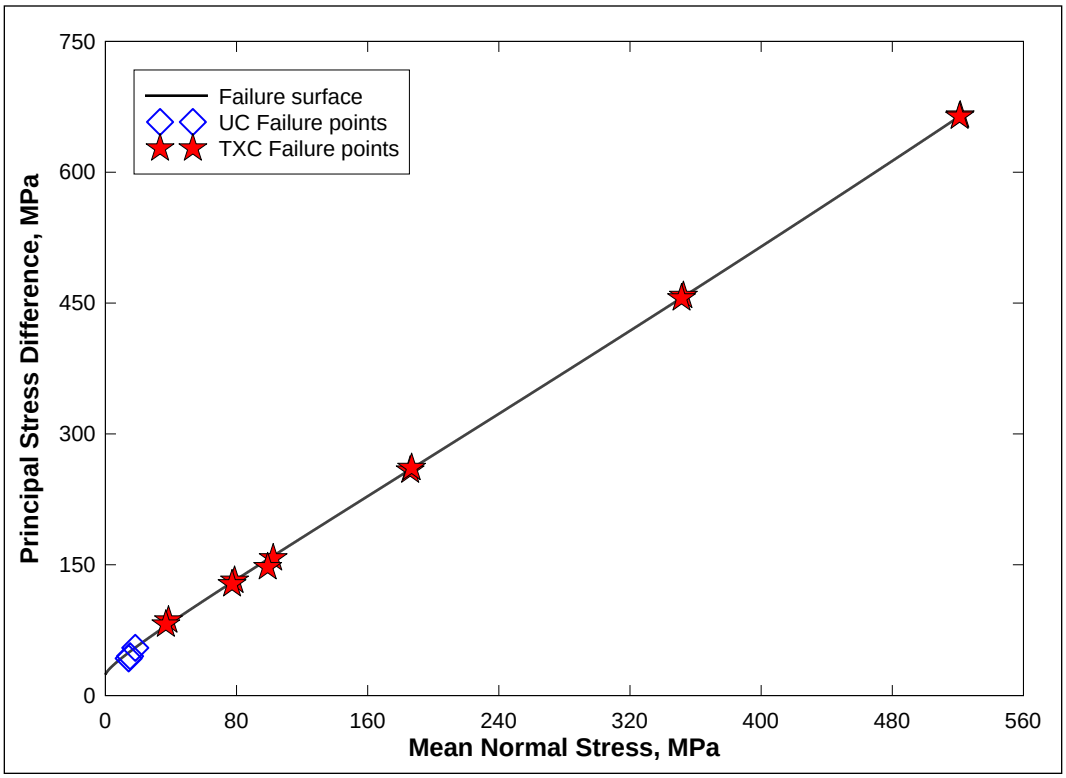

Figure 26. Failure data from UC and TXC tests and recommended failure surface.

Direct-pull (DP) tests

Extension failure data were successfully obtained from two DP tests. To prepare these specimens for testing, threaded caps are attached to the ends of the sample with a high-strength epoxy and allowed to cure for several days. Once the specimen was mounted into the DP apparatus, tensile stress was applied axially by a manually-operated hydraulic pump until failure of the sample occurred. These tests were performed without any application of confining pressure. The stress paths and failure data from the two DP tests are plotted in Figure 27 as principal stress difference versus mean normal stress. The average tensile strength of the DP test specimens occurred at an approximate principal stress difference of -4.0 MPa and at a mean normal stress of -1.4 MPa. The absolute value of the tensile strength of the brick is 8.4% of its unconfined, compressive strength.

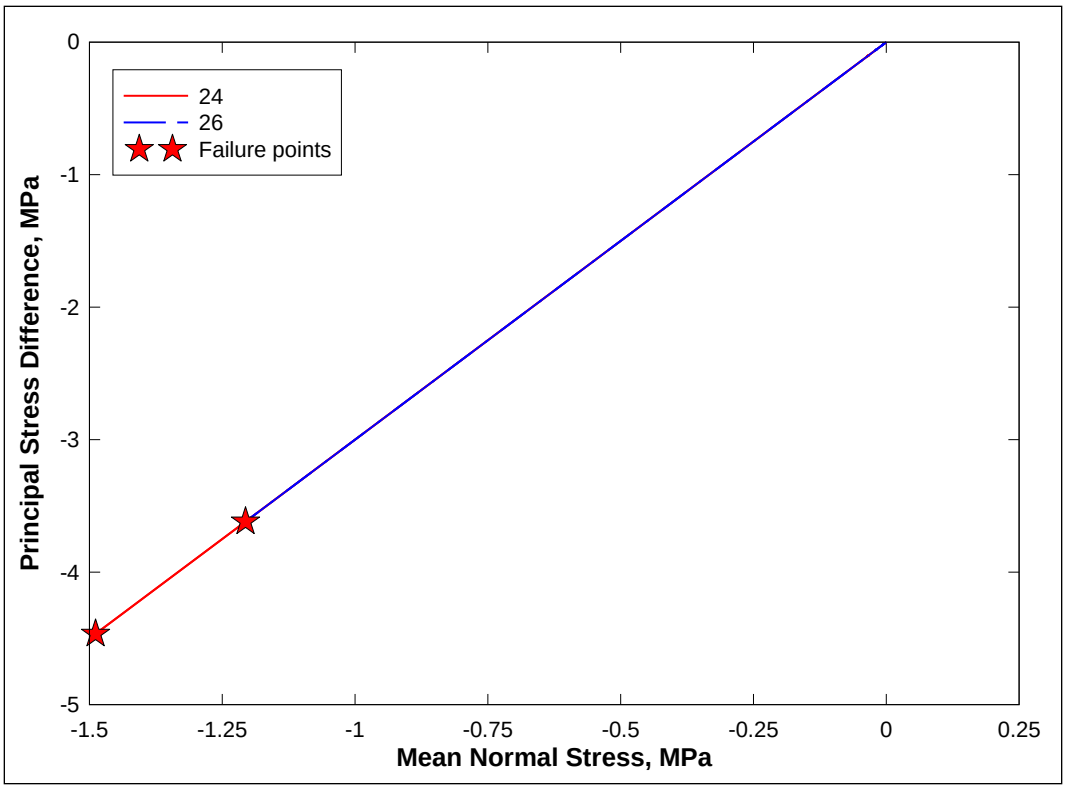

Figure 27. Stress paths and failure data from DP tests.

Uniaxial strain (UX) tests

One-dimensional compressibility data were obtained from two undrained, UX tests with lateral stress measurements. Data from the tests are plotted in Figures 28 through 30. The stress-strain data from the UX tests are plotted in Figure 28, the pressure-volume data are plotted in Figure 29,

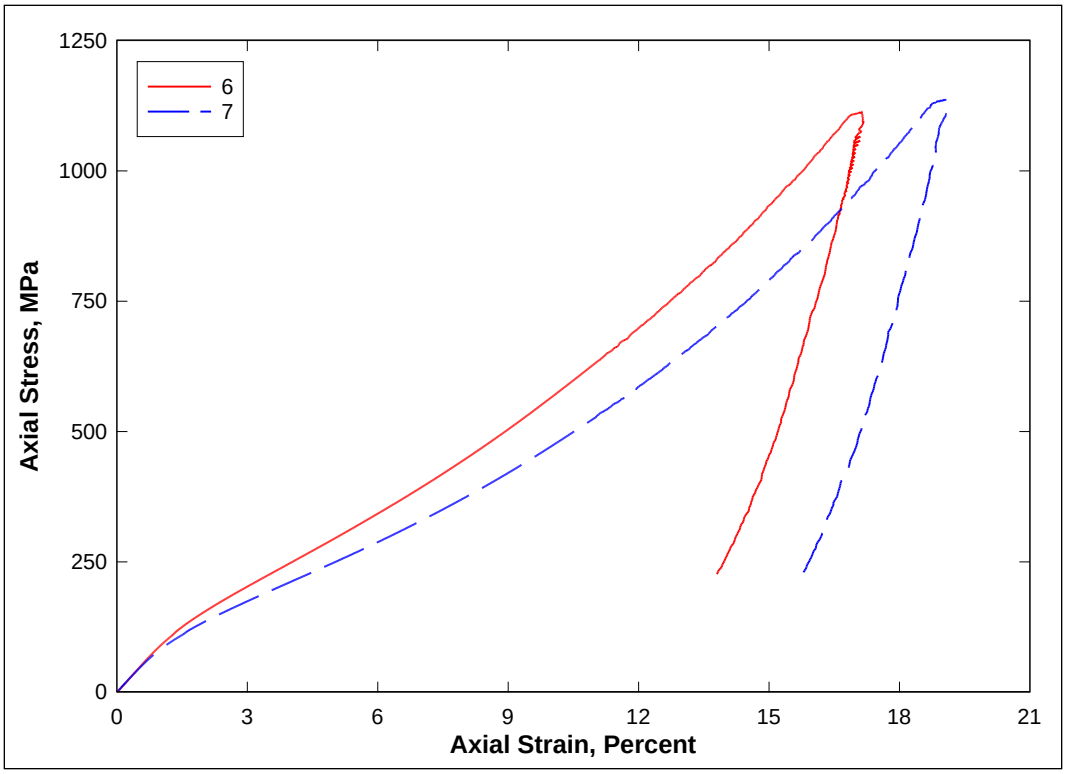

Figure 28. Stress-strain responses from UX tests.

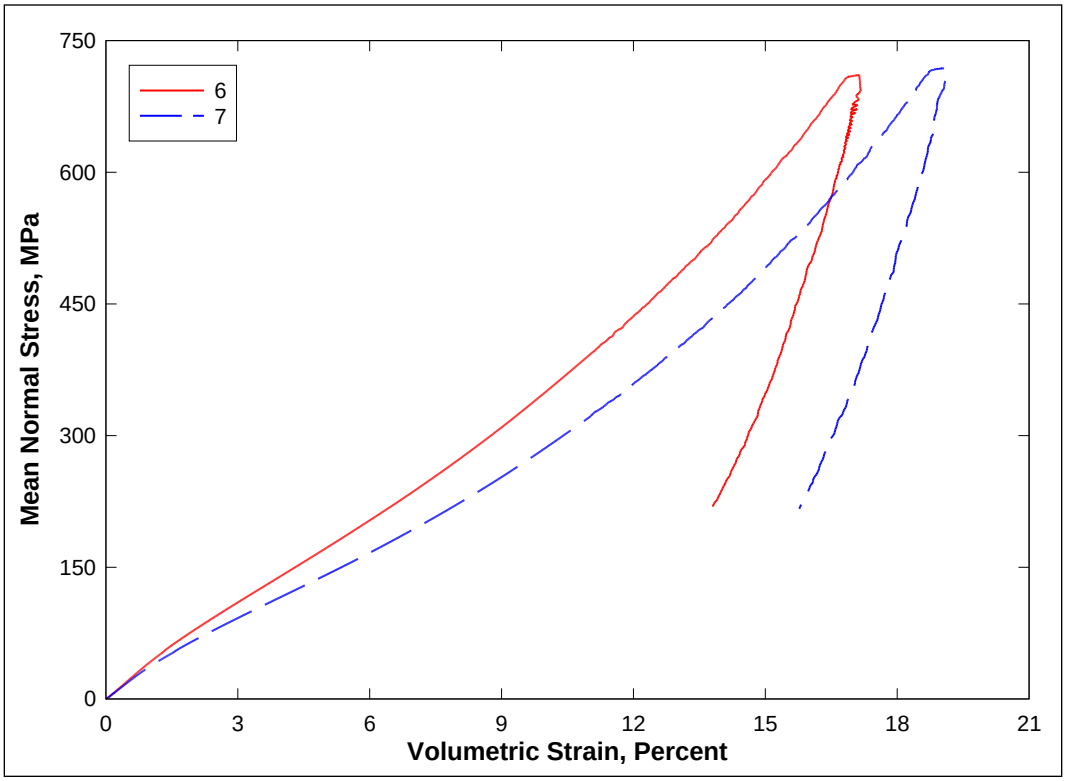

Figure 29. Pressure-volume data from UX tests.

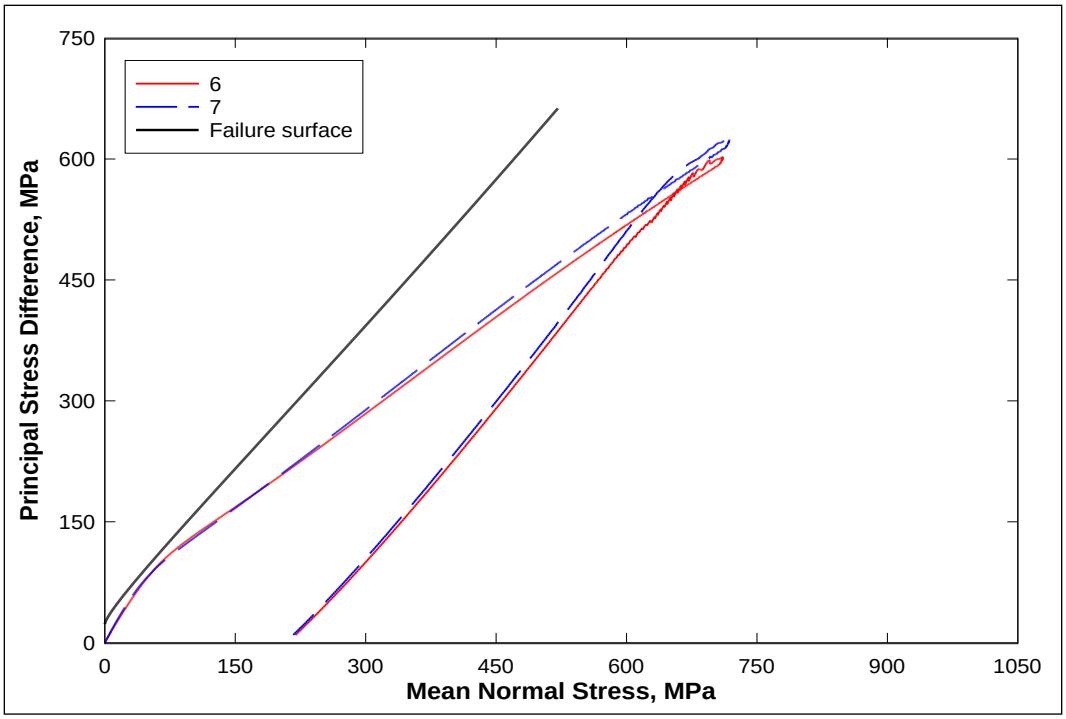

Figure 30. Stress paths from UX tests and failure surface from TXC tests.

and the stress paths with the TXC failure surface data are plotted in Figure 30. The UX responses indicate that the test specimens did not approach a saturated state, i.e., the volumetric strains achieved during the tests were far less than the volumes of air in the specimens. Also, these do not exhibit the unexplained large variations in compressibility that were shown for HC responses.

From the UX stress-strain loading data (Figure 28), an initial constrained modulus (M) of 9.0 GPa was calculated. The UX test data may also be plotted as principal stress difference versus mean normal stress (Figure 30), the slope of which is twice the shear modulus divided by the bulk modulus ($2G/K$). Considering comparable UX and HC specimens 6 and 27, respectively, which had essentially the same initial dry densities (1.869 mg/m^3), an initial shear modulus of 3.3 GPa was calculated from the constrained modulus and the initial bulk modulus, K, of specimen 27 (4.6 GPa). These two values may be used to calculate other elastic constants, such as an initial Young's modulus of 8.0 GPa and a Poisson's ratio of 0.21.

The stress paths from the UX tests and the failure surface are plotted in Figure 30. The UX stress paths almost reach the recommended TXC failure surface at low stresses before the paths soften slightly. The stress paths

soften after the ceramic bonds begin to break, causing the data to plot below the failure surface. The initial dry densities for test specimens 6 and 7 were 1.870 and 1.859 Mg/m^3, respectively. The pressure-volume responses from the HC and UX tests are compared in Figure 31. Again comparing UX and HC specimens 6 and 27, respectively, which had essentially the same initial values of dry density, shear induced compaction is evident due to the greater volumetric strain experienced by specimen 6 at equal values of mean normal stress.

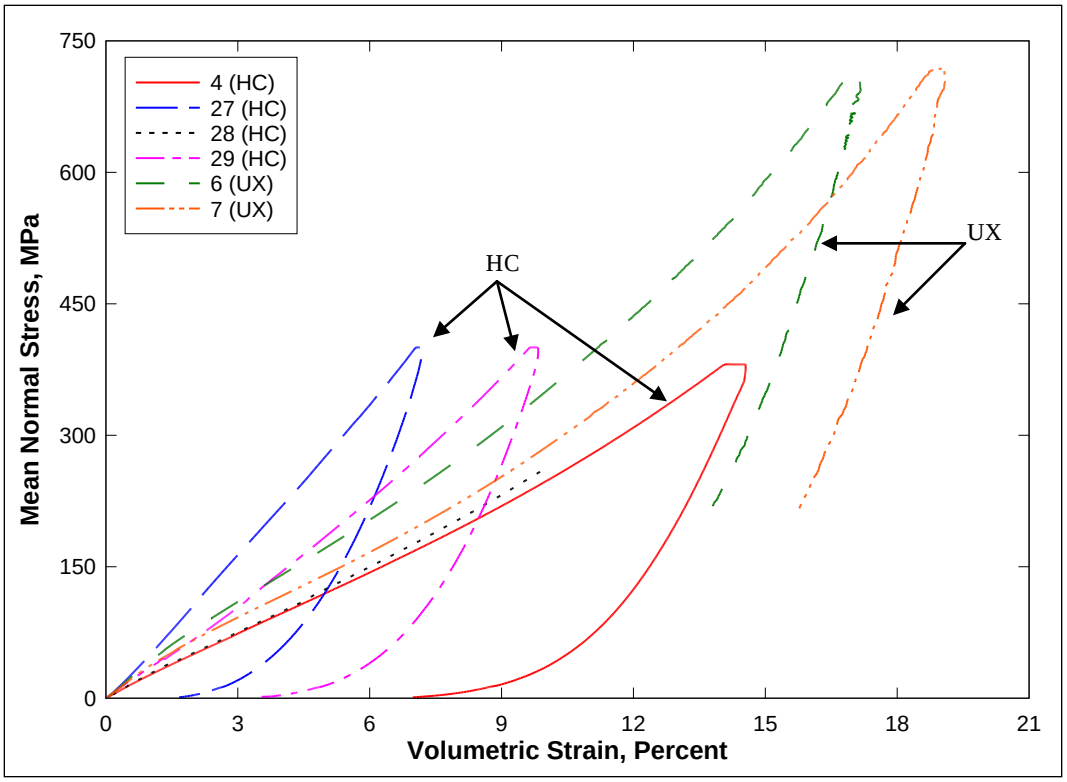

Figure 31. Comparison of pressure-volume data from HC and UX tests.

Strain path tests

One special type of strain-path test was conducted during this test program. UX/CV refers to tests with uniaxial-strain loading followed by constant-volumetric-strain loading with an axial-to-radial-strain ratio (ARSR) of -2.0. Results from two UX/CV tests conducted at two levels of peak radial stress during the initial UX phase are shown in Figures 32 through 35. The stress-strain data from the UX/CV tests are plotted in Figure 32, the pressure-volume data are plotted in Figure 33, the stress paths with the TXC failure surface are plotted in Figure 34, and the strain paths are plotted in Figure 35.

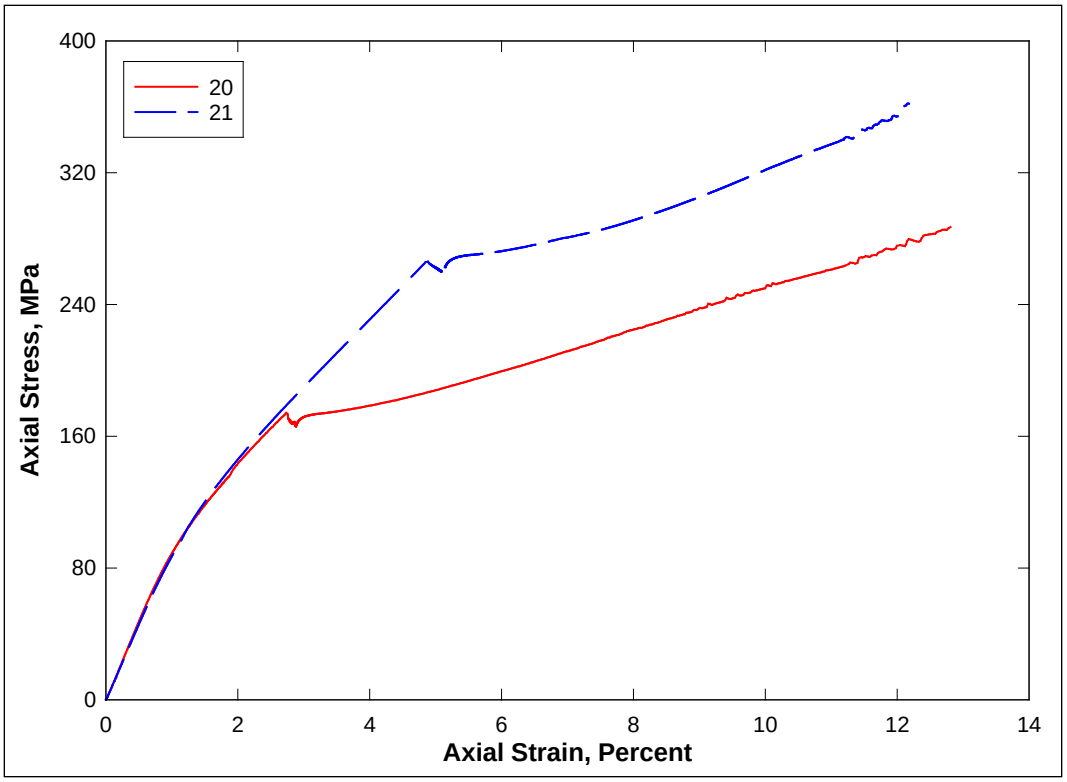

Figure 32. Stress-strain responses from UX/CV tests.

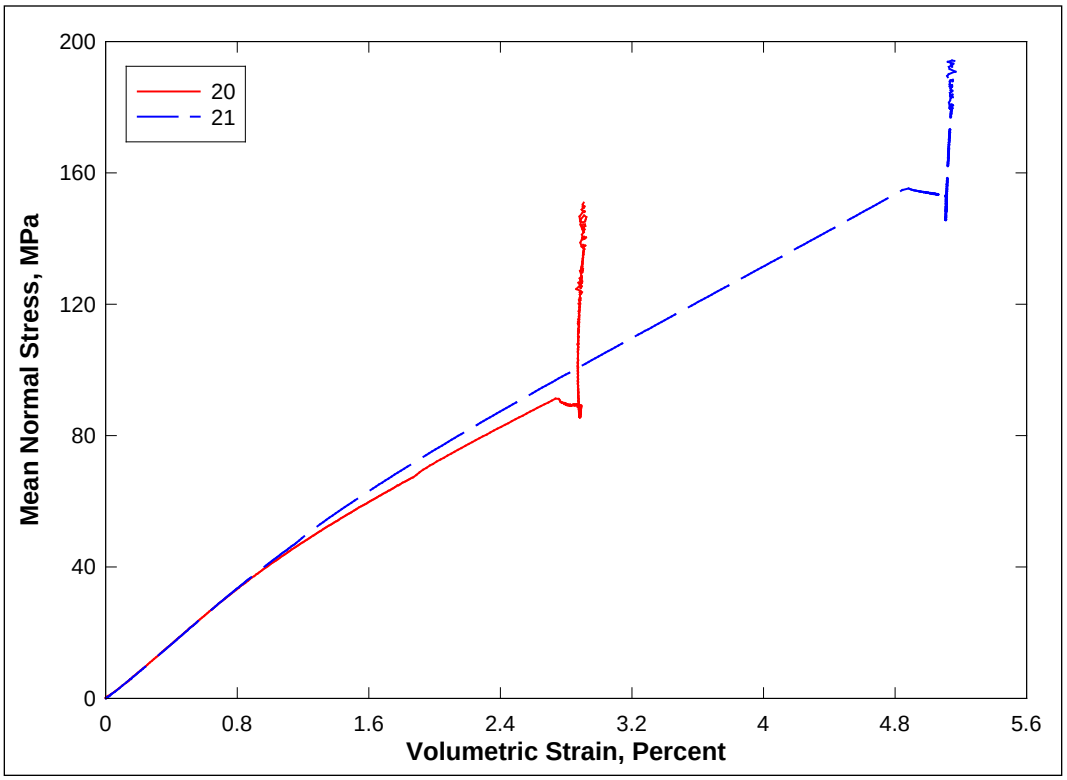

Figure 33. Pressure-volume data from UX/CV tests.

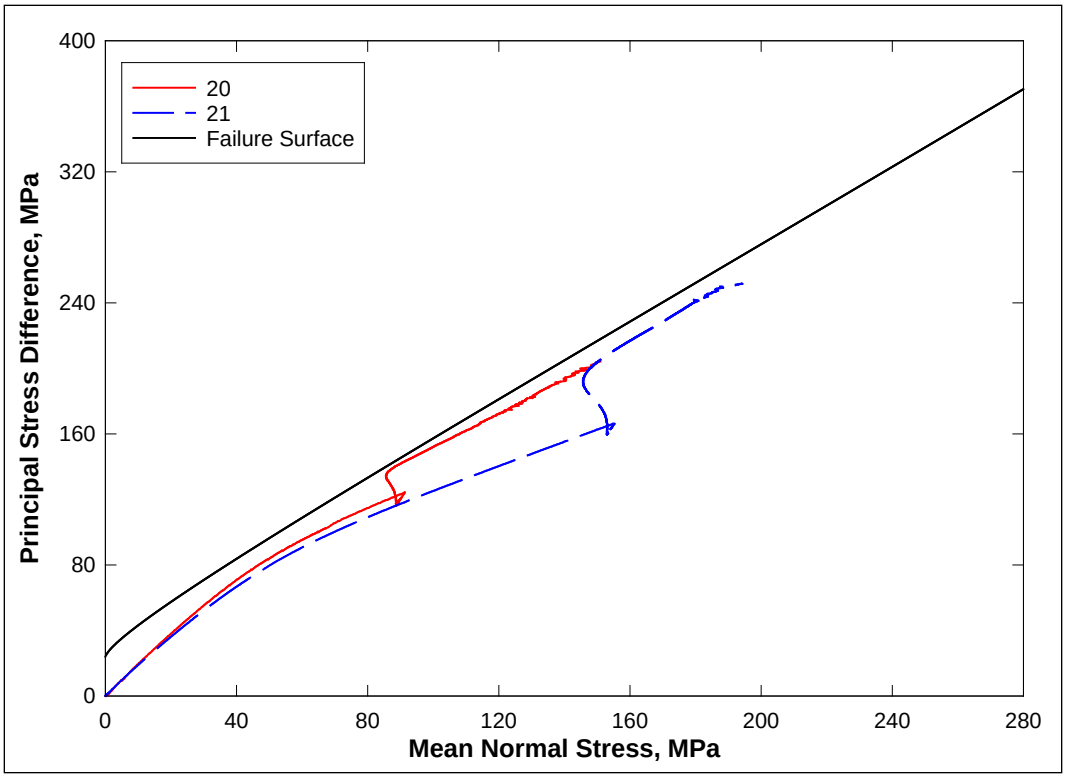

Figure 34. Stress paths from UX/CV tests and failure surface from TXC tests.

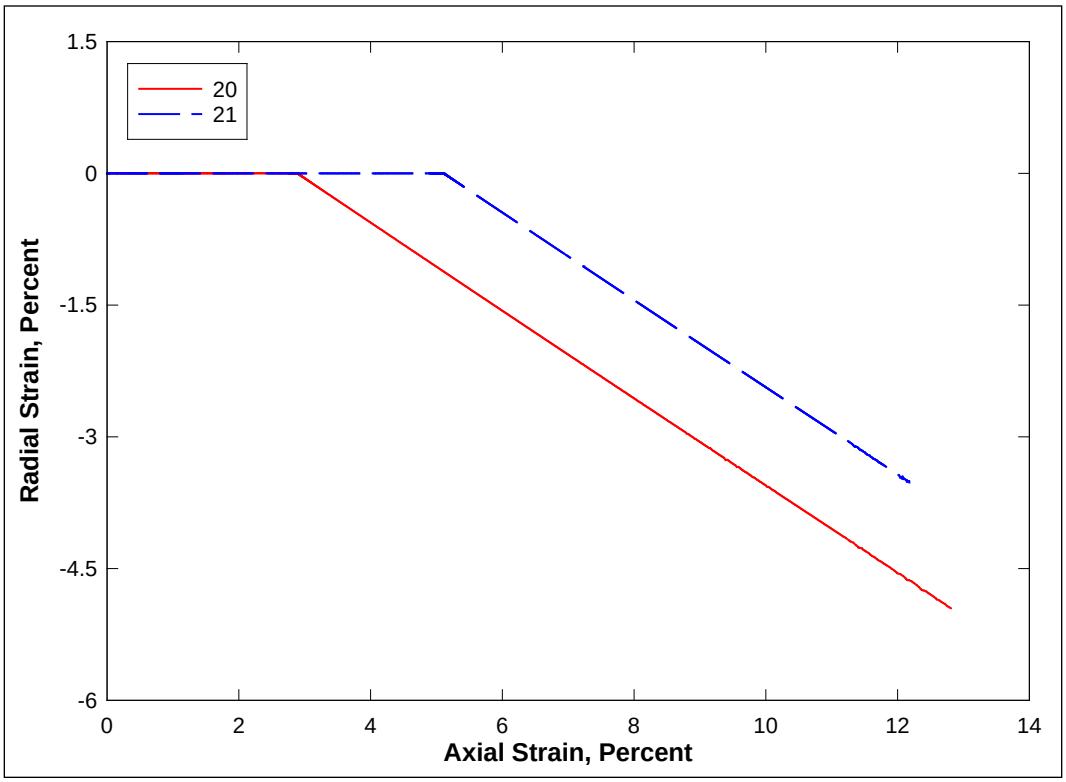

Figure 35. Strain paths from UX/CV tests.

When loading along the constant-volume strain path, the specimens tend to increase in volume due to the material's inherent shear-induced dilation characteristics near the failure surface. Increasing levels of pressure are required to maintain constant-volume boundary conditions (Figure 33). The CV portions of the stress-path data in Figure 34 initially exhibit an increase in principal stress difference with a slight decrease in mean normal stress followed by an increase in both principal stress difference and mean normal stress. During the CV loading, the data plot just below the failure surface developed from the TXC tests. This is mostly due to the lower dry densities of the UX/CV specimens. The average initial dry density of the TXC specimens was 1.870 Mg/m^3, whereas the initial dry densities of test specimens 20 and 21 were 1.859 and 1.867 Mg/m^3, respectively. These differences in the dry densities explain the UX/CV stress paths plotting just below the failure surface. Typically, the limiting surface for the UX/CV stress paths will be the TXC failure surface, assuming the initial dry densities of the UX/CV specimens are similar in value to the average initial dry density of the TXC specimens.

4 Summary

Personnel of the ERDC Geotechnical and Structures Laboratory conducted a laboratory investigation to characterize the strength and constitutive property behavior of Talley brick. A total of 24 successful mechanical property tests were conducted and consisted of three hydrostatic compression (HC) tests, three unconfined compression tests (UC), 12 triaxial compression (TXC) tests, two direct-pull (DP) tests, two uniaxial strain (UX) tests, and two uniaxial-strain-load/constant-volumetric-strain-load (UX/CV) tests. In addition to the mechanical property tests, nondestructive, pulse-velocity measurements were performed on each specimen prior to testing.

Conclusions

The overall quality of the test data was very good; limited scatter was observed in the data over repeated loading paths with the exception of HC compressibility responses. Creep was observed during the HC tests and the hydrostatic loading phases of the TXC tests. Results from the TXC tests exhibited a continuous increase in principal stress difference with corresponding increases in confining stress, indicating that the brick did not reach a fully saturated state. A compression failure surface was developed from the results of TXC tests conducted at six levels of confining pressure and from the results of the UC tests. High confining pressures are needed in order to define the material's brittle-to-ductile failure mode transition. The results for the DP tests were used to determine the tensile strength of Talley brick. From the observed data, Talley brick can withstand more deviatoric stress in compression than in tension before failure occurs. The absolute value of the tensile strength of the brick is 8.4% of its unconfined, compressive strength of 47.5 MPa. During the constant-volume loading, the material followed closely to the failure surface developed from the TXC tests, therefore, validating the compression failure surface.

References

American Society for Testing and Materials. 2005. *Annual Book of ASTM Standards 2005*. Philadelphia, PA.

_____. 2005a. Designation C 39-05. Standard test method for compressive strength of concrete specimens.

_____. 2005b. Designation C 42-04. Standard test method for obtaining and testing drilled cores and sawed beams of concrete.

_____. 2005c. Designation C 597-02. Standard test method for pulse velocity through concrete.

_____. 2005d. Designation D 2216-05. Standard test method for laboratory determination of water (moisture) content of soil and rock by mass.

_____. 2005e. Designation D 4543-04. Standard test method for preparing rock core specimens and determining dimensional and shape tolerances.

Bishop, A. W., and D. J. Henkel. 1962. *The measurement of soil properties in the triaxial test*. London: Edward Arnold, Ltd. 72-74.

TALLEY BRICK
Test No. 4

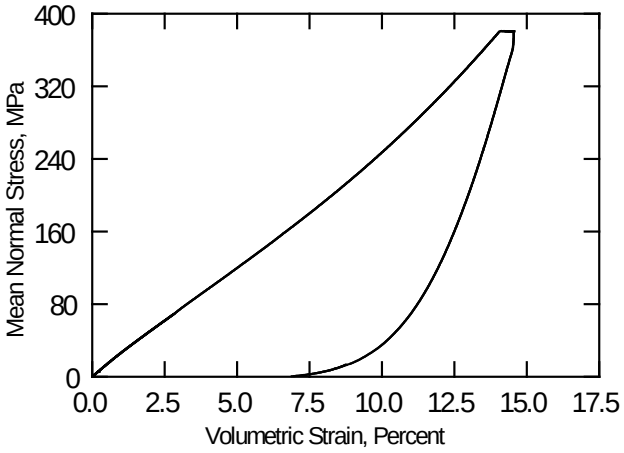

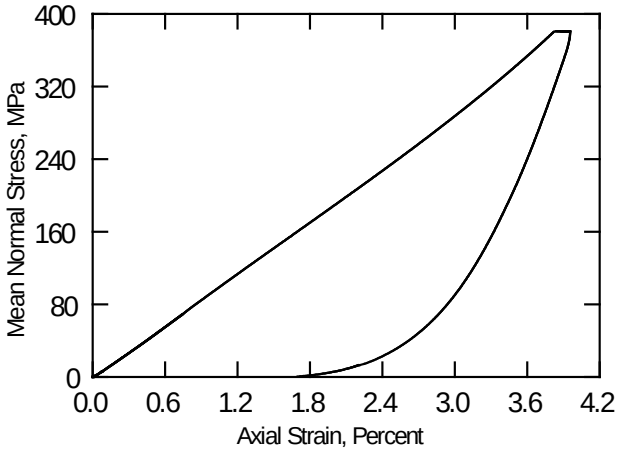

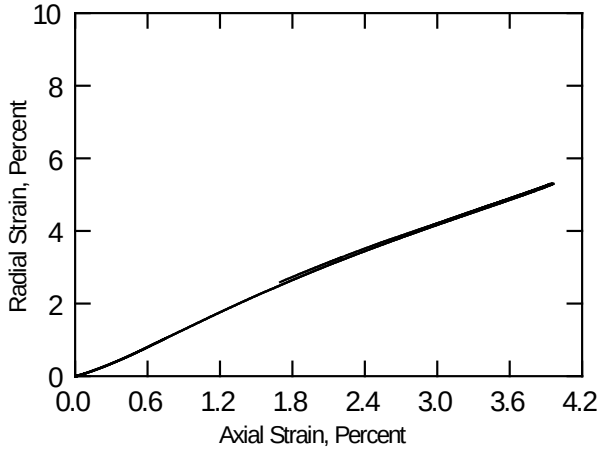

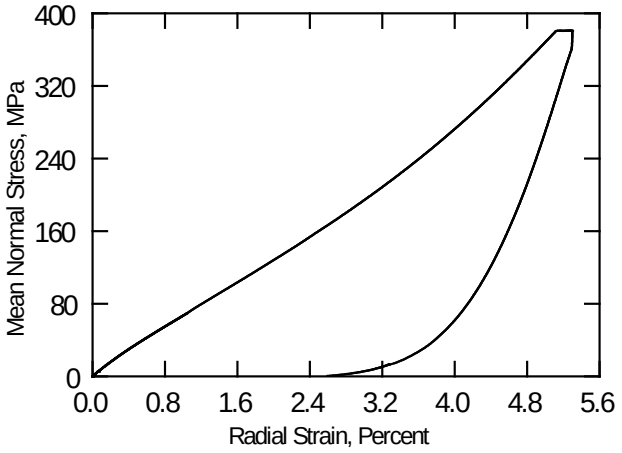

Plate 1

TALLEY BRICK
Test No. 27

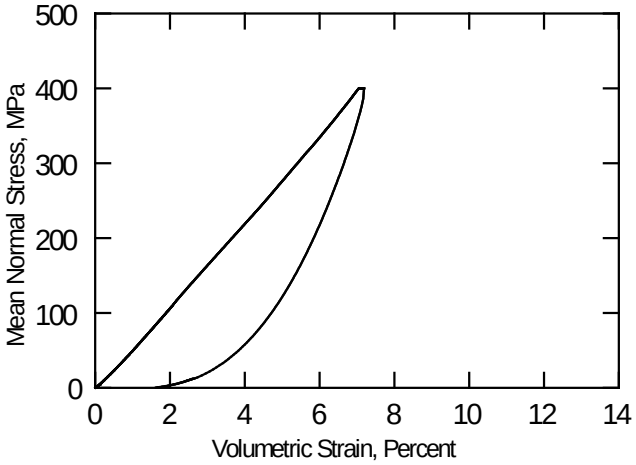

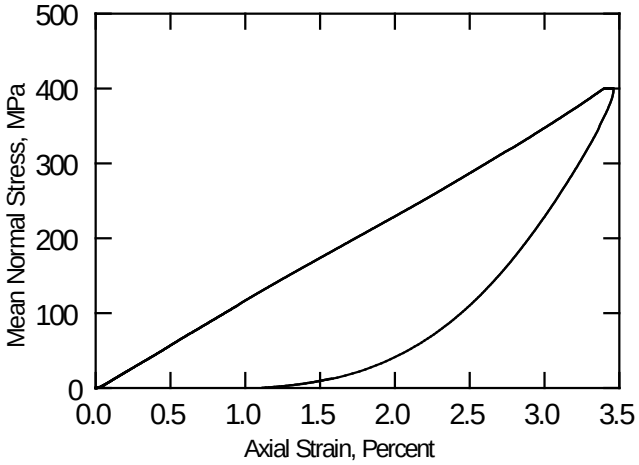

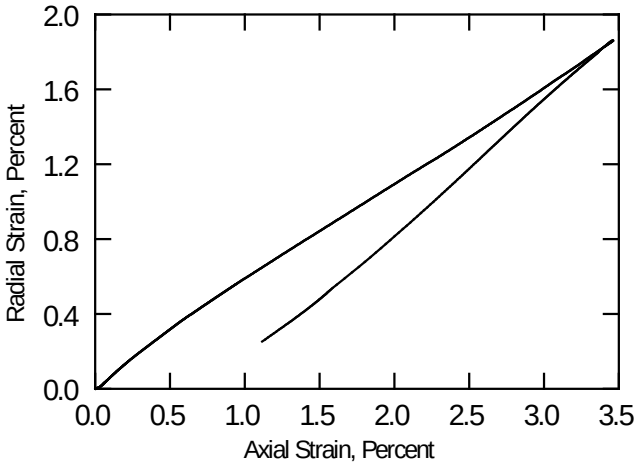

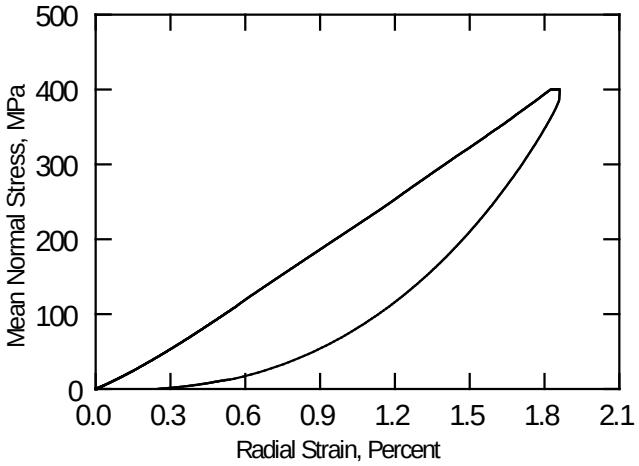

Plate 2

TALLEY BRICK
Test No. 28

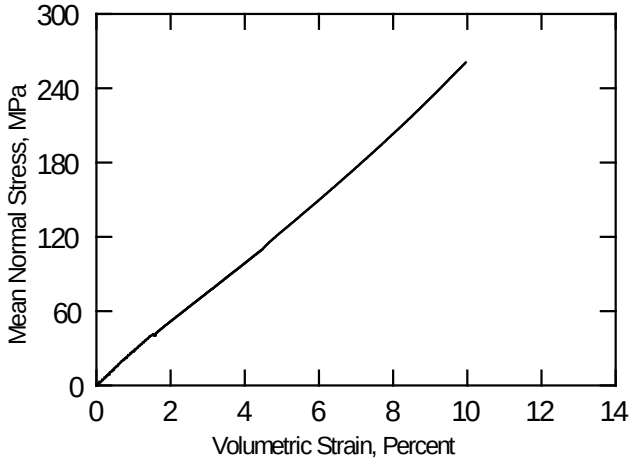

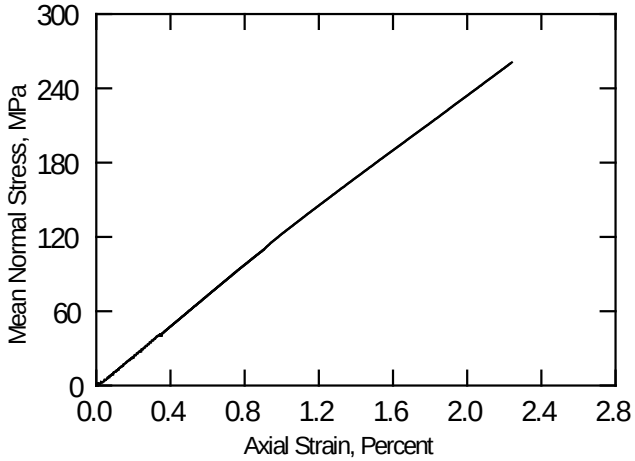

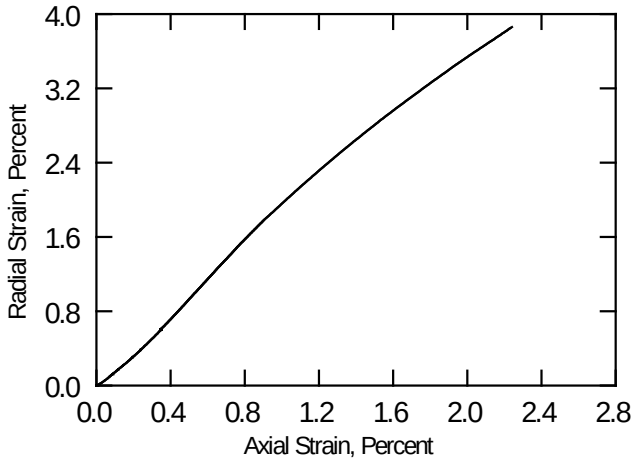

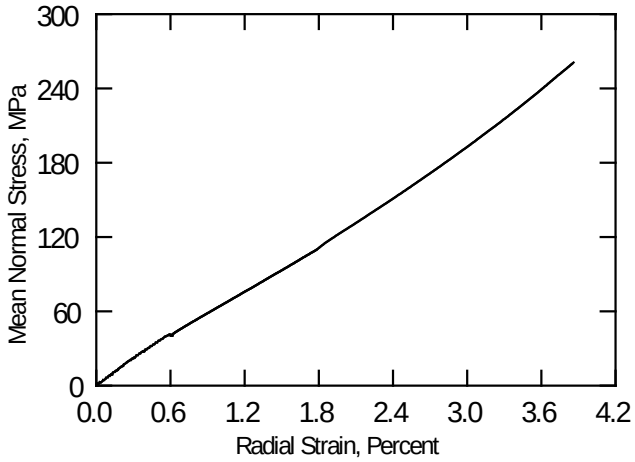

Plate 3

TALLEY BRICK
Test No. 29

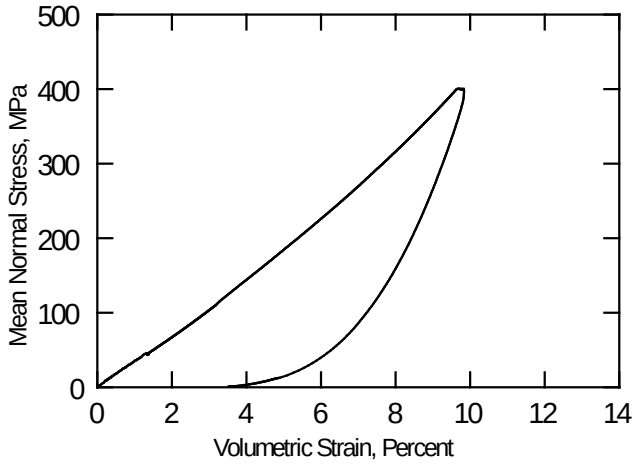

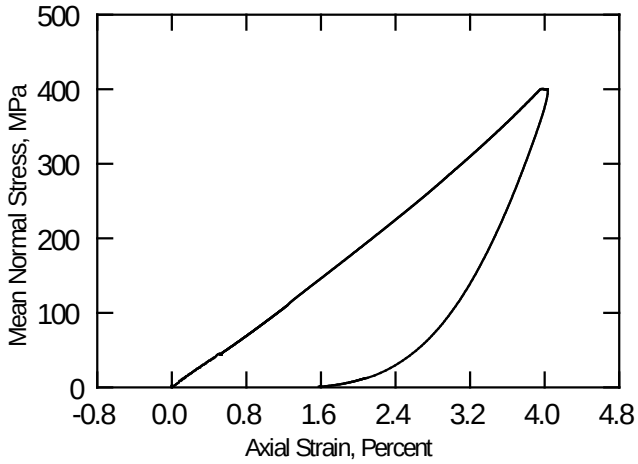

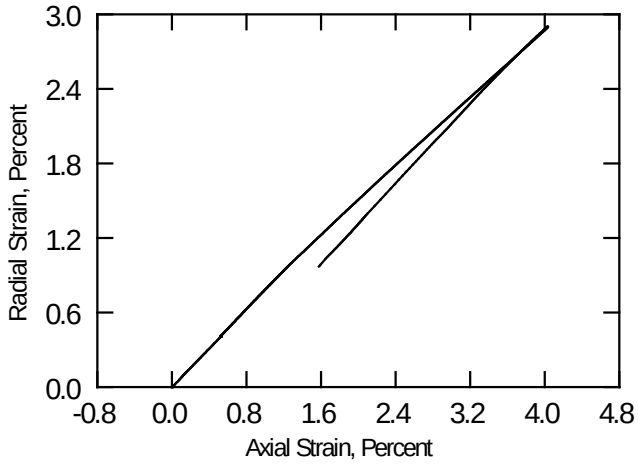

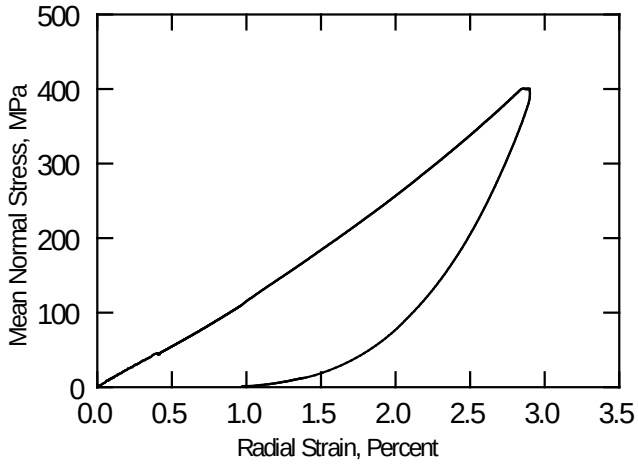

Plate 4

TALLEY BRICK
Test No. 1

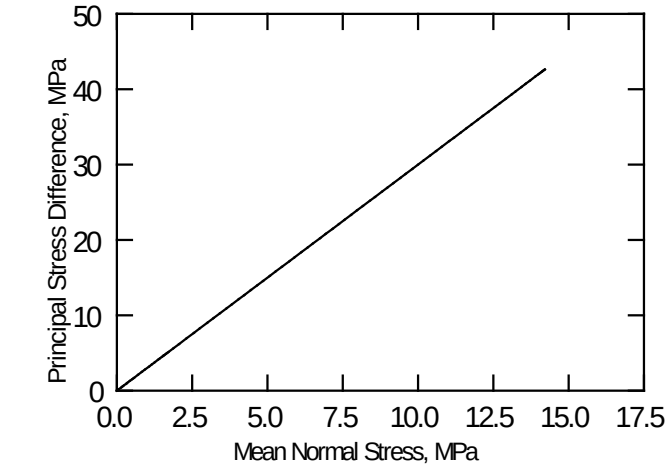

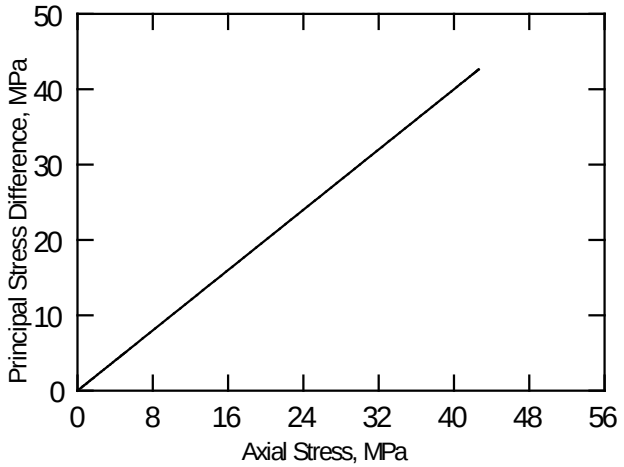

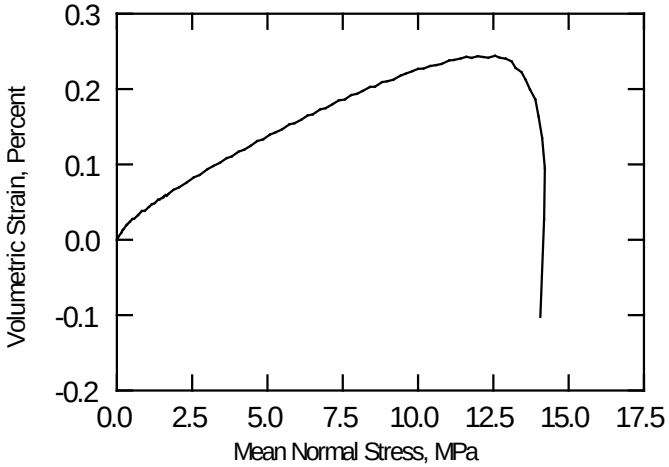

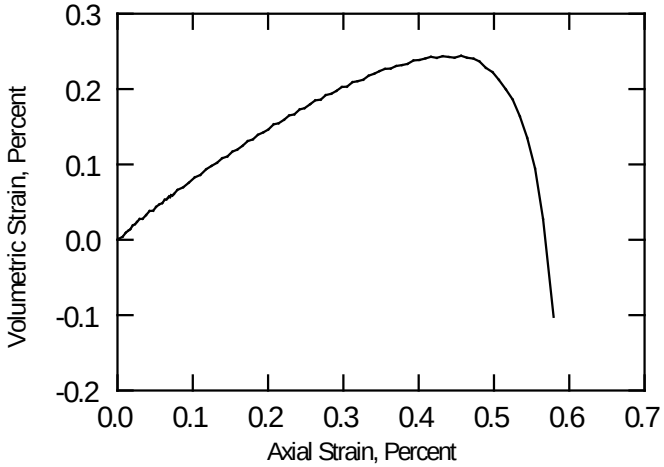

Plate 5

TALLEY BRICK
Test No. 2

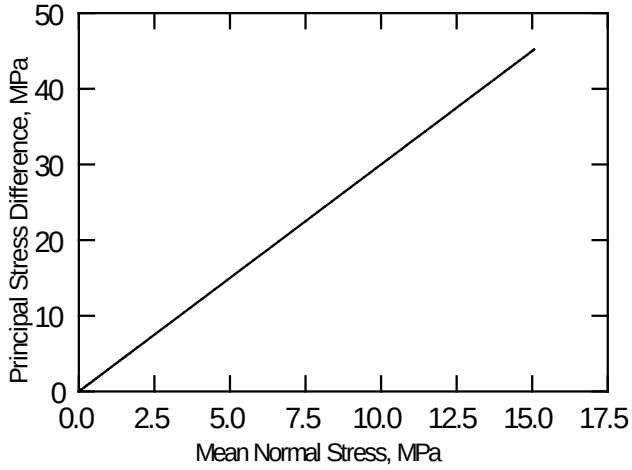

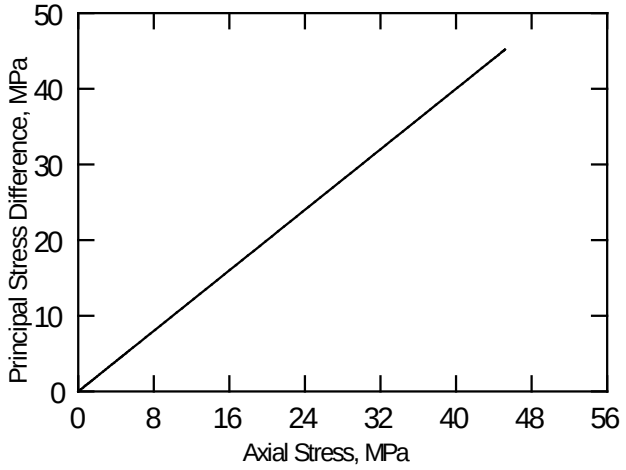

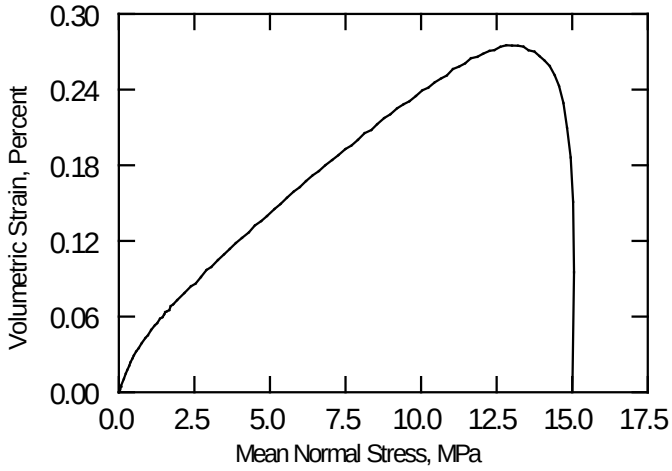

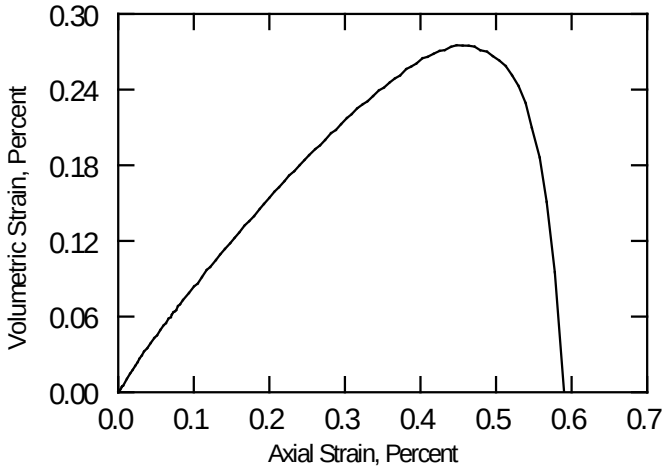

Plate 6

TALLEY BRICK
Test No. 3

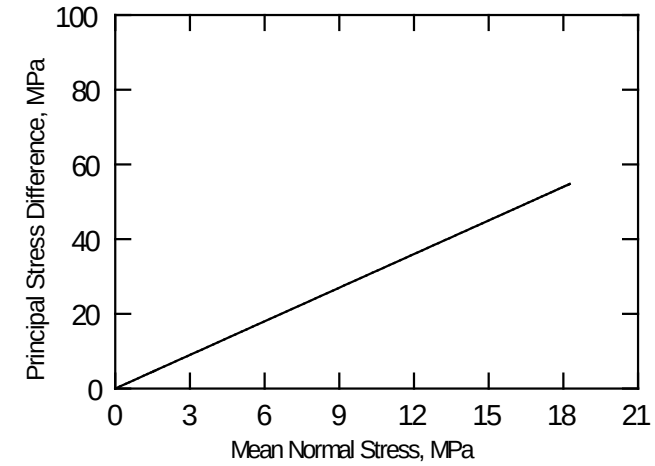

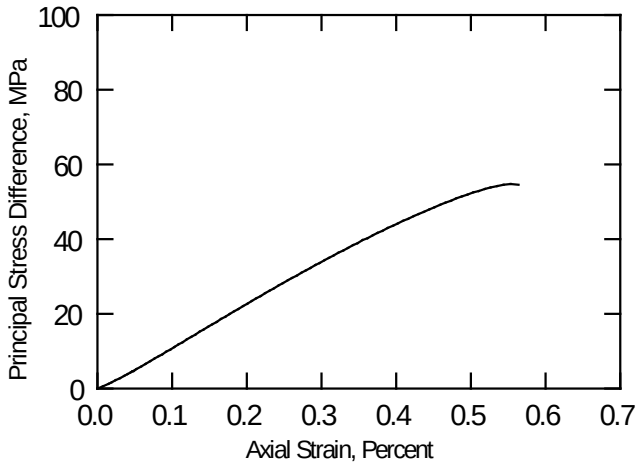

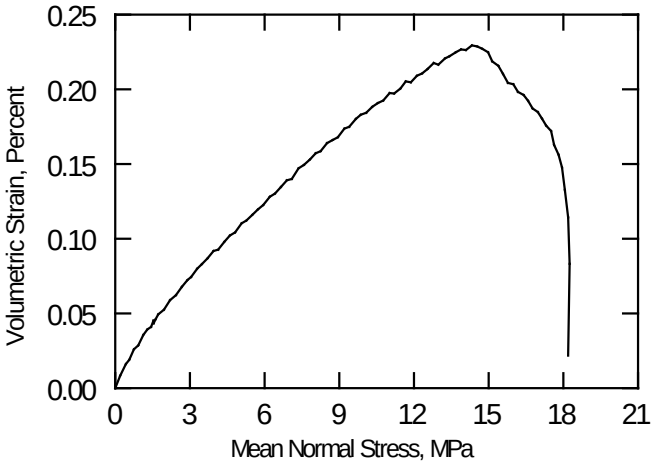

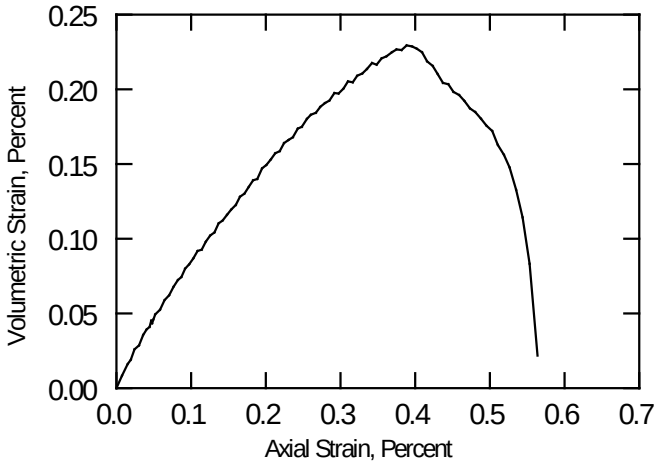

Plate 7

TALLEY BRICK
Test No. 8

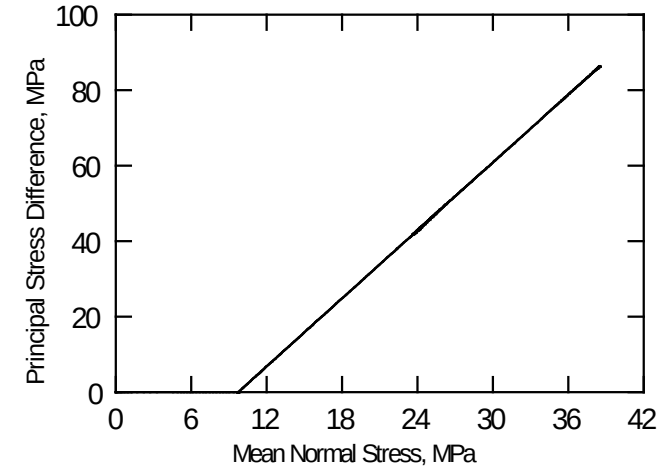

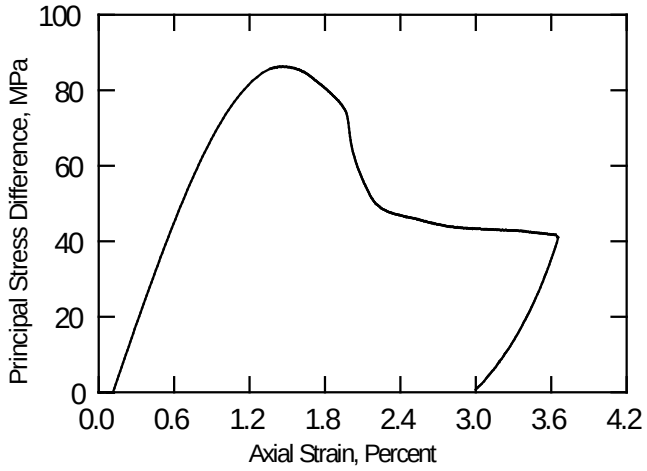

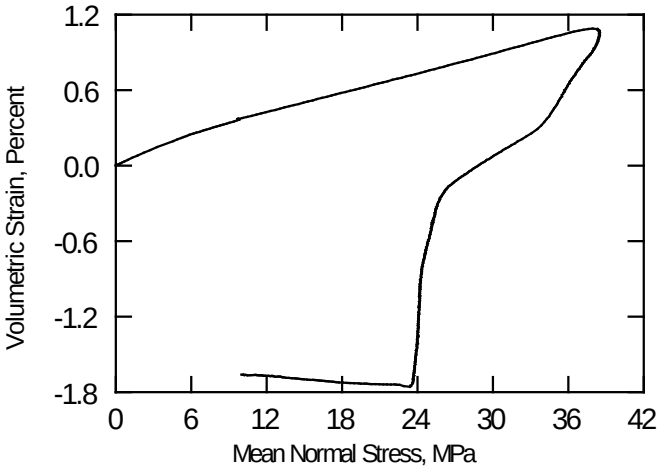

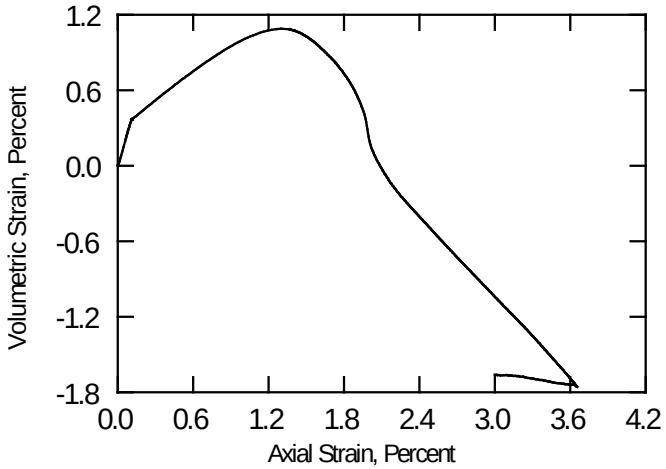

Plate 8

TALLEY BRICK
Test No. 9

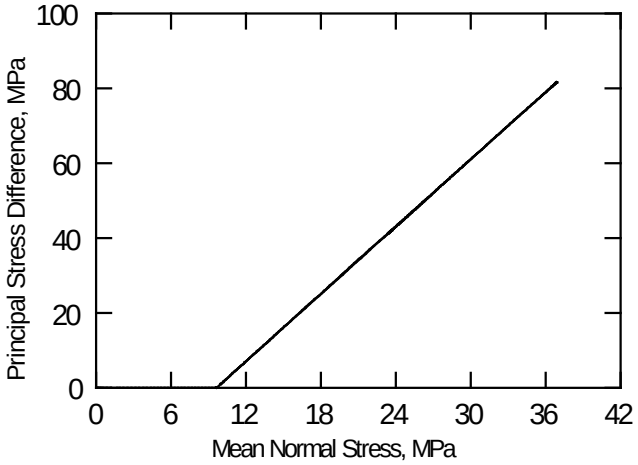

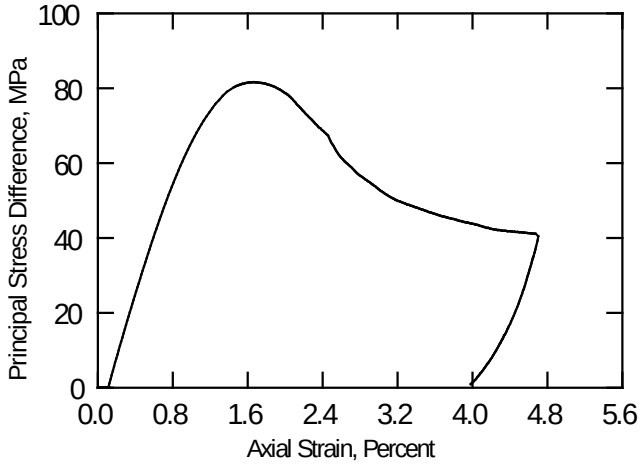

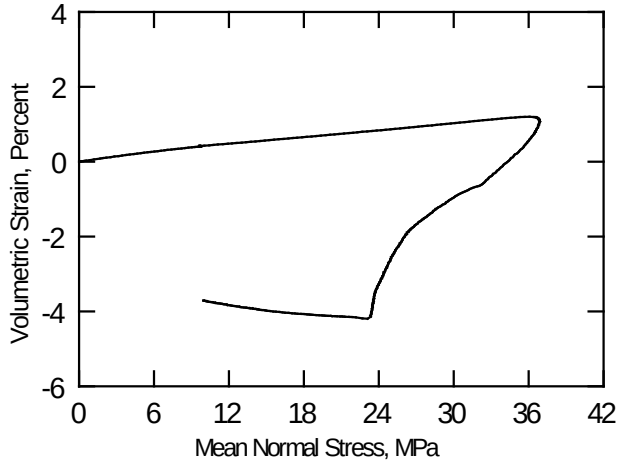

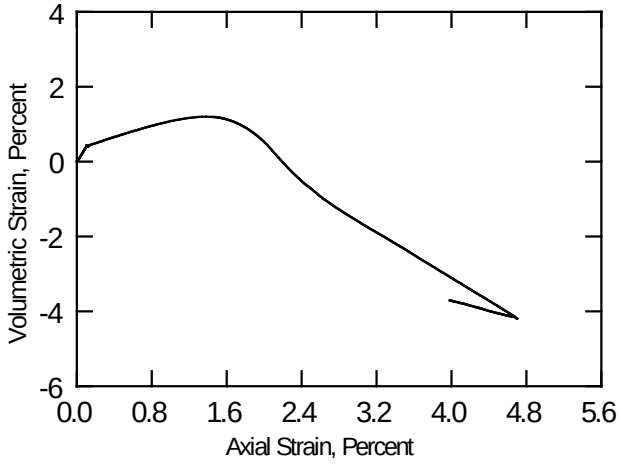

Plate 9

TALLEY BRICK
Test No. 10

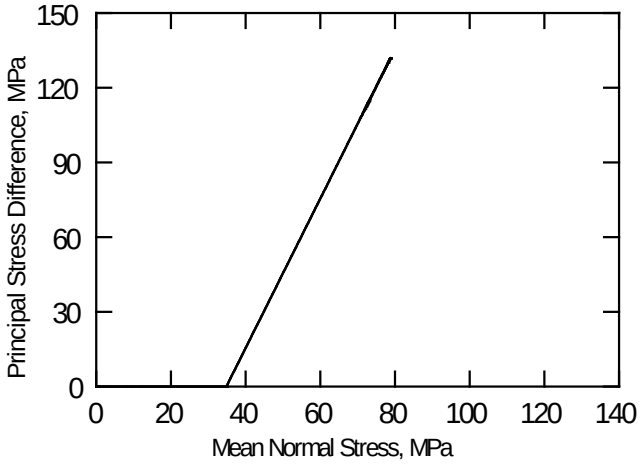

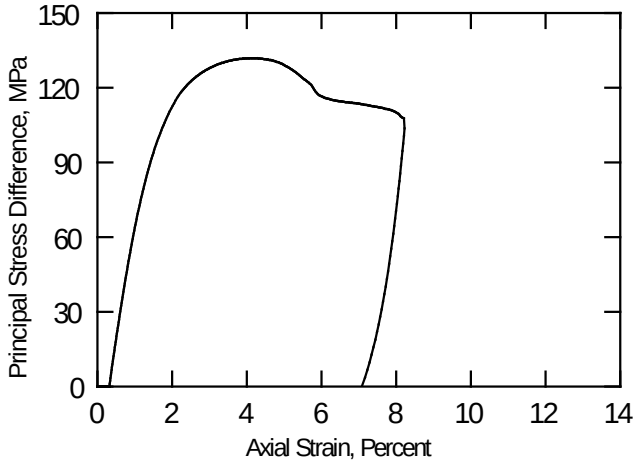

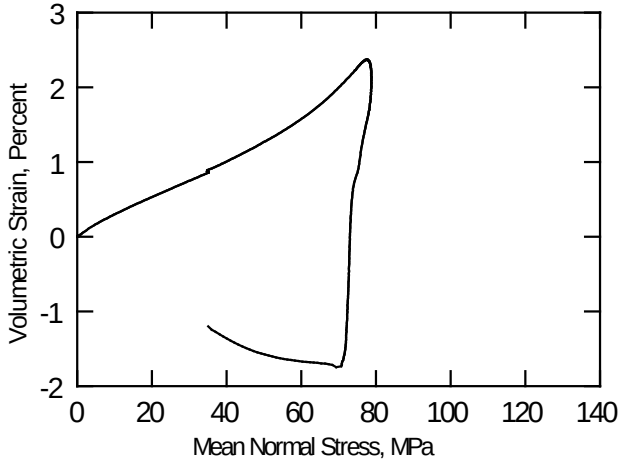

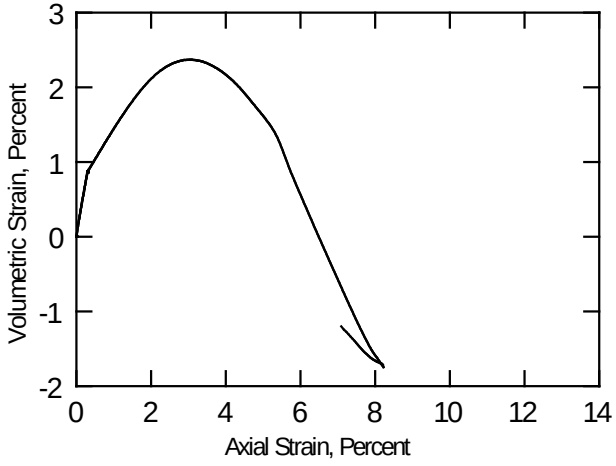

Plate 10

TALLEY BRICK
Test No. 11

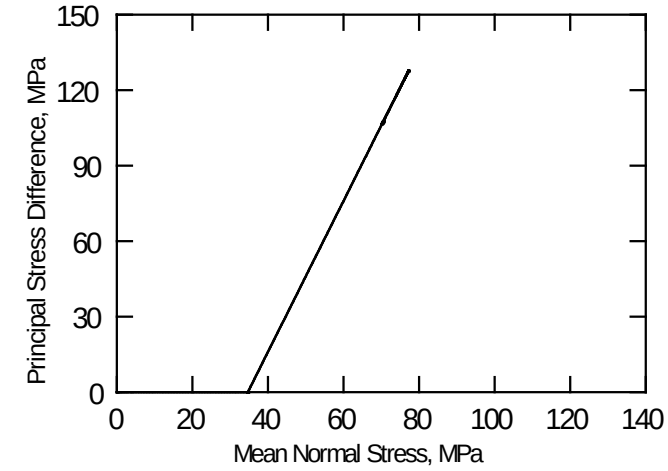

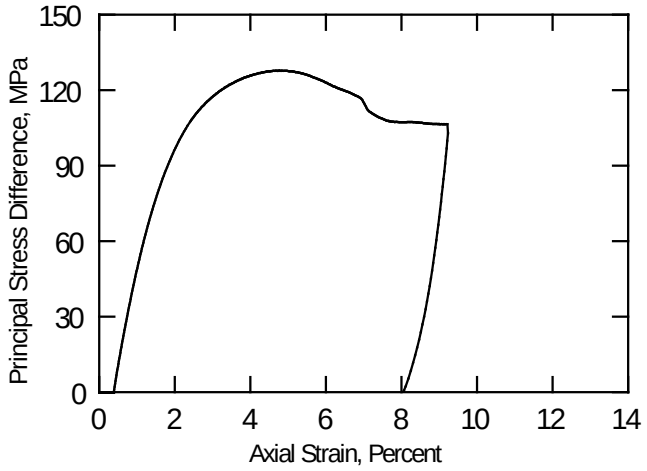

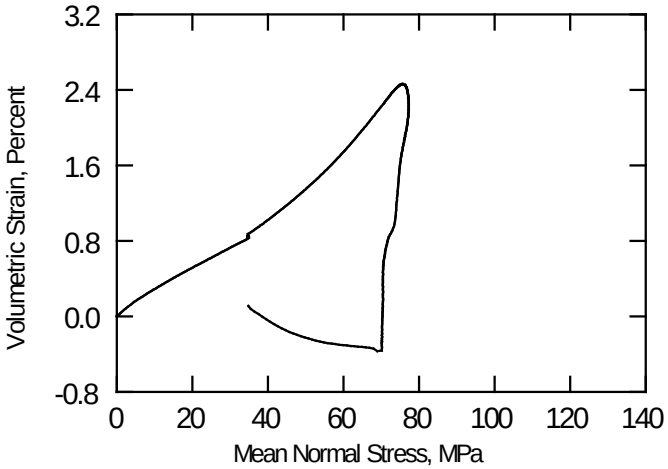

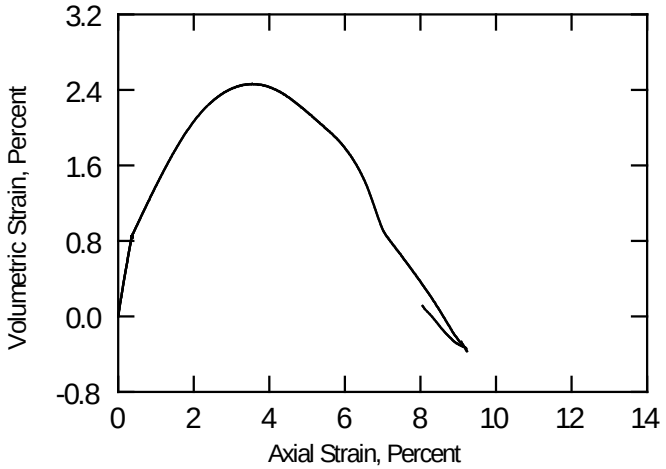

Plate 11

TALLEY BRICK
Test No. 12

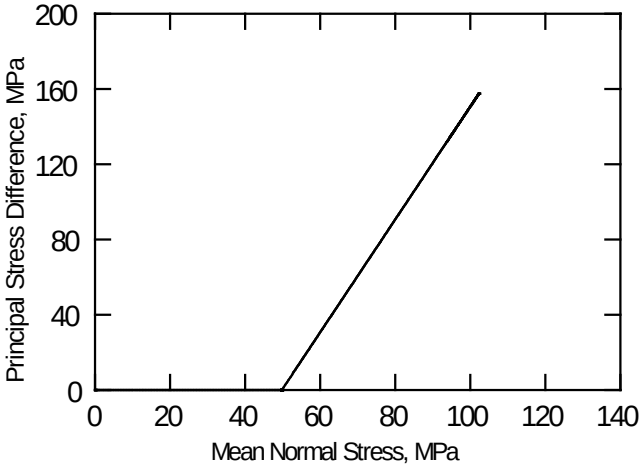

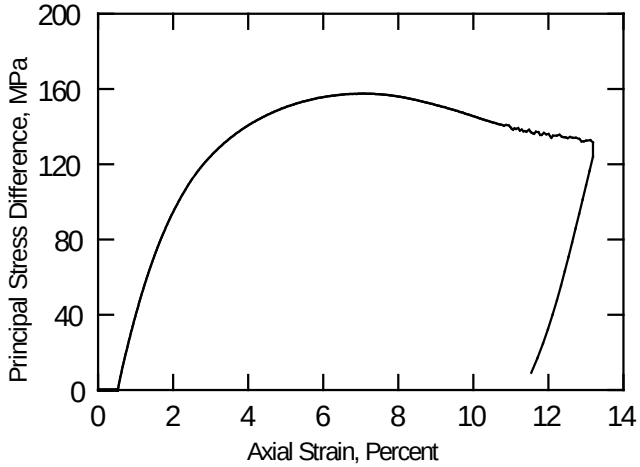

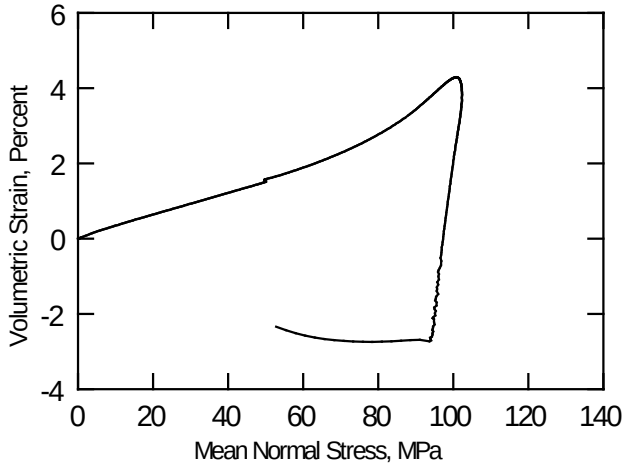

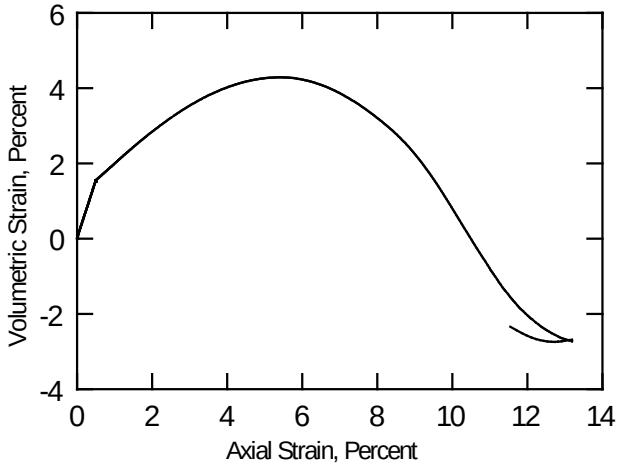

Plate 12

TALLEY BRICK
Test No. 13

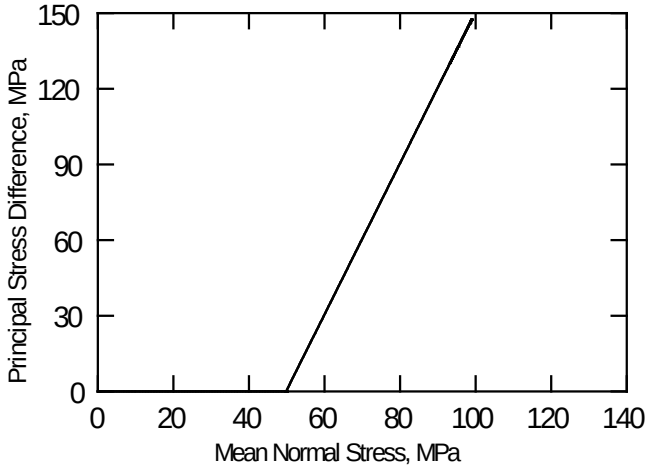

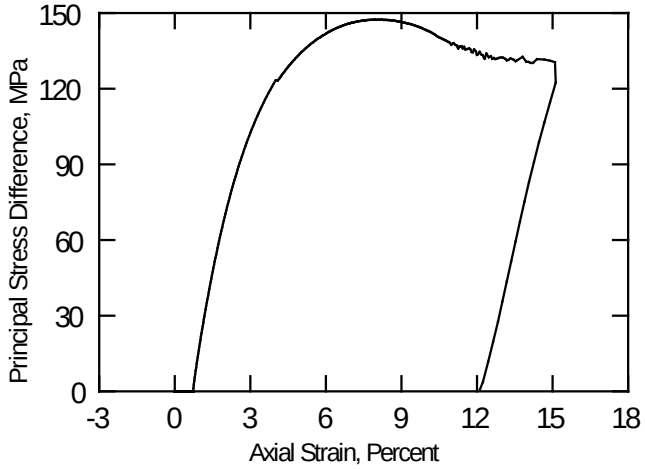

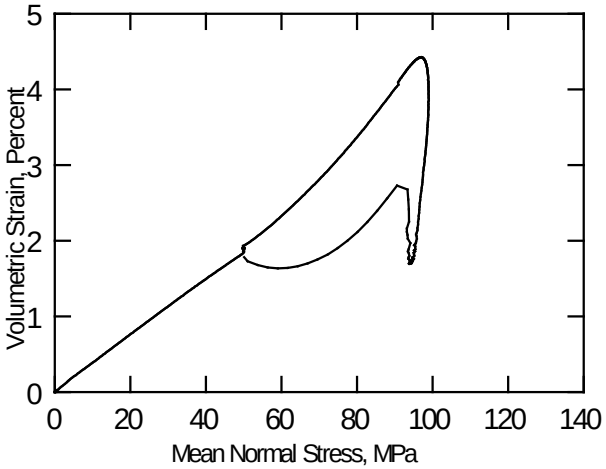

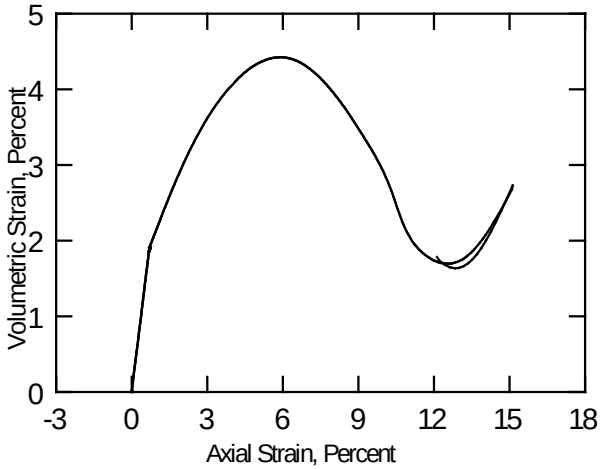

Plate 13

TALLEY BRICK
Test No. 14

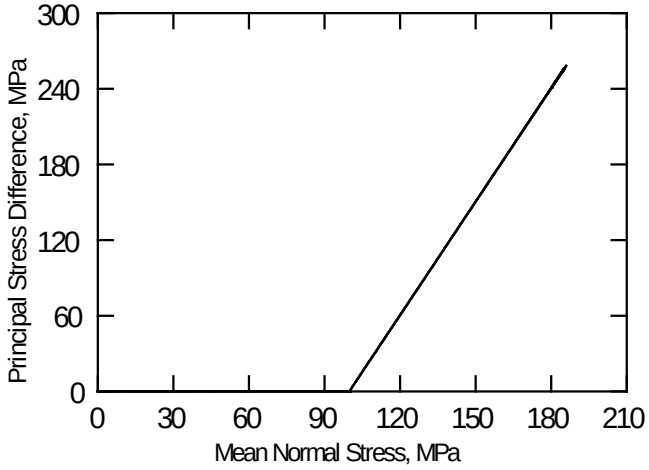

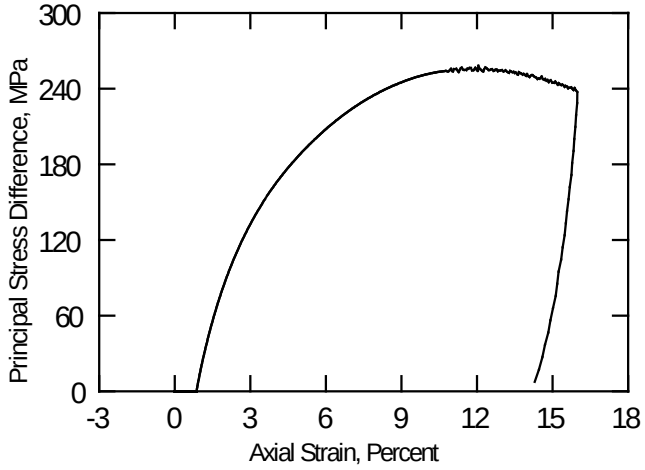

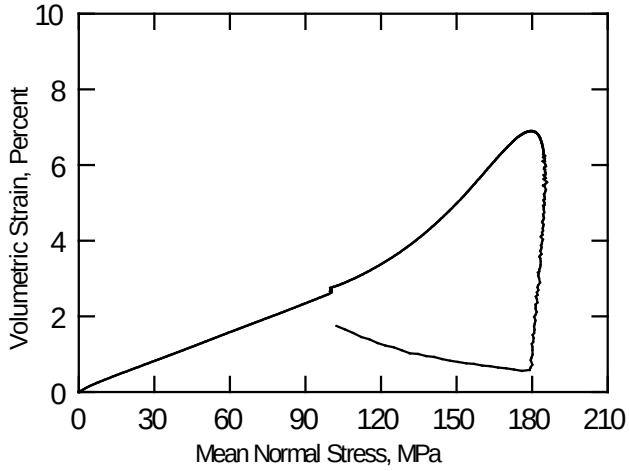

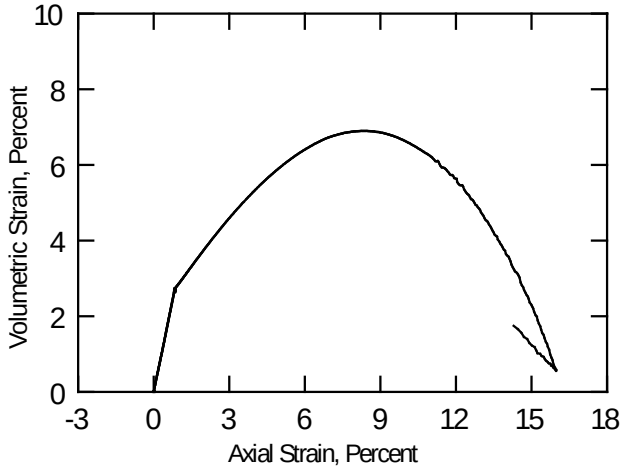

Plate 14

TALLEY BRICK
Test No. 15

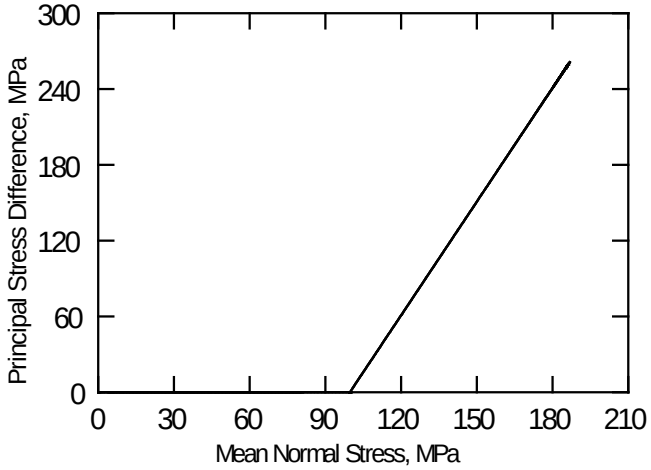

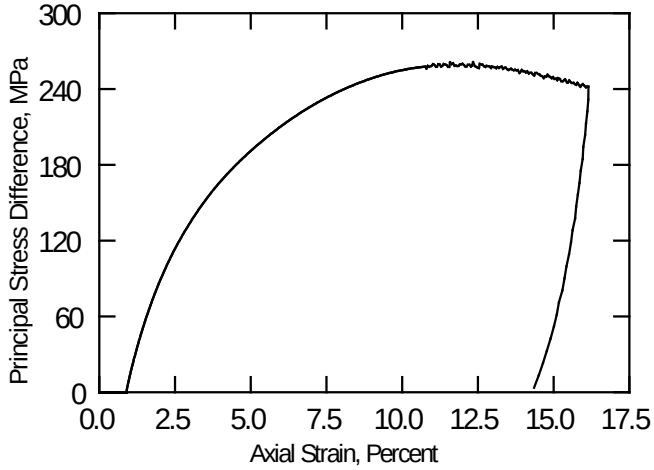

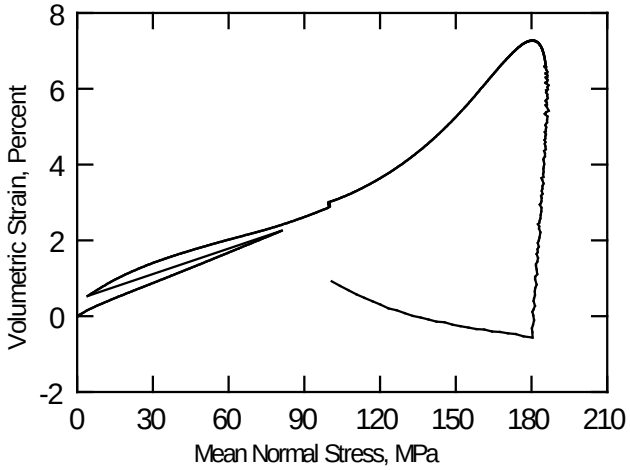

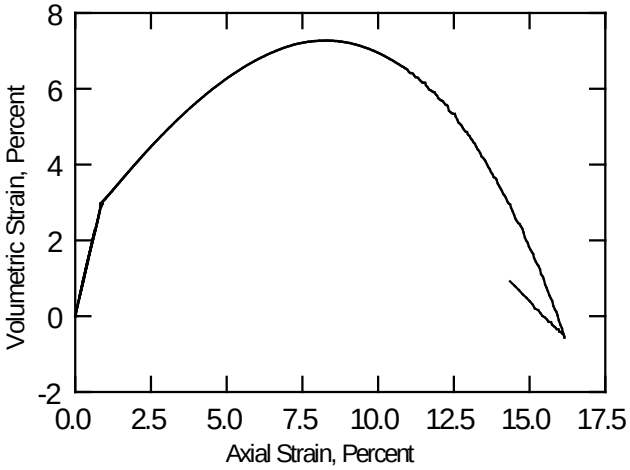

Plate 15

TALLEY BRICK
Test No. 16

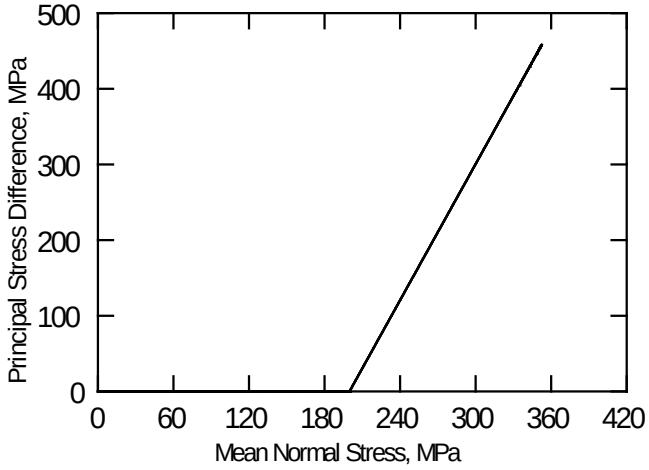

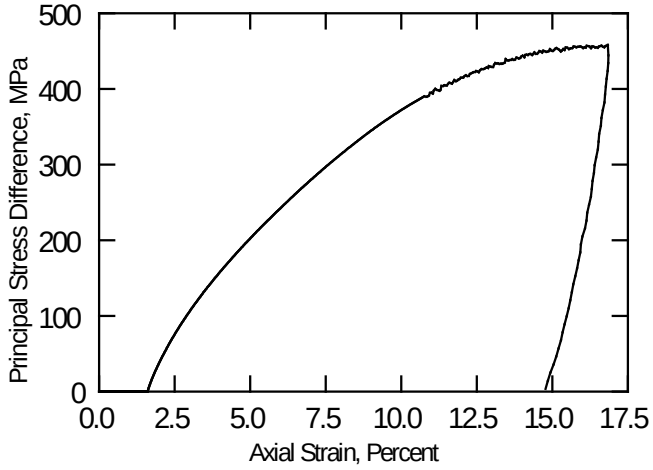

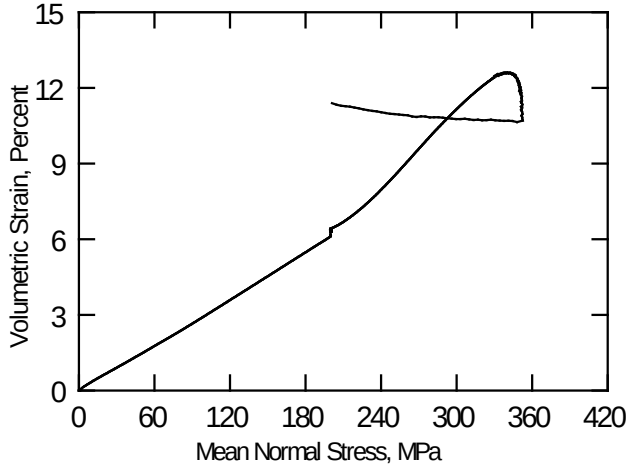

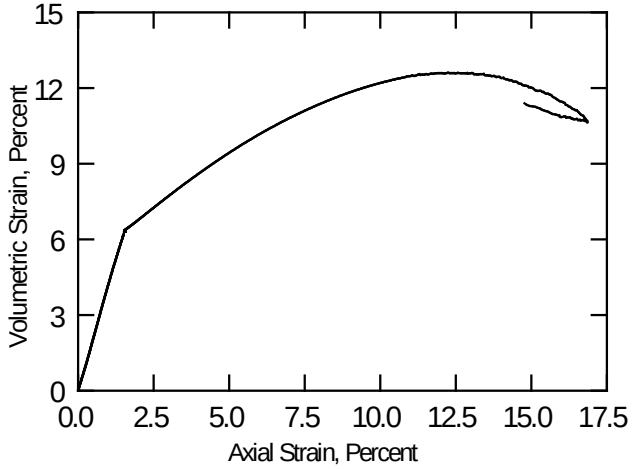

Plate 16

TALLEY BRICK
Test No. 17

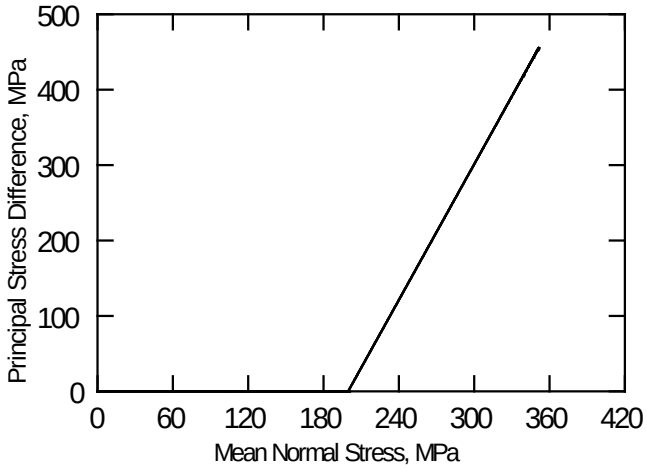

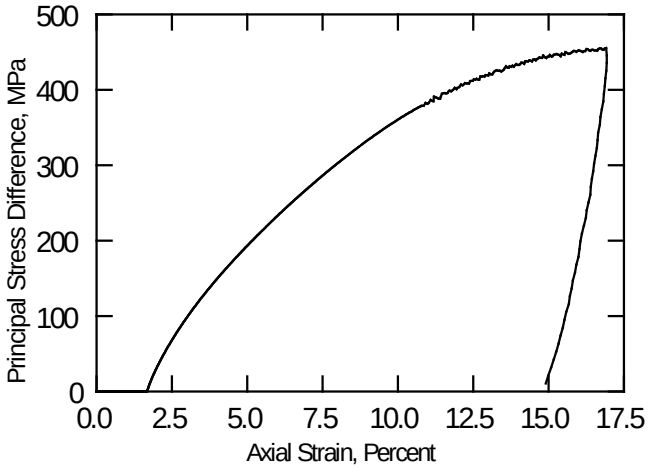

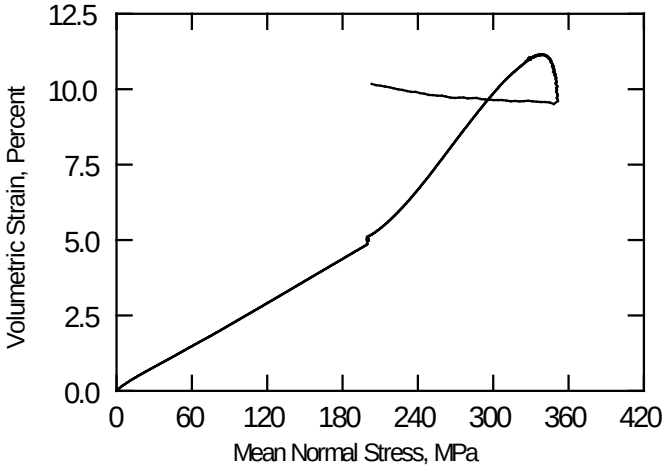

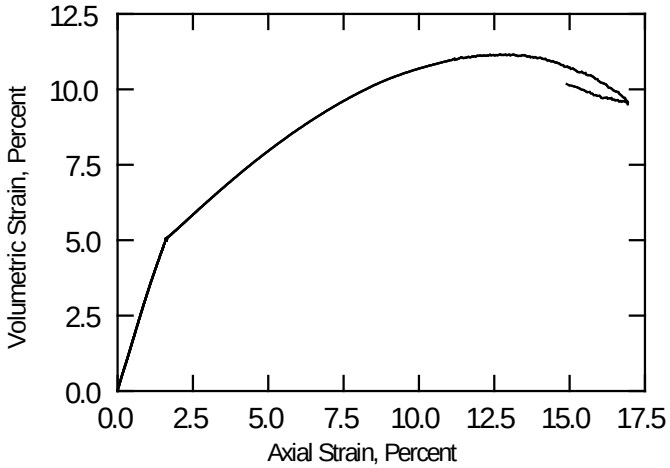

Plate 17

TALLEY BRICK
Test No. 22

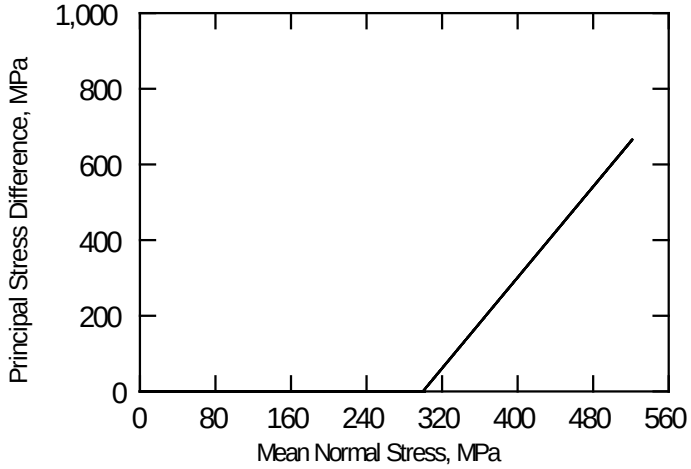

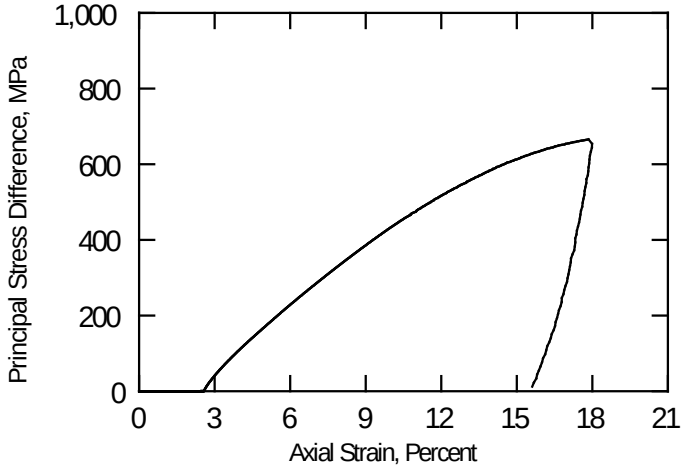

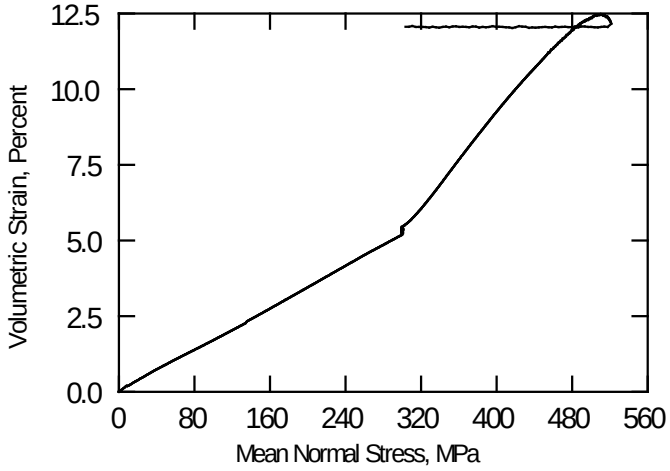

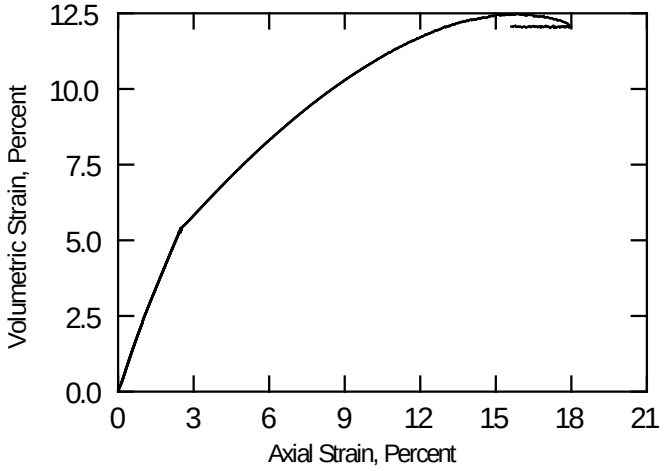

Plate 18

TALLEY BRICK
Test No. 23

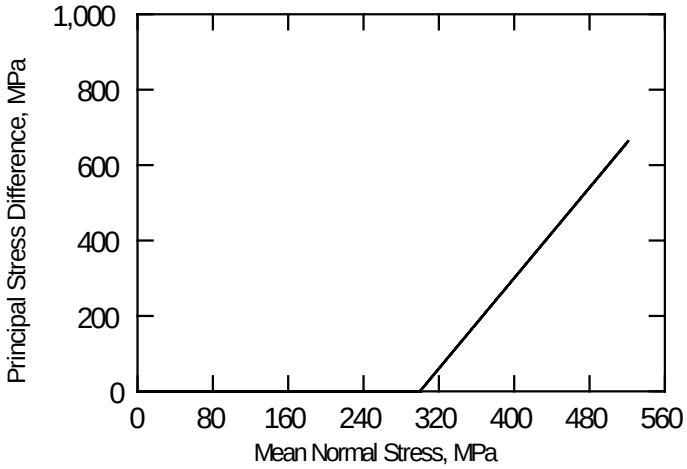

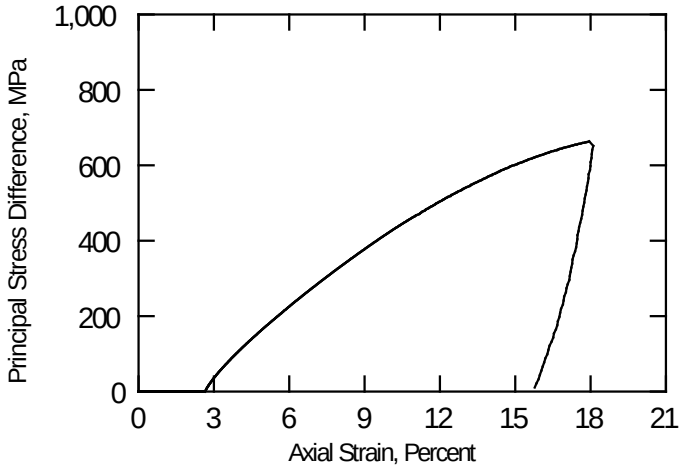

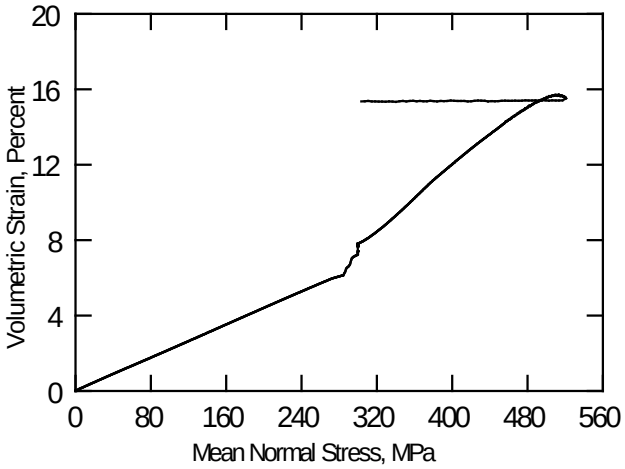

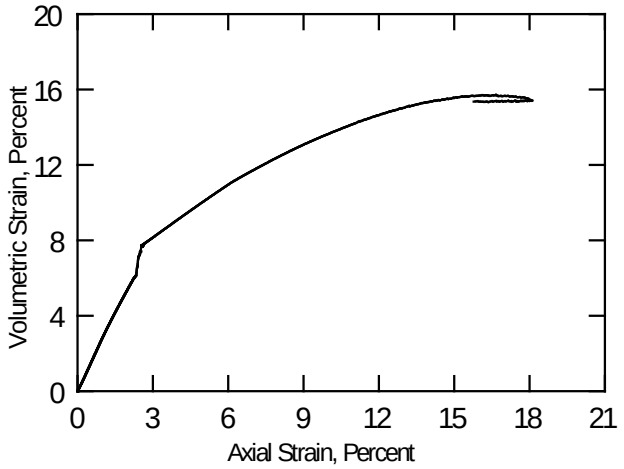

Plate 19

TALLEY BRICK
Test No. 6

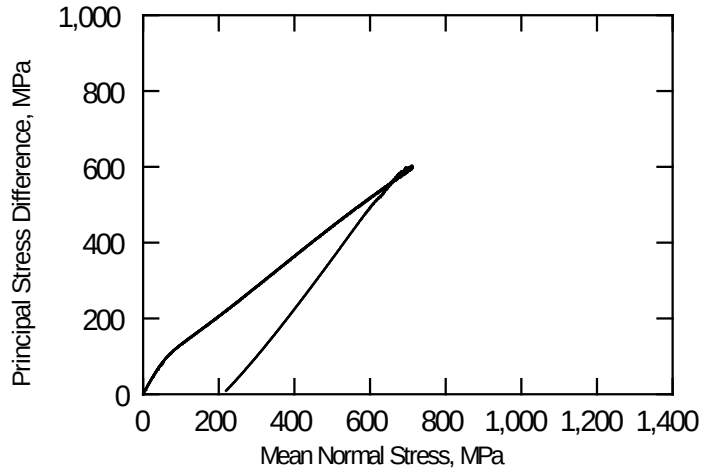

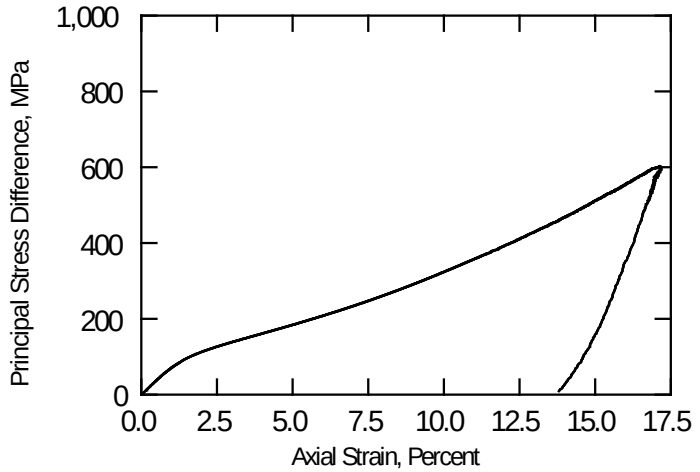

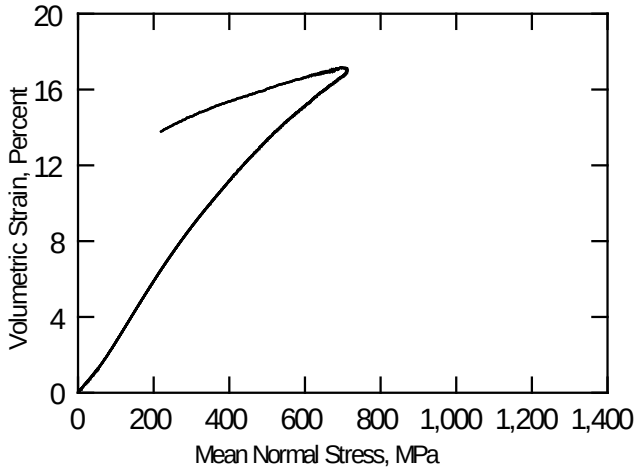

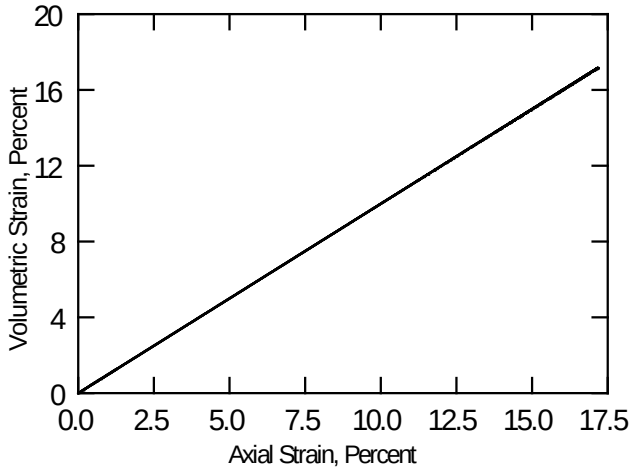

Plate 20

TALLEY BRICK
Test No. 7

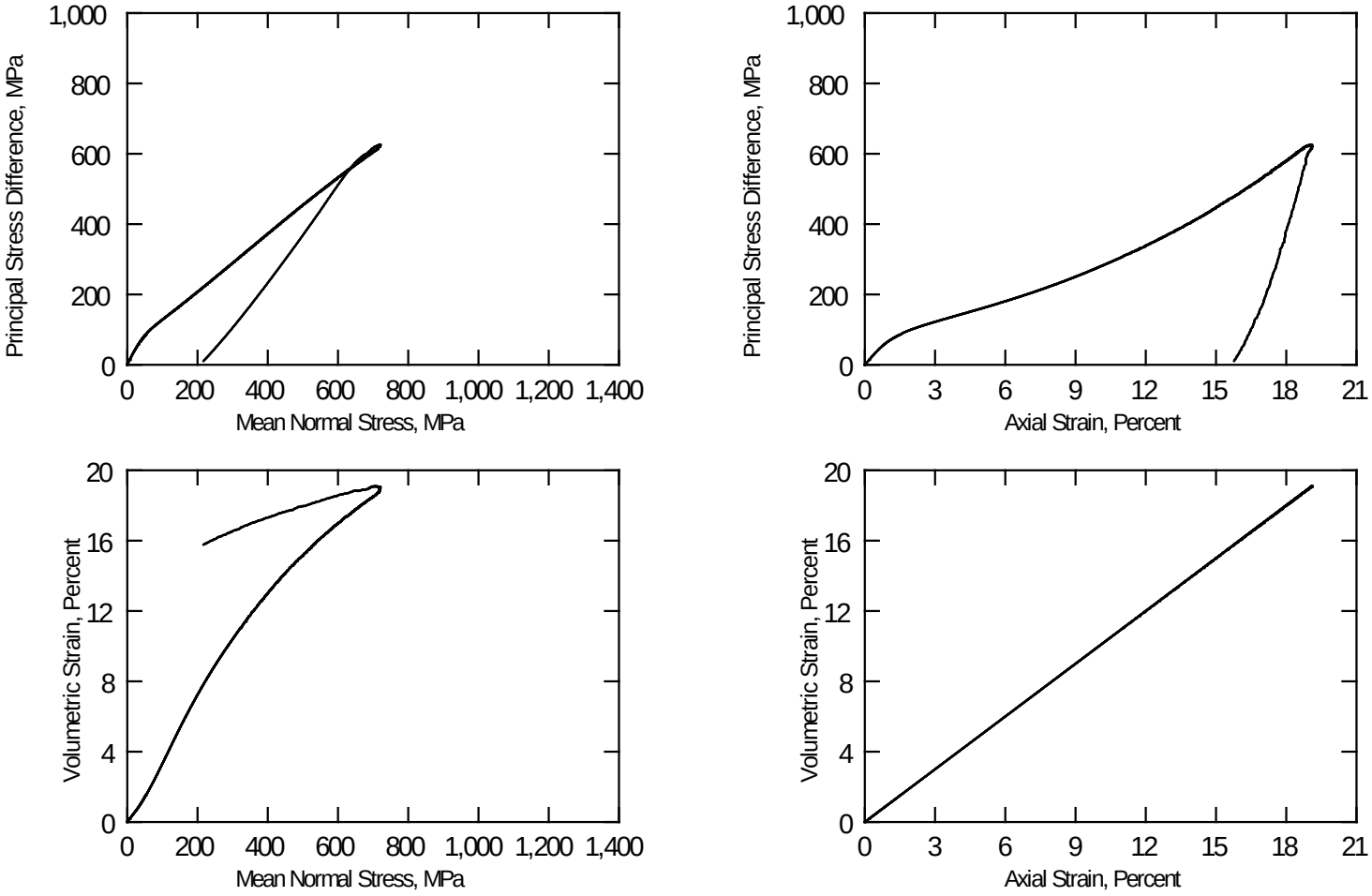

Plate 21

TALLEY BRICK
Test No. 20

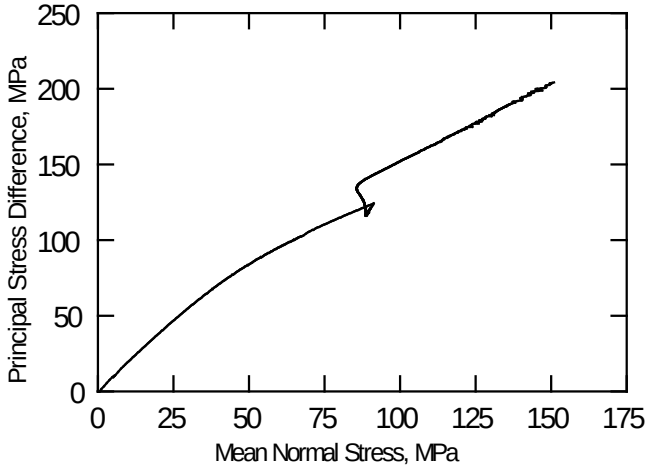

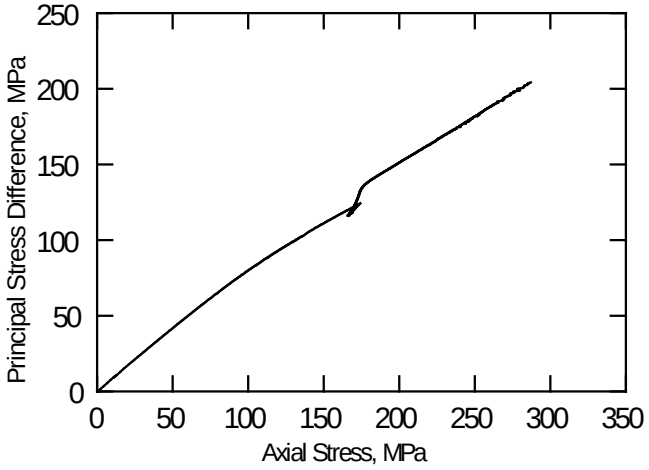

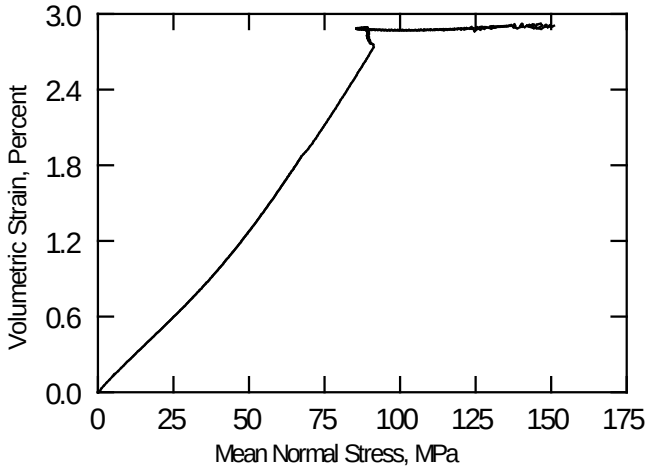

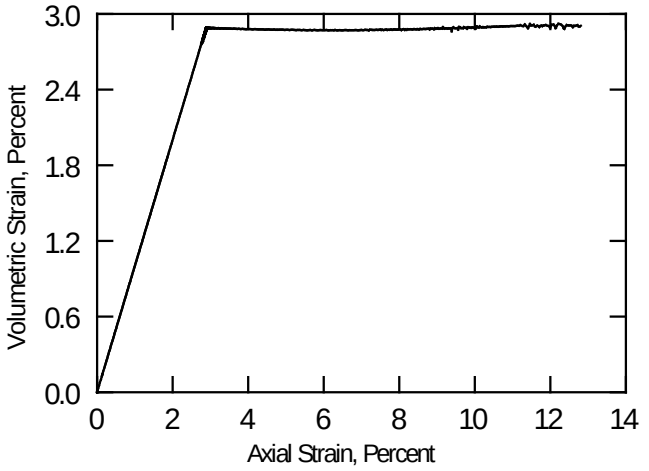

Plate 22

TALLEY BRICK
Test No. 21

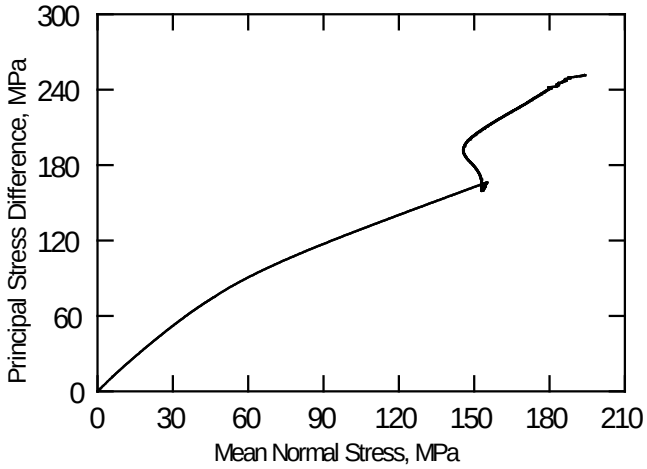

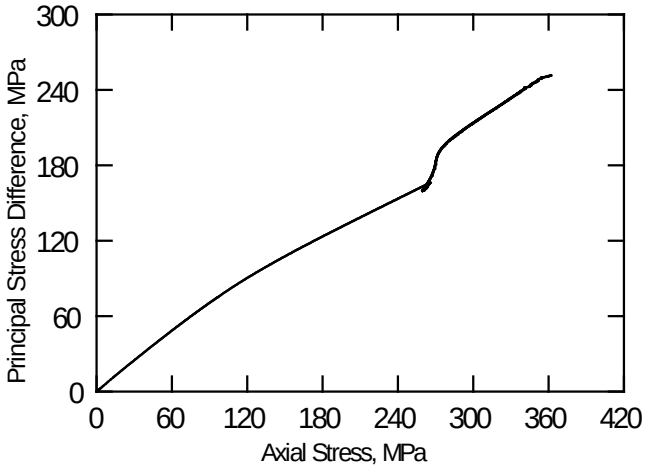

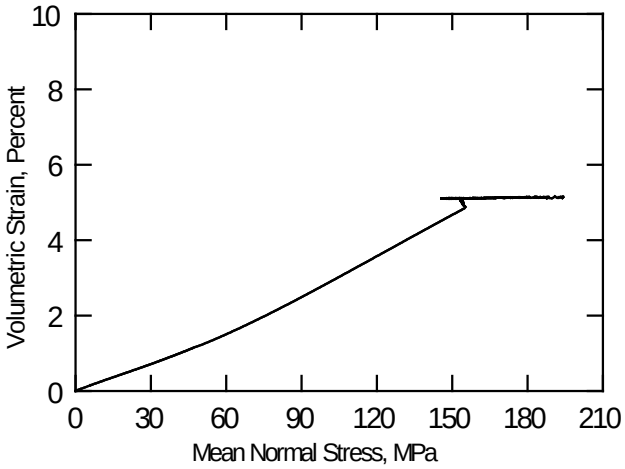

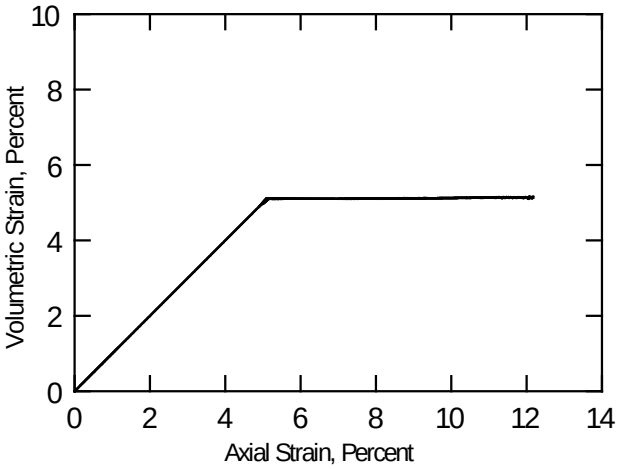

Plate 23

DISTRIBUTION LIST

DEPARTMENT OF DEFENSE

Defense Technical Information Center
ATTN: TC
8725 John Kingman Road
Suite 0944
Fort Belvoir, VA 22060-6218

Director
Defense Threat Reduction Agency
ATTN: CSX (Mr. M. E. Giltrud)
CXSS (Dr. Seung Lee)
CXSS (Dr. Young G. Sohn)
8725 John J. Kingman Road, MSC 6201
Fort Belvoir, VA 22060-6201

Director
Defense Intelligence Agency
ATTN: Dr. Anthony Kee
Unclassified Library
Building 6000
Bolling Air Force Base
Washington, DC 20340-5100

Commander
Field Command, Defense Threat Reduction Agency
ATTN: TDTPI (Dr. Phil Randles)
1680 Texas St., SE
Kirtland AFB, NM 87117-5669

DEPARTMENT OF THE ARMY

Commander
US Army Corps of Engineers
ATTN: CENAD-ET (Mr. Mohan Singh)
CESS (Mr. Ray Navidi)
Washington, DC 20314-1000

Commander
US Army Engineer District, Omaha
ATTN: CENWO-ED-S (Mr. Bruce Walton)
CENWO-ED-S (Mr. Bill Seipel)
215 North 17th Street
Omaha, NE 68102-4978

Commander
US Army Engineer School
ATTN: Technical Library
320 Manscen Loop
Fort Leonard Wood, MO 65473-5000

Director
US Army Research Laboratory
ATTN: Technical Library
RDRL-SL (Mr. R. Coates)
RDRL-SLB-E (Mr. D. Fordyce)
RDRL-SLB-W Mr. W. Mermagan)
RDRL-WML-H (Mr. Steve Schraml)
RDRL-WML-H (Mr. Richard Summers)
RDRL-WML-H (Mr. Robert Phillabaum)
RDRL-WML-H (Mr. Tim Farrand)
RDRL-WML-H (Mr. Christopher Meyer)
RDRL-WMP-F (Mr. David Fox)
Aberdeen Proving Ground, MD 21005-5066

Commander
US Army Research Laboratory
ATTN: Technical Library
2800 Powder Mill Road
Adelphi, MD 20783-1145

Director
US Army ARDEC
ATTN: Technical Library
RDAR-MEE-W (Dr. Bill Ng)
RDAR-EIP (Mr. Henry Kerwien)
RDAR-MEE-W (Mr. L. Thompson)
AMSTRA-AR-AEM-L (Dave Okken)
RDAR-MEE-W, Bldg. 3022 (Arthur S. Daniels)
Picatinny, NJ 07806-5000

Director
US Army AMRDEC
ATTN: RDMR-WDP-S (Mr. Thomas Gill)
Bldg 5400
Redstone Arsenal, AL. 35898-5000

DEPARTMENT OF THE NAVY

Commander
Naval Air Warfare Center
Weapons Division
ATTN: Mr. Kelly Minnick, Code 478200D
China Lake, CA 93555

Commander
Naval Surface Warfare Center
Dahlgren Division
ATTN: (Mr. Michael Hopson)
ATTN: (Dr. Carl Dyka)
17320 Dahlgren Road
Dahlgren, VA 22448-5100

Commander
Naval Surface Warfare Center
Indian Head Division
ATTN: (Mr. Roger Ilamni)
101 Strauss Ave., Bldg 301
Indian Head, Maryland 20640-5035

Naval Postgraduate School
ATTN: Mechanical Engineering Dept.
(Dr. Morris Driels)
Monterey, CA 93943

DEPARTMENT OF THE AIR FORCE

Air Force Institute of Technology
Air University
ATTN: Technical Library
Wright-Patterson AFB, OH 45433

Air Force Research Laboratory, Munitions Directorate
AFRL/RWPLT, ATTN: Mr. Norman S. Gagnon
AFRL/RWPLT, ATTN: Mr. Steve Standley
AFRL/RWPLT, ATTN: Mr. David Watts
AFRL/RWPLT, ATTN: Mr. Bruce Patterson
AFRL/RWPLT, ATTN: Mr. Mark Green
101 W Eglin Blvd, Suite 309
Eglin AFB, FL 32542-6810

DEPARTMENT OF ENERGY

Lawrence Livermore National Laboratory
ATTN: Technical Library
MS L-126 (Dr. Charles Noble)
P.O. Box 808
Livermore, CA 94550-0622

Sandia National Laboratories
ATTN: Dept 1160 (Douglas Dederman)
Dept 7141 (Technical Library, M/S 0889)
P.O. Box 5800
Albuquerque, NM 87185-0303

Sandia National Laboratories
ATTN: Technical Library
Dept. 9042 (Dr. Tracy Vogler)
P. O. Box 969
Livermore, CA 94551-0969

OTHER US GOVERNMENT

Mr. Larry Nuss
Mr. Tom Lippert
Denver Federal Center
Bldg. 67; Mail Code 86-68110
PO Box 25007
Denver, CO 80225-0007

Dr. Andrew A. Prinaris
U.S. Nuclear Regulatory Commission
T4F25M
Washington, DC 20555-0001

DEPARTMENT OF DEFENSE CONTRACTORS

Mr. S. E. Blouin
Applied Research Associates, Inc.
Box 120A, Waterman Road
South Royalton, VT 05068

Dr. Scott Furlow
Applied Research Associates, Inc.
6320 Southwest Blvd, Suite 103
Ft. Worth, TX 67109

Mr. Barry Bingham
Applied Research Associates, Inc.
4300 San Mateo Blvd., NE, Suite A220
Albuquerque, NM 87110

Dr. James K. Gran
SRI International
Poulter Laboratory
333 Rowenswood Avenue
Menlo Park, CA 94025
Dr. Y. Marvin Ito
Mr. H. D. Zimmerman
L-3 Communications Titan Group
9410 Topanga Canyon Blvd., Suite 104
Chatsworth, CA 91311-5758

Mr. Howard S. Levine
Weidlinger Associates
4410 El Camino Real, Suite 110
Los Altos, CA 94022

Dr. Gordon Johnson
Southwest Research Institute
5353 Wayzata Boulevard
Suite 607
Minneapolis, MN 55415

Nammo Talley
ATTN: Nick Duke
Will Betush
Matt O'Neal
Dominic Jezierski
Rick Ventura
P.O. Box 34299
Mesa, AZ 85277-4299

General Dynamics-OTS
ATTN: Dan Boeka
2950 Merced Street, Suite 131
San Leandro, CA 94577

General Dynamics-OTS
ATTN: David Saito
115 Hart St.
Niceville, FL 32578

Bob Waits (Test Area 1)
ERC, Inc.
4901 Corporate Drive NW, Suite E
Huntsville, AL 35805-6219

UNIVERSITIES

Dr. Philip Gullet
P.O. Box 9546
235L Walker Engineering Building
Department of Civil Engineering
Mississippi State, MS 39762

Dr. David Littlefield
Department of Mechanical Engineering
1530 3rd Avenue South
HOEHN 330B
Birmingham, AL 35294-4440

REPORT DOCUMENTATION PAGE

Form Approved
OMB No. 0704-0188

1. REPORT DATE *(DD-MM-YYYY)*	2. REPORT TYPE	3. DATES COVERED *(From - To)*
August 2011	Final report	

4. TITLE AND SUBTITLE

Laboratory Characterization of Talley Brick

5a. CONTRACT NUMBER

5b. GRANT NUMBER

5c. PROGRAM ELEMENT NUMBER

6. AUTHOR(S)

Hannah B. Beatty, Steven S. Graham, Erin M. Williams, and Paul A. Reed

5d. PROJECT NUMBER

5e. TASK NUMBER

5f. WORK UNIT NUMBER

7. PERFORMING ORGANIZATION NAME(S) AND ADDRESS(ES)

U.S. Army Engineer Research and Development Center
Geotechnical and Structures Laboratory
3909 Halls Ferry Road
Vicksburg, MS 39180-6199

8. PERFORMING ORGANIZATION REPORT NUMBER

ERDC/GSL TR-11-29

9. SPONSORING / MONITORING AGENCY NAME(S) AND ADDRESS(ES)

Headquarters, U.S. Army Corps of Engineers
Washington, DC 20314-1000

10. SPONSOR/MONITOR'S ACRONYM(S)

11. SPONSOR/MONITOR'S REPORT NUMBER(S)

12. DISTRIBUTION / AVAILABILITY STATEMENT

Approved for public release; distribution is unlimited.

13. SUPPLEMENTARY NOTES

14. ABSTRACT

Personnel of the Geotechnical and Structures Laboratory, U.S. Army Engineer Research and Development Center conducted a laboratory investigation to characterize the strength and constitutive property behavior of Talley brick. A total of 24 mechanical property tests were successfully completed, i.e., three hydrostatic compression tests, three unconfined compression (UC) tests, 12 triaxial compression (TXC) tests, two uniaxial strain (UX) tests, two uniaxial-strain-load/constant-volumetric-strain-load (UX/CV) tests, and two direct-pull (DP) tests. In addition to the mechanical property tests, nondestructive, pulse-velocity measurements were obtained from each specimen. The TXC tests exhibited a continuous increase in maximum principal stress difference with increasing confining stress. A compression failure surface was developed from the TXC test results at six levels of confining pressure and from the results of the UC tests. The results of the DP tests were used to determine the unconfined tensile strength of Talley brick. The Talley brick specimens displayed tensile strengths of less than 10% of the unconfined compressive strength. The UX/CV stress-path data intersect and then follow the failure surface developed from the TXC tests, as expected.

15. SUBJECT TERMS

Compression tests
Brick
Material properties
Extension tests
Material characterization

16. SECURITY CLASSIFICATION OF:			17. LIMITATION OF ABSTRACT	18. NUMBER OF PAGES	19a. NAME OF RESPONSIBLE PERSON
a. REPORT	b. ABSTRACT	c. THIS PAGE			19b. TELEPHONE NUMBER *(include area code)*
UNCLASSIFIED	UNCLASSIFIED	UNCLASSIFIED		69	